Machine Learning Based Myoelectric Control

Towards Clinical Application

Janne Hahne

Machine Learning Based Myoelectric Control

Towards Clinical Application

Dipl.-Ing. Janne Hahne
geb. in Berlin

Prüfungsausschuss
  Vorsitzender: Prof. Dr. Benjamin Blankertz
  Gutachter: Prof. Dr. Klaus-Robert Müller
                        Prof. Dr. Lucas C. Parra
                        Prof. Dr. Dario Farina

Tag der wissenschaftlichen Aussprache: 18.1.2016

Berlin, 2016

D 83

Abstract

Electromyographic (EMG) signals are used to control electrically powered hand and arm prostheses. In recent years the number of actuated joints in clinically available prostheses has increased significantly. However, the control strategies have not kept up with this development and limit the potential of these devices. Typically there are used only two electrodes on antagonistic muscle groups to control a single degree of freedom (DOF). To actuate other DOFs, the active prosthetic joint has to be selected by co-contraction or other heuristics, which is slow and does not allow for natural and fluent movements.

Significant research has been conducted in the past decades to overcome these limitations, mainly focusing on classification-based approaches. But these efforts had almost no impact on the clinical practice so far. The main reason for this is the lack of reliability under real-world conditions. In this thesis it is demonstrated that the reliability and robustness of the classification-based approach can be significantly increased by means of optimized spatial filters, which enhance the signal characteristics in raw-signal domain.

As the classification-based approach has still limitations regarding the flexibility of combining different motions, regression-based control techniques are explored, which allow for an independent simultaneous and proportional control of multiple DOFs. Four control methods are analyzed offline with a special focus on clinical applicability, namely linear regression (LR), mixture of linear experts (ME), multilayer perceptrons (MLP) and kernel ridge regression (KRR). Results show that the simple and computationally efficient methods LR and ME can perform as well as the more complex non-linear methods MLP and KRR if a proper feature representation is used. Furthermore, two DOFs of the wrist are linearly separable, which allows to estimate combined motions with high precision, even when trained with non-combined movements only.

For adaptive control techniques a training of both the user and the algorithm, is required. This is a long process which typically requires several iterations of alternated (re)training of the algorithm and testing and correcting by the user. A novel training strategy is introduced for regression-based control, in which the user and the algorithm can adapt concurrently. In a real-time study the benefits of this co-adaptive learning approach are demonstrated in comparison with conventional training. With this approach all ten able-bodied subjects and the two persons with congenital limb deficiency, who participated in the study, reached an independent, simultaneous and natural control of two DOFs within a very short time. Due to its minimal computational requirements the regression model can be readily applied on a microcontroller available on prosthetic devices. This is demonstrated by an implementation on an embedded system that fulfills clinical requirements. In tests with a physical hand prosthesis a subject with transradial amputation learned reliable simultaneous and proportional control the two DOFs.

Zusammenfassung

Elektromyographische Signale werden verwendet um elektrisch angetriebene Hand- und Armprothesen zu steuern. In den letzten Jahren hat sich die Anzahl der aktiven Gelenke bei klinisch verfügbaren Prothesen signifikant erhöht. Die Entwicklung der Steuerungsalgorithmen konnte mit dieser Entwicklung allerdings nicht mithalten und bildet momentan den Flaschenhals, der den Nutzen neuartiger Prothesen limitiert. Typischer Weise werden nur zwei EMG-Elektroden auf antagonistischen Muskelgruppen benutzt, um einen einzelnen Freiheitsgrad zu steuern. Um weitere Funktionen anzusteuern, ist ein Wechsel des aktiven Gelenks mittels einer Kokontraktion oder einer anderen Heuristik notwendig. Dies ist langsam und ermöglicht keine flüssigen, natürlichen Bewegungsabläufe.

Trotz beachtlicher Anstrengungen diese Einschränkungen mit Hilfe von Klassifizierungsalgorithmen zu überwinden, haben die Forschungsansätze in diesem Bereich die klinische Praxis kaum beeinflusst. Die Hauptgründe dafür sind die mangelnde Zuverlässigkeit unter realen Bedingungen. In dieser Arbeit wird gezeigt, dass sich die Zuverlässigkeit und Robustheit der Klassifikation durch den Einsatz optimierter räumlicher Filter, die die Signaleigenschaften im Rohsignal-Raum verbessern, signifikant steigern lässt.

Da der Klassifizierungsansatz jedoch nur eingeschränkte Möglichkeiten bietet verschiedene Bewegungen zu kombinieren, werden insbesondere auch Regressionsverfahren betrachtet, die eine unabhängige simultane Proportionalsteuerung mehrerer Funktionen ermöglichen. Ein Besonderer Schwerpunkt der Untersuchungen dieser Arbeit ist die klinische Anwendbarkeit. Vier Methoden, *Lineare Regression (LR)* einschließlich der Erweiterung *Mixture of Linear Experts (ME)*, *Multilayer Perceptrons (MLP)* und *Kernel Ridge Regression (KRR)* werden offline analysiert. Dabei schneiden die einfachen Methoden LR und ME mit geringen rechentechnischen Anforderungen nicht schlechter als die komplexeren, nichtlinearen Methoden MLP und KRR ab, sofern geeignete Feature-Repräsentationen der Signale verwendet werden.

Klassifikations- und Regressionsverfahren erfordern ein Training, sowohl des Anwenders, als auch des Algorithmus. Dies ist oft ein langwieriger Prozess der viele Iterationen aus wechselseitigem (neu)trainieren des Algorithmus und des Testens und Korrigierens durch den Nutzer benötigt. Hier wird ein neuer Trainingsansatz für Regressionssteuerungen präsentiert, bei dem Anwender und Algorithmus gleichzeitig lernen können. In einer Echtzeitstudie wird gezeigt, dass dieser Ansatz des koadaptieven Lernens erhebliche Vorteile gegenüber konventionellem Training hat. Mit dieser Methode konnten alle getesteten Versuchspersonen mit normaler Anatomie und zwei Personen mit angeborener Fehlbildung des Unterarms innerhalb kürzester Zeit zwei Freiheitsgrade simultan und proportional steuern. Die verwendeten Algorithmen kommen mit minimaler Rechenleistung aus und lassen sich problemlos auf den vorhandenen Mikrocontrollern einer Prothese verwenden. Dies wird durch die Implementierung auf einem minimalistischen eingebetteten Echtzeitsystem demonstriert, dass die wichtigsten klinischen An-

forderungen erfüllt. In Tests mit einer elektrischen Handprothese, konnte die Versuchs-person mit transradialer Amputation die beiden Freiheitsgrade der Prothese zuverlässig simultan und proportional steuern.

Acknowledgements

I am deeply grateful for all people who helped me in conducting this work. Especially I would like to thank my supervisor Klaus-Robert Müller, who always supported me, trusted me and gave me all freedom I could wish for my work. His fast and unbureaucratic help and the great input I got on Machine Learning have been invaluable for this thesis.

Second, I would like to thank Lucas C. Parra. His input in signal processing and adaptive algorithms shaped large parts of this work. Especially his helpfulness and the huge amount of time he spent in many discussions with me have been an incredible support.

I further would like to thank Dario Farina. His expertise in electromyography and his help in analyzing the data have been of unestimable value. Without the experimental support by him and his group large parts of this work would not have been possible.

I further would like to thank Sven Dähne for his continuous input and the restless discussions to optimize the details of the experimental designs. Special thanks go also to Han-Jeong Hwang who has not only been an irreplaceable support with the statistics but provided also unconditional help in planning and conducting the experiments. His diligence and tireless passion for the details significantly improved our common studies. I further would like to thank all other people who supported this work including Felix Bießmann, Ning Jiang, Claudia Sanelli, Michael Tangermann, Hubertus Rehbaum, Frank Meinecke, Bernhard Graimann and Hans Dietl. I am very thankful for the technical and administrative support by Dominik Kühne and Andrea Gerdes.

Special thanks deserve my wife Petra and our children Jon and Nina for their patience and for covering my back during this work.

Contents

List of Symbols

$\boldsymbol{x}(t)$, $\boldsymbol{X}$ - raw-data (vector at time t, matrix with samples as column vectors)

$\boldsymbol{s}(t)$, $\boldsymbol{S}$ - components in vector and matrix form

$\boldsymbol{\phi}(t)$, $\boldsymbol{\Phi}$ - features in vector and matrix form

$\boldsymbol{y}(t)$, $\boldsymbol{Y}$ - class or regression labels in vector and matrix form

$\boldsymbol{w}$, $\boldsymbol{W}$ - linear mapping vector, matrix with multiple mappings in columns.

$\boldsymbol{A}$ - spatial patterns (forward model)

$\mathbf{I}$ - identity matrix

$\boldsymbol{\Sigma}$ - covariance matrix

$\boldsymbol{D}$ - diagonal matrix

λ_i^c - eigenvalue i for class c

D_X, D_Φ, D_Y - dimensionality of $\boldsymbol{X}$, $\boldsymbol{\Phi}$ and $\boldsymbol{Y}$.

N_X, N_Φ - number of samples, in raw-signal and feature domain

N_c - number of classes

$\sigma(x)$ - sigmoid function

$h(\boldsymbol{x})$ - non-linear mapping for kernel methods

γ - kernel width for Gaussian kernel function

r and θ - radius and angle in polar coordinates

Abbreviations

ADC - analog to digital converter

BCI - brain computer interface

CSP - common spatial patterns

DOF - degree of freedom

EEG - electroencephalography

EMA - exponential moving average filter

EMG - electromyography, electromyographic

IC - integrated circuit

IED - inter electrode distance

KRR - kernel ridge regression

LDA - linear discriminant analysis

LR - linear regression

MAV - mean absolute value

MC - microcontroller

ME - mixture of linear experts

MLP - multilayer perceptron (artificial neuronal network)

MVC - maximum voluntary contraction

OvO - one versus one

OvR - one versus rest

PCA - principal component analysis

PWM - pulse width modulation

QDA - quadratic discriminant analysis

RLS - recursive least squares

RMS - root mean square

SNR - signal to noise ratio

VAR - variance

1 Introduction

Losing a hand in an accident is often a highly traumatic experience for the affected person. Moreover, it typically comes along with a radical change of life, as in many cases the professional occupation cannot be continued and simple activities of daily living like eating, dressing/undressing or cooking may become very difficult. Even though hand prostheses may never be able to fully replace the original limb, they can provide important practical and also psychological support to the user. The most common control-signals for actuated upper limb prostheses are electromyographic (EMG) signals, which are small electrical potentials that muscles generate during contractions.

Great advances in mechatronics in the past years led to the development of several highly functional commercially available prostheses with individually actuated digits that have the capability of decreasing the gap between the artificial device and the actual limb. However, so far there exists no controller that is capable of extracting a sufficiently high number of control signals from the intention of the user, to make full use of the advanced hardware. Despite several decades of research on myoelectric control aiming to improve this human-machine interface and impressive results in the literature, so far this had almost no impact on the clinical practice. The clinical state of the art allows for controlling only one degree of freedom (DOF) at a time and the user has to switch between the active joints or pre-defined grip patterns. The reason for this mismatch between academic results and its applicability is that in most academic studies many clinically relevant factors were excluded and that the methods become unreliable under real-world conditions.

The aim of this work is to develop novel control strategies for myoelectric hand prostheses that are applicable also under real-world conditions and have the potential to increase the quality of life for prosthesis users. Therefore, this thesis will be focusing on factors of practical relevance.

1.1 Outline of this Thesis

Chapter 2 introduces the neurophysiology, underlying the generation of electromyographic signals and provides an overview on the history of upper-limb prostheses and control techniques. Research approaches will be summarized that have been described in the literature, including classification and regression-based techniques. In chapter 3, the concept of spatial filters will be introduced and applied to classification-based myoelectric control with the aim to increase the reliability and robustness of this approach. In particular, different multiclass extensions of a technique known as as common spa-

tial patterns (CSP) are investigated. The robustness to real-world issues is evaluated by including a variation of the arm position and by adding artificial sensor-noise. Chapter 4 compares previously applied regression techniques for independent simultaneous and proportional control of multiple DOFs with novel approaches. In this comparison a special emphasis on clinical relevant factors is given. Based on these offline investigations, a real-time control is developed. It is evaluated in chapter 5 in a closed-loop, which allows the user to adapt to the provided feedback. A novel and promising training approach is introduced and carefully investigated in a real-time study, in which both the user and the algorithm learn simultaneously. The usability of the developed techniques is demonstrated on an embedded system used to independently control two DOFs of a real prosthesis by a subject with upper limb deficiency.

1.2 Scientific Contribution

This is the first work that applies common spatial patterns in the context of myoelectric control. These spatial filters are optimized in a supervised training procedure for each user individually and enhance the relevant information in raw-signal domain. This does not only improve classification accuracy and robustness but also gives access to filter-patterns that allow for a physiological interpretation of the results.

Regression has been proposed recently to archive simultaneous and proportional control of multiple degrees of freedom. In this work two previously applied methods (linear regression and multilayer perceptrons) are compared with two methods that are novel in this context (mixture of experts and kernel ridge regression). Systematic investigations of the relationship between EMG features and joint angles revealed that relatively simple and computationally significantly more efficient methods can perform equally well as more complicated and computationally expensive techniques. This is very important for a future transfer into a clinical application as the algorithms are required to run on a minimalistic hardware with low power consumption to be integrated into a prosthesis. For the first time it is systematically investigated how the amount and the diversity of training data influences the performance. Useful suggestions can be derived from this analysis on training protocols for a practical clinical application of the methods.

Finally this is the first realization of co-adaptive learning in myoelectric control. The real-time study demonstrates that this novel closed-loop training concept is much more efficient than conventionally applied open-loop calibration or alternating phases of human and machine learning that are usually present when a conventional trained system is evaluated and retrained in case of insufficient performance.

Large parts of the results have been published previously by the author in peer reviewed journal and conference publications. An overview on the related publications is given below. The author wants to thank his co-authors for allowing to use materials of joint publications in this thesis.

1.3 List of Publications

The following publications are included in large parts in this thesis.
Journal publications:

[1] J. M. Hahne, B. Graimann, and K.-R. Müller, "Spatial filtering for robust myoelectric control", IEEE Transactions on Biomedical Engineering, vol. 59, no. 5, pp. 1436 - 1443, May 2012

[2] J. M. Hahne, F. Biessmann, N. Jiang, H. Rehbaum, F. Meinecke, K.-R. Müller, D. Farina, and L. Parra, "Linear and non-linear regression techniques for simultaneous and proportional myoelectric control", IEEE Transactions on Neural Systems and Rehabilitation Engineering, vol. 22, no. 2, pp. 269 - 279, Mar. 2014.

[3] J. M. Hahne, S. Dähne, H.-J. Hwang, K.-R. Müller, L. Parra, "Concurrent Adaptation of Human and Machine Improves Simultaneous and Proportional Myoelectric Control", IEEE Transactions on Neural Systems and Rehabilitation Engineering, vol. 23, no. 4, Jul. 2015

Conference contributions:

[4] J. M. Hahne, H. Rehbaum, F. Biessmann, F. Meinecke, K.-R. Müller, N. Jiang, D. Farina, and L. Parra, "Simultaneous and proportional control of 2D wrist movements with myoelectric signals", in 2012 IEEE International Workshop on Machine Learning for Signal Processing (MLSP), Sep. 2012.

[5] J. M. Hahne, S. Dähne, D. Farina, L. Parra, K.-R. Müller, "Separability of Wrist Motions in Simultaneous and Proportional Myoelectric Control", Bernstein Conference, Göttingen, Sep. 2014, DOI:10.12751/nncn.bc2014.0226

[6] J. M. Hahne, K.-R. Müller, D. Farina, "An Embedded System for Simultaneous and Proportional Myoelectric Control of Upper Limb Prostheses", in 2015 37th Annual International Conference of the IEEE Engineering in Medicine and Biology Society (EMBC), 2015.

The following publications are related to this work but have not been included into the thesis.
Journal publications:

[7] H.-J. Hwang, J. M. Hahne, K.-R. Müller, "Channel Selection for Simultaneous and Proportional Myoelectric Prosthesis Control of Multiple Degrees-of-Freedom", Journal of Neural Engineering, Journal of neural engineering, vol. 11, no. 5, Aug. 2014

[8] J.-P. Kauppi, J. M. Hahne, K.-R. Müller, Aapo Hyvärinen, "Three-way analysis of spectrospatial electromyography data: classification and interpretation", Plos One, vol. 10, no. 6, June 2015

[9] M. M.-C. Vidovic, H.-J. Hwang, S. Amsüss, J. M. Hahne, D. Farina, K.-R. Müller, "Improving the Robustness of Myoelectric Pattern Recognition for Upper Limb Prostheses by Covariate Shift Adaptation", IEEE Transactions on Neural Systems and Rehabilitation Engineering, in Press, 2015.

Conference contributions:

[10] J. M. Hahne, J. M. Herrmann, D. Hofmann, M. Paulus, B. Graimann, "Electrode configuration for multifunctional, myoprostheses", presented on the congress of the International Society of Electrophysiology and Kinesiology (ISEK), Aalborg, 2010

[11] D. Hofmann, A. Biess, J. M. Hahne, B. Graimann, J. M. Herrmann, "Spatial information in multi-electrode data for myoprostheses", presented on the congress of the International Society of Electrophysiology and Kinesiology (ISEK), Aalborg, 2010

[12] D. Hofmann, A. Biess, J. M. Hahne, B. Graimann, J. M. Herrmann, "Information theoretical analysis of high density electromyographic data for prostheses control", in Front. Comput. Neurosci. Conference Abstract: Bernstein Conference on Computational Neuroscience. DOI: 10.3389/conf. fncom, 2010, Bd. 132.

[13] H.-J. Hwang, J. M. Hahne, K.-R. Müller, "Channel selection for simultaneous myoelectric prosthesis control", in 2014 International Winter Workshop on Brain-Computer Interface (BCI), 2014.

[14] H.-J. Hwang, J. M. Hahne, K.-R. Müller, "Impact of Arm Position Change on the Performance of Simultaneous and Proportional Myoelectric Control", International BioMedical Engineering Conference (IBEC), 2014.

[15] S. Dähne, J. M. Hahne, P. Pawletta, K.-R. Müller, "Boosting simultaneous and proportional myoelectric control by combining source power correlation (SPoC) and linear regression", Bernstein Conference, Göttingen 2014, DOI: 10.12751/nncn. bc2014.0225

[16] M. M.-C. Vidovic, L.P. Paredes, H.-J. Hwang, S. Amsüss, J. Pahl, J. M. Hahne, B. Graimann, D. Farina, and K.-R. Müller, "Covariate shift adaptation in emg pattern recognition for prostheticdevice control", in 2014 36th Annual International Conference of the IEEE Engineering in Medicine and Biology Society (EMBC), 2014.

2 Fundamentals

2.1 Electromyography

Electromyographic signals are small electrical potentials that are generated in muscles during contraction. All body movements are driven by muscles that apply forces to the skeleton when contracting. Muscles are composed of fibers that shorten after activation by depolarization of the cell-membrane. They are controlled by the central nervous system (CMS) via motor neurons. All muscle fibers that are controlled by one motor neuron form a motor unit (MU) and contract always simultaneously. The number of muscle fibers per MU varies within and across muscles and amounts to several hundred [Buchthal and Schmalbruch, 1980]. Also the number of MU per muscle differs across muscles and falls in the range of 100 - 400 units for the muscles relevant for myoelectric control [Al-Faiz and Al-Mashhadany, 2009]. To activate a MU, local depolarizations of the motor neurons membrane (action potentials) travel along the axons from the spinal cord towards the muscles. At the neuro-muscular junction, each neural action potential triggers the release of neurotransmitters, which cause a local depolarization of all muscle fibers of that MU. The depolarization starts in the innervation zone, typically located in the central section of the muscle. A motor unit action potential (MUAP) propagates in both directions of the muscle fibers and causes the contraction of all fibers of that MU. Two factors are determining the force level: the number of activated MUs and the firing rates of the individual MUs [Despopoulos and Silbernagl, 2003].

Invasive recodings with needle-electrodes (which are also used for certain medical diagnostics) have a very high selectivity and allow to directly detect individual MUAPS. Due to the volume conduction of the tissue, the local depolarizations of the individual MUs superimpose and form the surface electromyogram (sEMG) measured on the skin. Both the number of activated MUs and the firing rates are reflected in the amplitude of the sEMG. It consists of frequencies in the range of approximately 0 - 500 Hz. The amplitude increases with the contraction force and can reach levels in the range of a few millivolts for strong contractions. Although recent developments in high density EMG recording and signal processing techniques allowed to reconstruct MUAP spike trains at low contraction levels even non-invasively [Holobar et al., 2010, Glaser et al., 2013], for myoelectric control typically more global features are extracted from the sEMG.

For medical diagnostics and research proposes, the EMG is often recorded with Ag/AgCl-Electrodes in combination with conductive electrode gel. This minimizes the electrode-skin impedance and disturbing half-cell potentials and allows to record at very low
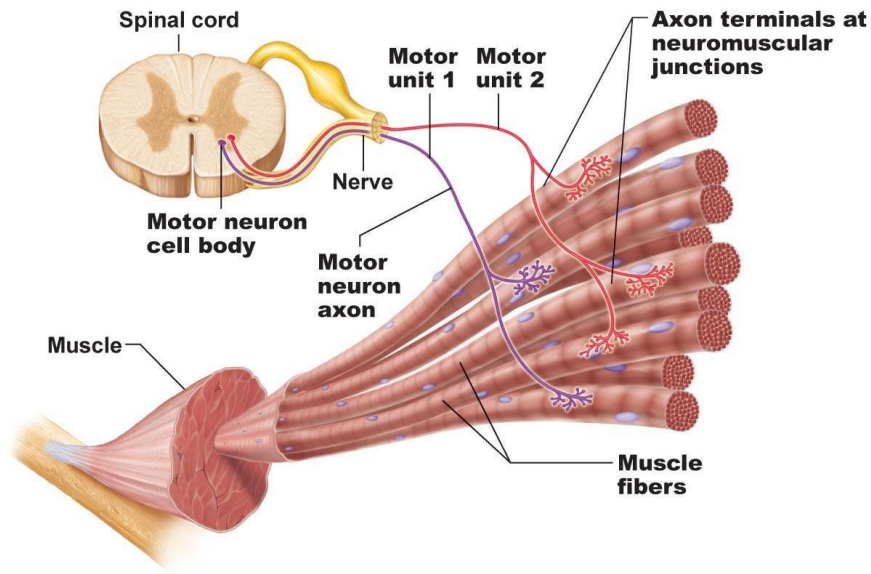
Figure 2.1: Schematic illustration of the neuromuscular system showing two motor units. Reprinted from [Marieb and Hoehn, 2013] with permission of Pearson Education, Inc., Upper Saddle River, NJ

noise levels [Clancy et al., 2002]. For a long-term use in prosthetics, electrodes with gel are not suitable, and typically dry steel-electrodes are used instead. Due to the increased impedances, dry electrodes typically have higher noise levels and require more advanced amplifiers designs [Chi et al., 2010]. Because of its relation to muscle-force, the EMG can be used as a consciously controllable user input for devices such as myoelectric hand prostheses [Muzumdar, 2004].

2.2 Upper Limb Prostheses

The number of trauma related amputations and congenital limb deficiencies of the upper extremity in developed countries per year and 100.000 inhabitants is in the range of 0.5 - 1 for the hand, 0.05 - 0.2 for below the elbow (transradial) and 0.05 - 0.1 for above elbow (transhumoral) cases [Dillingham et al., 1998, James and Luff, 2006, Kutzenberger and Hackl, 2006]. Prostheses are artificial replacements of a missing body part. First indications for artificial limb-replacements are found already on mosaics and vases from pre-historic times [Putti, 2005]. A famous and one of the oldest still existing examples for mechanical hands is the "iron hand" (Fig. 2.2) of Gottfried ("Götz") von Berlichingen (1481 - 1562). It is made from metal and includes sophisticated mechanics which allows to close and lock the fingers in different positions with the intact hand to grasp and hold objects.
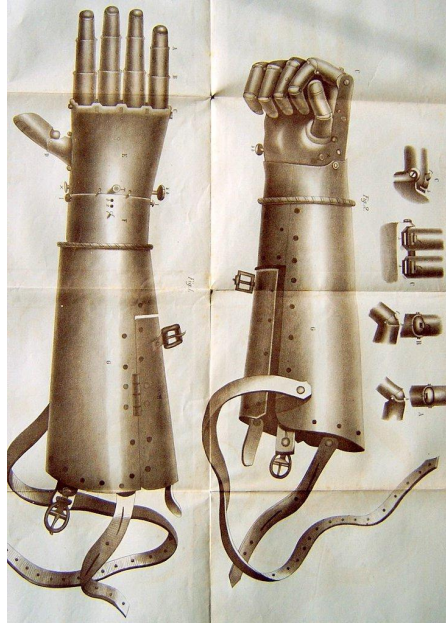
Figure 2.2: Historic example of mechanical upper limb prosthesis: The second version of the "iron hand" of Götz von Berlichingen, manufactured around 1530 (Drawing by Christian von Mechel 1815, picture from [Berlichingen-Rossach, 1861], public domain).

More recent examples of body-powered mechanical devices use cable-controls for directly actuating the mechanic to open or close the device (Fig. 2.3). They are still very popular because of their low costs, low weight and very high robustness [Berning et al., 2014]. As the device is directly actuated by other muscles, the user obtains a direct force-feedback — a very useful feature that modern myoprostheses still miss. Drawback of the body-powered devices are the relatively low grip force and the limitation to a single actuated DOF.

The first research prototypes for electrically powered hand prostheses which use the EMG as control source were introduced after the 2nd world war in Germany [Reiter, 1948] and the first commercially available devices were developed in the 1960's in Russia [Sherman, 1964]. Over many decades myoelectric-prostheses had only one actuated DOF for opening and closing the hand and optionally a second one for a rotation of the wrist. In the last years, great advances were achieved in the development of highly functional electrically powered hand prostheses with a high number of actuated joints. Currently at least four manufacturers offer multifunctional hand prostheses with six to eleven actuated joints (Fig. 2.4) [Belter et al., 2013] and there exist research prototypes with up to 20 active joints [Miguelez, 2011, Fite et al., 2008, Cipriani et al., 2011a]. In the design of new prostheses, there are always trade-offs between functionality (number of joints and actuators), maximal grip strength, complexity, anatomical correctness on one

Figure 2.3: Modern example of a body powered, cable driven prosthesis: Split-hook from Fillauer (picture used with permission of Fillauer).

side and costs, weight, size and mechanical robustness on the other side. In many hardware designs some of the joints are therefore mechanically coupled to reduce the number of actuators, which reduces the weight, costs and size and can increase grip strength. Until now no controller for independent control of more than one DOF is clinically available (see sec. 2.3.1), the actuators are typically coupled by the controller (e.g. all fingers open or close simultaneously) and different programs are selected heuristically to access different grip patterns or control different joints.

2.3 Myoelectric Control

Despite several decades of research on advanced myoelectric control algorithms all manufacturers of myoelectric hand prostheses still use the same simple control strategy that was introduced in the 1960's. Only very recently a start-up company has introduced a classification-based controller that can be used in combination with the hand-prostheses of the most important manufacturers [Coapt-LLC, 2015]. In this section the clinical state of the art is described and an overview on the research-approaches that are found in the literature is provided. The properties of the most important approaches are summarized in figure 2.6.

2.3.1 Clinically Available Control Techniques

Clinically available myoelectric control techniques are relatively simple. Individuals with hand amputation usually maintain a phantom feeling for their lost limb and movements
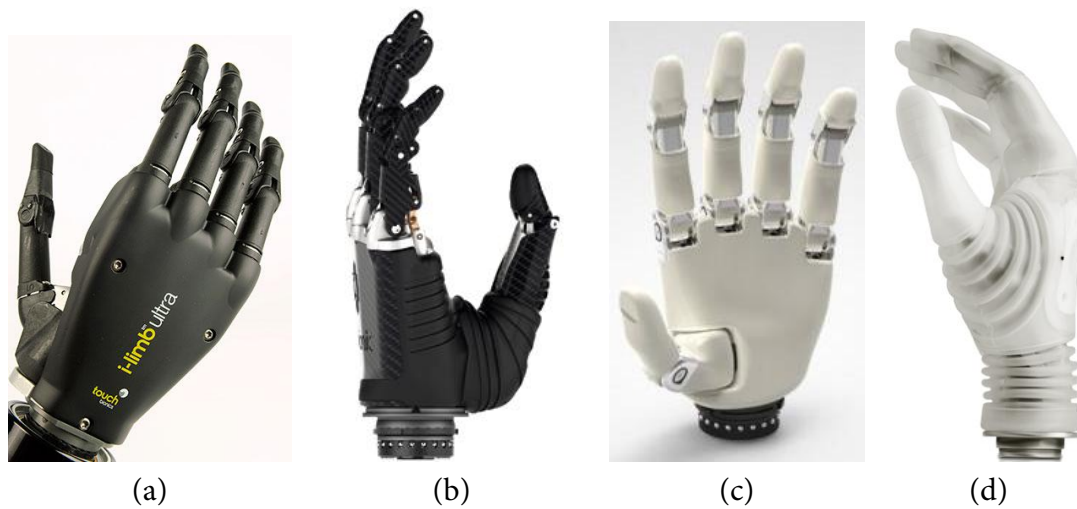
Figure 2.4: Examples of clinically available multifunctional hand prostheses: (a) Touch bionics "i-limb ultra", (b) RLS Steeper Group "Bebionic", (c) Vincent Systems "Evolution 2", Otto Bock "Michelangelo". All pictures are provided by the manufacturers and used with permission.

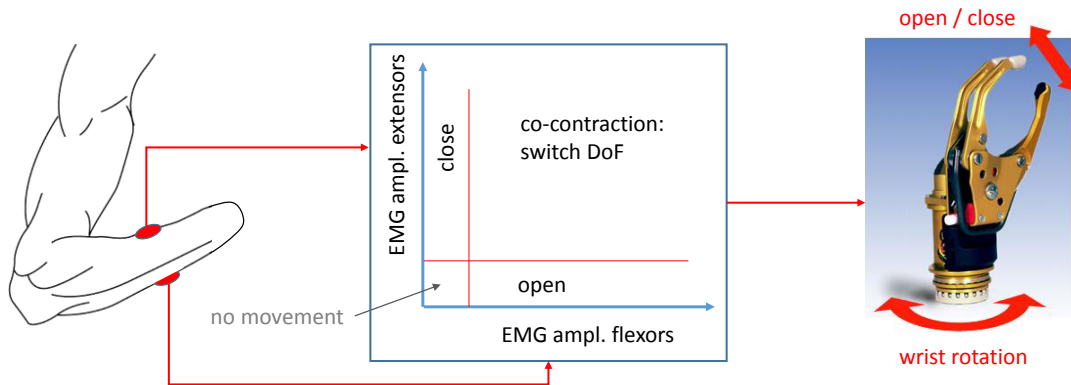Figure 2.5: Clinical state of the art. The amplitudes of two electrodes on antagonistic muscles are used to control one DOF. Above threshold levels on the flexor electrode close the prosthesis and the opposite for the extensor electrode. The signal amplitude is mapped to the speed or grip-force of the prosthesis. When both muscles are activated together, this co-contraction triggers the switching to another DOF.

with the phantom hand cause contractions of the residual muscles in the forearm. To control a hand prosthesis, they typically perform muscle contractions, corresponding to extensions and flexions of the wrist. Bipolar EMG signals obtained from the residual extensors and flexors are used as control inputs and the signals are directly mapped into one DOF [Muzumdar, 2004]. Activity at the extensor-electrode opens the prosthetic hand, and activity at the flexors closes it. The movements the subject has to perform to control the prosthesis are not identical to the movements executed by the prosthesis, but the contraction patterns related to the activated muscles are spatially well separated and allow for a very robust control. Within very short time the association is learned by the user and the control becomes intuitive.

A proportional control is possible, i.e. by varying the muscle force, the user can control the speed of the prosthesis. If an object is touched, the grip-force is controlled instead of the velocity. With this method, referred to as *direct control*, it is not possible to control more than one DOF at a time. Simply extending direct control to more DOFs is not possible with surface EMG because usually there are not enough independently activatable control sites available. An exception is given by targeted muscle reinnervation (TMR), a surgical procedure, where additional control sites are obtained by transferring the nerves that used to control the lost limb into other, still existing muscles, which are spatial well separated. There is ongoing research to develop electrode implants that pick up the signals directly at the muscles [Herberts et al., 1968, Weir et al., 2009, Baker et al., 2010, Lewis et al., 2013, Prabhav et al., 2014]. This can potentially give a higher number of distinct input signals even without TMR and may also allow to extend direct control to more than one DOF [Smith et al., 2014, Pasquina et al., 2015].

For all other users, additional functions like a rotation of the wrist are controlled by switching the active DOF. This can be achieved by a co-contraction where both muscle-groups are activated for a short time together. Then the same two control signals as for the first DOF are used to control another DOF (Fig. 2.5). Other clinically available functions such as individually actuated fingers cannot be controlled independently at all. Instead, only pre-defined trajectories and grip patterns have to be selected heuristically, e.g. by manual switching. This control scheme is very cumbersome, time consuming and limits the benefit of additional prostheses functions [Amsuess et al., 2014b].

2.3.2 Classification-Based Approaches

To obtain more advanced control signals, research in the last decades has focused mainly on classification-based approaches. Even if the signals of more than two electrodes are typically not independent, additional information can be obtained by increasing the number of channels. The electrodes are either placed in a targeted way on muscles that are involved in the specific contractions, or equally distributed over the entire region of interest. A classifier is trained to distinguish between different contraction patterns. Typically there are used four to ten electrodes and the features that are required as a clas-

sifier input are extracted from the filtered EMG-signals in a block-wise manner. Reviews on classification-based approaches are provided by [Zecca et al., 2002, Parker et al., 2006, Oskoei and Hu, 2007, Scheme and Englehart, 2011, Peerdeman et al., 2011]. A wide range of feature ensembles and classifiers has been investigated extensively. The explored features include simple time-domain features [Hudgins et al., 1993], such as the mean absolute value (MAV), variance (VAR), root mean square (RMS), number of zero crossings (ZC), number of slope sign changes (SSC) and wavelength (WL) and time-frequency sensitive features based on short-time Fourier transformation [Hannaford and Lehman, 1986], wavelet transformation [Englehart et al., 2001], wavelet packed transformation [Chu et al., 2006] and auto regressive [Graupe and Cline, 1975] models.

Proposed classifiers for myoelectric control include among others linear discriminant analysis (LDA) [Englehart and Hudgins, 2003], multi-layer perceptrons (MLPs) [Kelly et al., 1990], Gaussian mixture models [Huang et al., 2005, Castellini and van der Smagt, 2009], and support vector machines [Castellini et al., 2009]. Promising results have been achieved to classify dynamic muscle contractions with time-frequency-based features offline, but this scheme turned out to be unpractical in a real-time application. Returning to a rest-state between two contractions was needed and made the system again slow and cumbersome. Instead, a scheme with instantaneous classification of steady-state contractions was shown to be much more effective [Englehart and Hudgins, 2003].

Dimensionality reduction with principal component analysis (PCA) was suggested, to reduce the effect of overfitting, when limited amount of training data is available and feature ensembles lead to high dimensional feature spaces. In chapter 3 regularization of the classifier will be introduced as an alternative to handle high-dimensional feature-sets in myoelectric control. After a lot of effort has been put into the development and application of various features and classifiers, it became evident that a simple time-domain feature-set proposed by Hudgins [Hudgins et al., 1993] (MAV, ZC, SSC, WL) in combination with an LDA classifier performs equally well or better than other, less efficient methods [Englehart and Hudgins, 2003].

Classification rates above 90% have been reported consistently in multiclass tasks with eight and more classes for able-bodied subjects. But despite several decades of research and increasing classification performances, none of the approaches have influenced clinical practice so far.

The main reason for this limited transfer from research into clinical application is the lack of reliability of many approaches under real-world conditions [Almström et al., 1981, Lorrain et al., 2011, Jiang et al., 2012a, Farina et al., 2014]. Many studies that reported very high performance investigated only static contraction patterns with gelled electrodes under laboratory conditions and with fixed arm-position from single session recordings [Zecca et al., 2002, Oskoei and Hu, 2007]. The high performance levels obtained with the applied techniques often drop when natural variations in the EMG patterns and noise-sources that are typical for real-world conditions are introduced [Amsuss et al., 2013, He et al., 2015, Vidovic et al., 2015]. These non-stationarities [von Bünau et al.,

2009, Samek et al., 2012] may be caused by changed electrode impedances due to sweat or dry skin [Jiang et al., 2012a], altered arm position [Fougner et al., 2011, Radmand et al., 2014], mechanical load due to the weight of the prosthesis [Cipriani et al., 2011b, Roy et al., 2007], small shifts of electrode positioning [Hargrove et al., 2008, Young et al., 2011] or variations in the way the user performs the contractions. To be suitable for a clinical application, a method needs to be sufficiently robust against these factors.

A classifier provides only an estimation which movement is executed but not the level of contraction that is needed to control the velocity or grip force of a prosthesis. To obtain a proportional control, which is clinically important, the discrete signals of the classifier output can be combined with a force-estimate [Castellini and van der Smagt, 2009] that is typically achieved the averaged amplitude of all EMG channels [Jiang et al., 2012a]. For each class a specific scaling factor is applied to compensate for the fact that some movements are associated with significantly larger or more superficial muscles, which cause larger EMG amplitudes [Scheme et al., 2014]. Problematic with this approach is that variations in the force-level can degrade the classification accuracy [Al-Timemy et al., 2013]. It can have dramatic consequences when a contraction with strong EMG amplitude is misclassified as a class corresponding to smaller amplitudes. As the wrong scaling factor is applied, there can occur a false movement at a very high speed. This extended classification scheme provides direct access to all functions of the prosthesis, but does not allow for a simultaneous control of several DOFs. Thus, complex tasks still have to be split into several subtasks which have to be executed sequentially. Even classification-based approaches with combined classes [Young et al., 2013] do not provide independent control of multiple DOFs because the speed of each DOF cannot be controlled independently. Instead, combined movements are activated in fixed ratios only. For example, it is not possible to slowly open or close the hand while rotating the wrist at medium speed. Also smooth transitions from one movement to another that are required for a natural appearance are not possible.

2.3.3 Regression-Based Approaches

Contrary to classification, regressors do not decide for certain classes but estimate instead continuous multivariate outputs comprising all DOFs simultaneously [Fougner et al., 2012]. This allows for an *independent* simultaneous and proportional estimation and can facilitate a fluent and natural control, given an accurate estimation. The lack of such natural control is indeed one of the main limitations of the classification-based control approach [Jiang et al., 2012a].

One benefit in regression-based approaches is the possibility of intuitive correction by the user, when real-time feedback is provided. Since also small changes in the EMG-signals lead to a directed change in the control output, the user gets immediate feedback and may intuitively correct his contraction patterns. A recent real-time study based on regression control demonstrated a relatively high robustness against variations in arm

position [Hwang et al., 2014b].

To train a regressor, typically EMG data with known activation profiles (data labels) are required. [Jiang et al., 2009] and [Nielsen et al., 2011] measured the torques or forces of all related DOFs to obtain these labels. [Muceli and Farina, 2012] and [Jiang et al., 2012b] have shown that it is also possible to use joint-angles instead of forces for training. A direct comparison of these strategies is provided in [Ameri et al., 2014c].

A major challenge for regression methods in myoelectric control is to obtain accurate training labels in the absence of a limb. For unilateral amputees who represent the majority of the hand prostheses users, a supervised training is possible with a bilateral training strategy. The subjects perform bilateral mirrored contractions and the regressor is trained with forces or kinematics measured at the contra-lateral side. Another strategy that can be applied also for bilateral amputees is to use visual cues instead of measured kinematics or forces [Ameri et al., 2014b].

A few studies explored the possibility to use linear mappings for the regression [Jiang et al., 2009, Ziai and Menon, 2011], but mostly multilayer perceptrons (MLPs) were applied [Nielsen et al., 2011, Muceli and Farina, 2012, Jiang et al., 2012b, Ameri et al., 2014c]. [Ameri et al., 2014a] investigated recently also kernel methods for regression-based myoelectric control. In this thesis, the relationship between EMG-features and wrist angles, measured by a motion tracking system will be investigated in more detail and several linear and non-linear regression techniques will be compared under practical relevant conditions.
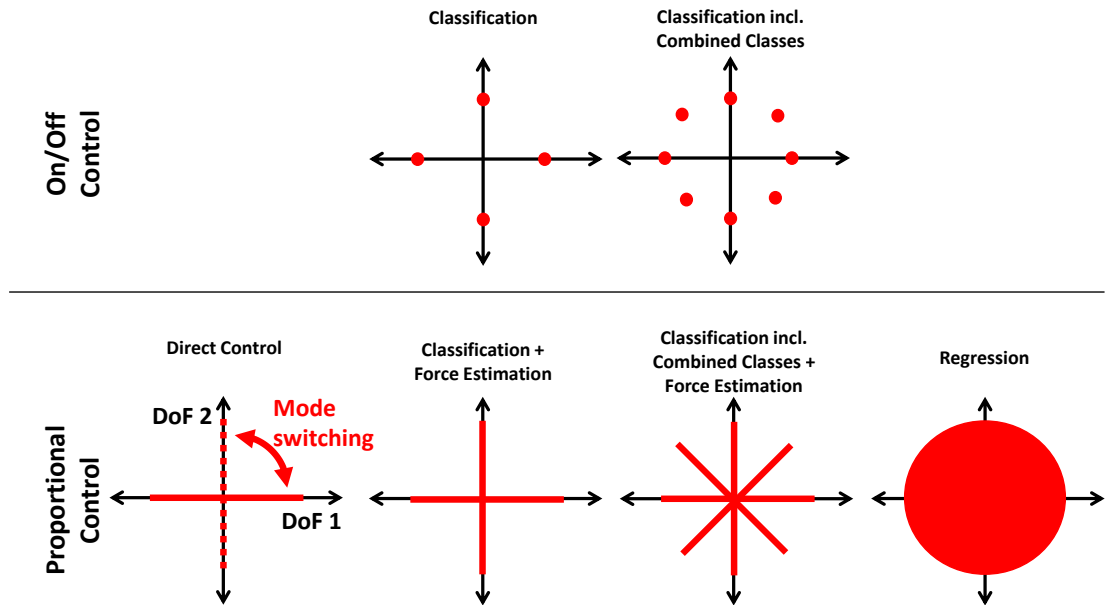
Figure 2.6: Comparison of the possible range of motion for different control strategies (illustrated for two DOFs): The industrial state of the art "direct control" allows for proportional control but is limited to one DOF at a time. Pure classification-based approaches allow for directly accessing several functions but still require a sequential execution of the movements. A proportional control can be added by an additional signal path for force-estimation and including combined classes allows for actuating more than one function at the same time. However, as simultaneous classes can be activated in a fixed ratio only, the range of possible motions is still limited. A fully independent and proportional control of several DOFs is possible with regression-based approaches.

3 Spatial Filters for Robust Classification

3.1 Introduction

The amplitude of myoelectric potentials measured on the skin does typically not exceed a few millivolts, which is relatively low compared to electromagnetic interferences and other noise-sources that can be several magnitudes larger. To extract the desired EMG signals, the signal to noise ratio (SNR) can be increased by temporal and spatial filtering. For removing DC offsets, motion artifacts, power-line interferences and noise outside the EMG frequency-band, temporal filters are applied. The idea of spatial filters is to combine multiple channels with the goal to enhance certain signal characteristics. If $\boldsymbol{x}(t)$ is a vector with D_X EMG-signals at time instance t, a linear, instantaneous spatial filter can be achieved by a simple vector multiplication:

$$s(t) = \boldsymbol{w}^\top \boldsymbol{x}(t) \tag{3.1}$$

The output of the filter $s(t)$ is called a *component* and the filter properties are determined by the *weight-vector* $\boldsymbol{w}$.

A bipolar derivation is used for clinically available myoelectric controllers and also in most research studies [Zecca et al., 2002, Oskoei and Hu, 2007]. This can be seen as a very simple spatial filter with the coefficients $\boldsymbol{w} = [\ 1 \quad -1\ ]^\top$, i.e. the potentials of two electrodes are subtracted. Since the interfering signals are usually very similar in adjacent regions, most of the noise cancels out while the locally varying EMG is enhanced if the electrodes are located properly. Other static spatial filters that involve more electrodes such as Laplacians, have been applied in EMG-research [Disselhorst-Klug et al., 1997, Merletti et al., 2009, Farina et al., 2003]. In this chapter a class of spatial filters is investigated that not only increases the signal to noise ratio, but is optimized to directly enhance information that is relevant for the classification task.

In the context of brain computer interfaces (BCI, [Vidal, 1973, Dornhege et al., 2007, Wolpaw and Wolpaw, 2012]) the performance of motor-imaginary movement classification was significantly improved by using subject specific spatial filters on the electroencephalography (EEG) signals. The filter weights $\boldsymbol{w}$ were optimized based on subject specific training data. In particular, Common Spatial Patterns (CSP, [Ramoser et al., 2000]) have shown to be very powerful for binary classification problems [Blankertz et al., 2008]. Also multiclass CSP has been suggested [Dornhege et al., 2004].

In the following sections, several multiclass extensions of CSP will be presented and applied to high dimensional EMG data of ten able-bodied subjects. In a classification task
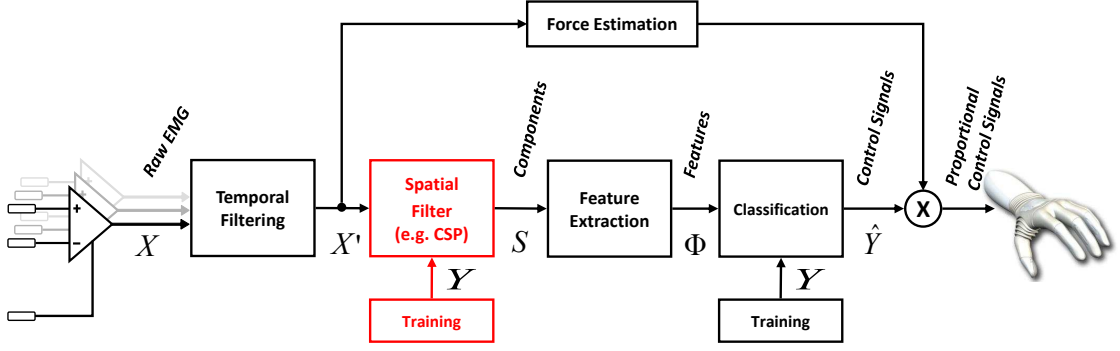
Figure 3.1: Typical signal processing chain for a classification-based myoelectric control system with added spatial filtering step. Both, the classifier and the spatial filter are trained in a supervised fashion. As the classifier estimates only the type of movement but not the force, an additional processing path is used to enable proportional control.

with six hand and wrist movements, the algorithms are compared to a classical pattern recognition approach in terms of classification accuracy and robustness. The trained filter coefficients give access to patterns that are physiological interpretable.

This chapter is based on prior publication in [Hahne et al., 2012a].

3.2 Common Spatial Patterns (CSP)

CSP is a supervised algorithm to obtain linear spatial filters that maximize the variance of one class and at the same time minimize the variance of a second class. Given that the information is coded in the variance, the classes become maximally separated. Thus, extracting features from the CSP-components instead of the EMG channels simplifies the task for the classifier. As the variance of the EMG increases with increasing muscle force and carries therefore the most important information, it is expected that CSP can improve classification-based myoelectric control.

Let $\boldsymbol{X_c} \in \mathbb{R}^{D_X \times N_{X_c}}$ denote a matrix which contains the multivariate EMG signals $\boldsymbol{x}(t)$ for N_{X_c} time instances during contractions of class c. With $\boldsymbol{\Sigma_c} = \frac{1}{N_{X_c}-1}\boldsymbol{X_c}\boldsymbol{X_c}^\top$ being the empirical covariance matrix of $\boldsymbol{X_c}$, the variance of the filter-output $s(t)$ is given by $\boldsymbol{w}^\top \boldsymbol{\Sigma_c} \boldsymbol{w}$ and the optimization problem can be formulated as:

$$\boldsymbol{w} = \arg\max_{\boldsymbol{w}} \frac{\boldsymbol{w}^\top \boldsymbol{\Sigma_1} \boldsymbol{w}}{\boldsymbol{w}^\top \boldsymbol{\Sigma_2} \boldsymbol{w}} \tag{3.2}$$

In many cases more than one filter is desired. One could repeat the optimization procedure iteratively with the additional constraint that the new filters are orthogonal to all
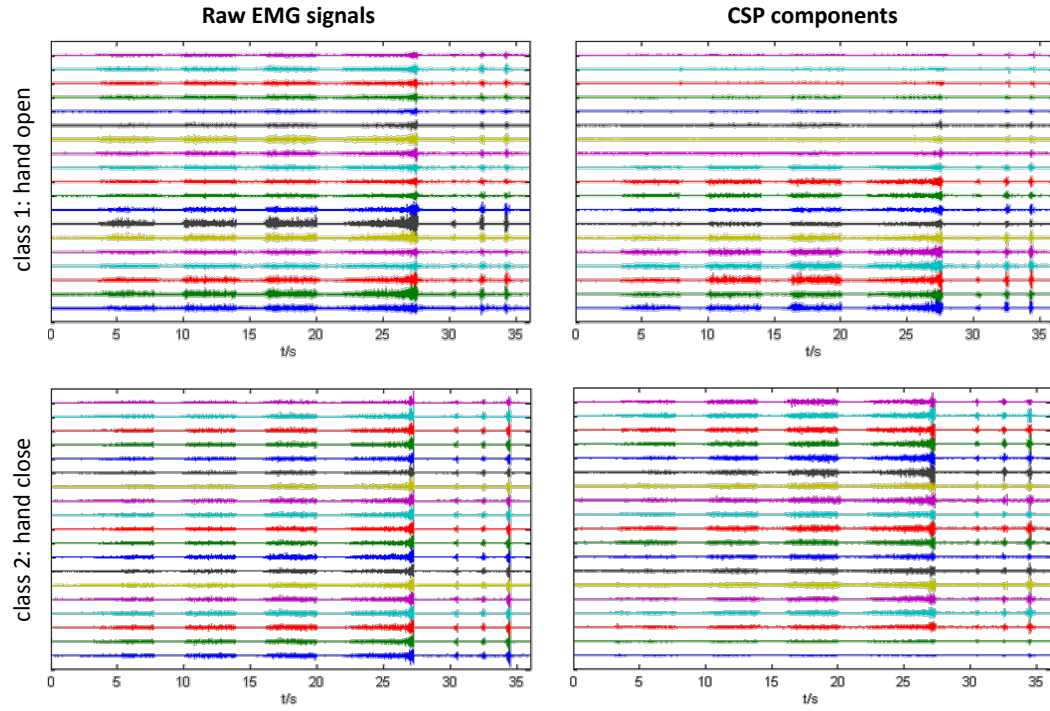
Figure 3.2: Demonstration of the CSP algorithm for 2-class EMG data. The left panels show raw EMG data and the right panels the corresponding CSP components for the movements *hand open* and *hand close*. While the variances of the raw signals are relative similar, they become clearly separated after transformation into CSP components.

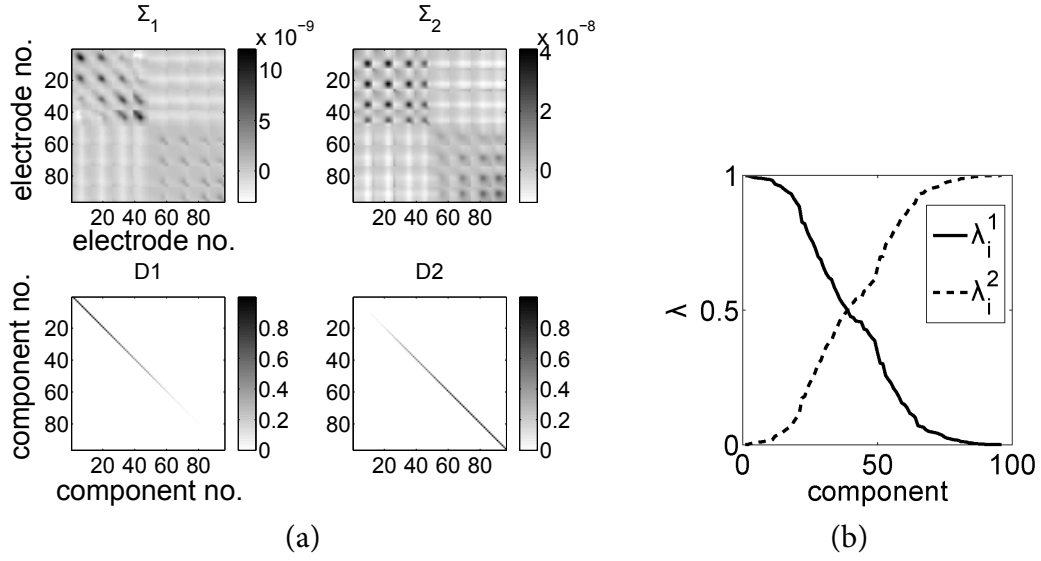previously defined filters. By this procedure D_X orthogonal weight vectors $\boldsymbol{w}_i$ could be obtained.

Figure 3.3: Simultaneous diagonalization of the covariance matrices for two classes with CSP: (a) Visualization of the covariance matrices Σ_1, Σ_2 and the diagonal matrices D_1 and D_2. (b) Eigenvalue spectra, extracted from the principal diagonals. The variances of the uncorrelated components S sum up to one and differ maximally in the first and last dimensions.

A direct solution for a full filter matrix with rank D_X is provided by solving the generalized eigenvalue problem $\Sigma_1 w = \lambda \Sigma_2 w$, i.e. finding the matrix W that diagonalizes both Σ_1 and Σ_2:

$$W \Sigma_1 W^\top = D_1 \qquad (3.3a)$$

$$W \Sigma_2 W^\top = D_2 \qquad (3.3b)$$

$$D_1 + D_2 = I \qquad (3.4)$$

$W \in \mathbb{R}^{D_X \times D_X}$ contains D_X spatial filters as row vectors. Applying W to the raw signals would give D_X components $S = W * X$. The variances of all components for inputs of class 1 are indicated by the corresponding eigenvalues λ_i^1 that form the principal diagonal of D_1. Similarly, the eigenvalues λ_i^2 in D_2 represent the variances for input signals of class 2. As indicated by (3.4), the eigenvalues λ_i^1 and λ_i^2 sum up to one for all components. Thus, choosing a component with high variance for one class has a low variance for the other.

Note that if both the temporal and the spatial filters are linear, the order of these processing steps can be exchanged which reduces computational load, if the number of spatial components D_S is smaller than the number of input channels D_X.

An example of covariance matrices for EMG signals of two classes, the corresponding diagonal matrices $\boldsymbol{D_1}$ and $\boldsymbol{D_2}$ and the eigenvalue spectra is shown in figure 3.3. The block structure of the covariance matrices is caused by the row wise positioning of the channels within electrode arrays.

Since the filters in $\boldsymbol{W}$ are sorted in a way that the eigenvalues in $\boldsymbol{D_1}$ are in descending order, the first and the last components have the best separation properties. However, when dealing with real biosignals, often more components are selected to increase the robustness [Blankertz et al., 2008]. This will be explored in more detail for a myoelectric control task in the experimental section 3.4.

3.3 Multiclass CSP

Although the classical CSP approach is limited to two classes, there are several options to extend CSP to more classes. One way is to combine several binary CSP filters in an one vs. rest or an one vs. one combination scheme. Another approach is to extend the optimization problem to a simultaneous diagonalization of more than two covariance matrices [Dornhege et al., 2004]. These extensions are introduced in the following sections.

3.3.1 One vs. Rest

In the one vs. rest (OvR) approach each filter is optimized to maximize the variance of the corresponding class and minimize the sum (or average) of the variances of all other classes:

$$\boldsymbol{w_c} = \arg\max_{\boldsymbol{w}} \frac{\boldsymbol{w_c}^\top \boldsymbol{\Sigma_c} \boldsymbol{w_c}}{\boldsymbol{w_c}^\top \left(\sum_{i \neq c} \boldsymbol{\Sigma_i} \right) \boldsymbol{w_c}} \tag{3.5}$$

This can be achieved by solving the generalized eigenvalue problem with $\boldsymbol{\Sigma_1} = \boldsymbol{\Sigma_c}$ and $\boldsymbol{\Sigma_2} = \sum_{i \neq c} \boldsymbol{\Sigma_i}$ for each class c. Only the filters with highest eigenvalues in $\boldsymbol{D_1}$ are selected, as the components that maximize the rest are of no interest. This is repeated for each class. The features of all selected components are concatenated and classified by a multiclass classifier.

In the OvR extension, the number of components is growing linearly with the number of classes. Since only the average of the other classes is minimized, there is no guarantee that each individual counter class results in a low variance output. Thus, the filters might be suboptimal in terms of separating properties.

3.3.2 One vs. One

In the one vs. one (OvO) approach the binary CSP algorithm is applied for all possible class combinations. The filters are chosen in the same way as in the binary case for each combination. The components have optimal separation properties for the classes belonging to each combination, but the response for unrelated classes is not determined. In this approach the number of filters grows quadratically with the number of classes. The number of combinations is $N_{comb} = (N_c^2 - N_c)/2$. Depending on the number of classes N_c and the number of components selected for each combination, this can result in a very large number of components and a high dimensional feature space. Given the limited amount of training data this can cause overfitting problems in the classification task that have to be compensated by regularization techniques. In the present approach, the features of all components are concatenated into one feature vector and applied to a multiclass classifier. An alternative would be to apply for each class combination a parallel classifier and combine the classification outputs. But in a pilot study this led to worse results than concatenating features of all combinations and is therefore not applied here. Nevertheless, this approach might be interesting to increase the robustness against false activations in a real-world scenario (see also [Scheme et al., 2011]).

3.3.3 Joint Diagonalization

Another approach is the simultaneous diagonalization of more than two covariance matrices, i.e. to optimize a filter matrix $\boldsymbol{W}$ that diagonalizes the covariance matrices of all classes:

$$\boldsymbol{W}\boldsymbol{\Sigma_c}\boldsymbol{W}^\top = \boldsymbol{D_c} \; ; \; c = 1...N_c \tag{3.6}$$

$$\sum_c \boldsymbol{D_c} = \boldsymbol{I} \tag{3.7}$$

Contrary to the two class case, the solution can be only approximated. Here the *ffdiag* algorithm described in [Ziehe et al., 2004] is used. Figure 3.4(a) shows an example of the approximated diagonal matrices for the six class problem described below for one representative subject. The standard error in the off-diagonal elements was always smaller than 5×10^{-3}, indicating a successful approximation.

The elements of the principal diagonals of D_c form the eigenvalue spectrum for class c. As in the binary case the eigenvalue λ_i^c indicates the variance (or power) of component i for signals of class c.

Selecting good components for classification is not as straight forward as in the binary case, where the component with the highest eigenvalue for one class has automatically the lowest eigenvalue for the other class. [Dornhege et al., 2004] compared different strategies in a BCI context. In this work the best results were obtained by simply adding for each

class the components with highest eigenvalues λ_i^c. If a component would be selected twice, the component with the next highest eigenvalue λ_j^c is selected for the class with lower eigenvalue λ_i^c. The eigenvalue spectra for an representative example are shown in figure 3.4(b). If λ_i^c is close to 1 for one class and very low for all other classes, this component has good separation properties. In the given example this is the case for some of the classes (e.g. component 75 for class 5). In other cases (e.g. class 1) the highest λ_i^c is much lower than 1 and the corresponding component will also capture power for other classes. The first components that are selected for each class are marked by vertical lines.
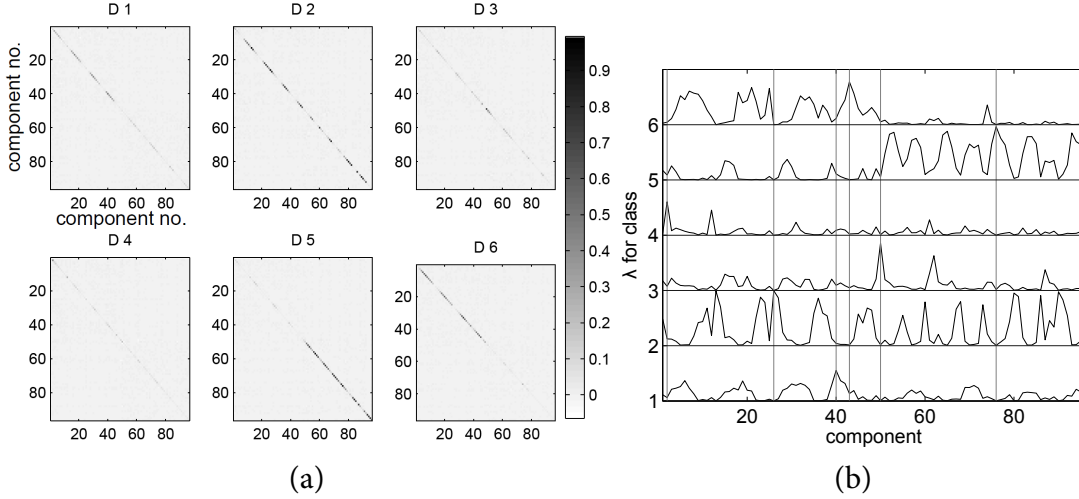

(a) (b)

Figure 3.4: Example of simultaneous joint diagonalization for a 6 class problem. (a): Diagonal matrices D_1 to D_6. Since the solution is only an approximation, the off-diagonal elements are very small but not exactly zero. (b): Eigenvalue spectra for all classes. As in the two class CSP algorithm, the eigenvalues of all classes sum up to one, but selecting components is not as straight forward. The gray lines indicate heuristically selected components for that the spectra strongly differ for different classes.

3.4 Experiments

3.4.1 Setup and Paradigm

For this study, 96 monopolar EMG signals were recorded from the non-dominant forearms of 10 able bodied subjects, five females and five males. "Brain Amp DC" biosignal amplifiers were used with a sampling frequency of 2500 Hz and two Ag/AgCl electrode arrays with an inter electrode distance of 8 mm (OT-Bioelettronica ELSCH064R3S). The arrays were placed on the forearm, at approximately one third of the distance from the

Figure 3.5: High density EMG electrode arrays mounted on the forearm of an able-bodied subject.

elbow to the wrist (Fig. 3.5). For a reproducible electrode placement in tangential direction, the location of the ulna was used as a reference position, which was identified by palpation. The approximate position of the electrodes relative to the forearm muscles is shown in figure 3.9.

The subjects were instructed to perform six different classes of hand movements (hand open, hand close, pronation, supination, wrist flexion, wrist extension) in five different arm positions (arm down, half lifted, extended to the front, in front of the body, in front of the face). A visual feedback was provided of the root mean square (200 ms moving window), averaged over all channels and scaled to maximum voluntary contraction (MVC) for each class. To adapt the scaling, the subjects performed an MVC for each class-position-combination in the beginning of the session.

Each trial was formed by a contraction of three seconds with approximately 40 % force. The trials were recorded in several runs, where each run contained each class-position-combination exactly once. In between two trials was a break of 4 seconds, in which the subject had to change the arm position. The order of trials within each run was randomized in class and position. When the subject or the experimenter noticed a failure (e.g. wrong or delayed contraction, wrong arm position) in the execution of a trial, it was marked during the experiment and not used in the evaluation of this study. The number of removed trials was very low for all subjects (0 to 0.83 % of trials, average $0.41\% \pm 0.28\%$). After each run the subject was allowed to have a break and relax for some minutes. Each subject performed 25 to 35 runs. In this way, 750 to 1050 trials were obtained from each subject. This is enough independent data for a proper statistical evaluation. For this study, only the static part of the contractions is used, i.e. the beginning and end of each contraction were removed. All signals were filtered with a highpass (500 Hz, 4th order Butterworth), a low pass (20 Hz, 4th order Butterworth) and a band stop filter (45 - 55 Hz, 2nd order Butterworth) to remove noise, movement artifacts and power-
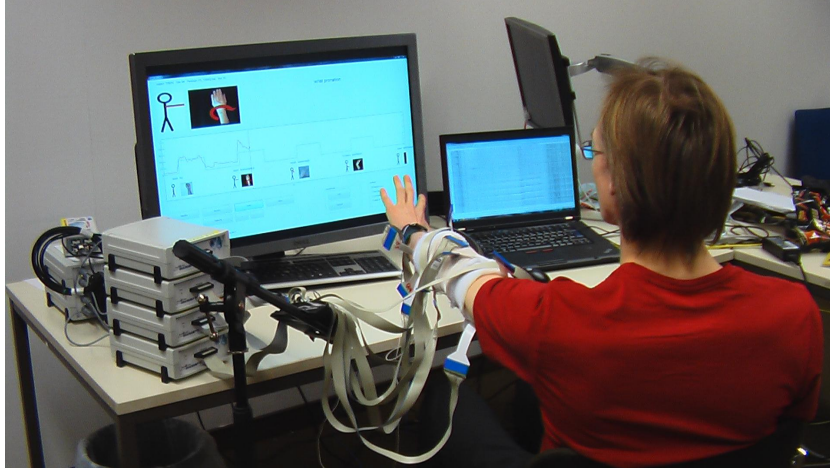
Figure 3.6: Data recording during the execution of the experimental paradigm. The subject is visually instructed to execute a certain contraction in a defined arm-position. To ensure stable contraction levels and minimal subject-related delays in the execution of the commands, the mean EMG amplitude across channels is provided as a real-time feedback. The subject follows pre-defined profiles with the feedback curve.

line interferences. The experiments are in accordance with the Declaration of Helsinki and approved by the local ethics commission (Ethikkommison Charité Berlin, approval number EA4/085/11).

3.4.2 Feature Extraction

In this study the features were extracted from overlapping blocks of 200 ms, with an increment of 50 ms. This scheme was chosen in order to fulfill the time constraints that would arise in a real-time application [Smith et al., 2011]. Longer window sizes would increase the classification accuracy, but cause also larger delays which reduces the usability of an online control system. The choice of 200 ms window length is a good compromise in this trade-off [Farrell and Weir, 2007].

To capture the discriminative information of the CSP-components, variance-sensitive features should be extracted. Instead of directly using the block-wise computed empirical variance, LOG-VAR features (eq. 3.8) are applied. The logarithm causes a compression of the value range which results in a feature distribution closer to Gaussian that is beneficial for the following classification step using Fischer LDA:

$$\boldsymbol{\phi}(t) = log\left[\frac{1}{N-1}\sum_{i \in \boldsymbol{b}_t} \boldsymbol{s}(i)^2\right] \tag{3.8}$$

where $\boldsymbol{b}_t$ contains the N (raw-data) sample-indices of block t.

3.4.3 Baseline Method

In order to compare the performance of the proposed algorithms, a commonly used method was implemented to obtain a baseline performance. A set of bipolar signals was derived by a couple-wise subtracting of monopolar channels with inter-electrode distance (IED) of 16 mm and aligned with the direction of the muscle fibers. From the bipolar signals the Hudgins feature set (mean absolute value, zero crossing, slope sign changes and wavelength, [Hudgins et al., 1993]) was extracted in the same scheme as for the other methods described in section 3.4.2. Englehart and Hudgins found that for steady-state EMG signals these rather simple features in combination with linear discriminant analysis outperform many other, more complex methods [Englehart and Hudgins, 2003]. This scheme was used in many other studies [Peerdeman et al., 2011].

3.4.4 Classification Scheme

For both classification of features extracted from CSP components and in BCI [Blankertz et al., 2008] and of the Hudgins feature set in myoelectric control, Fisher linear discriminant analysis (LDA) has been proposed. This is the optimal Bayes classifier for data that is Gaussian distributed and has the same covariances for all classes in feature space.

Each to be classified feature vector ϕ is assigned to that class c with highest probability regarding the following equations:

$$\hat{y} = \arg \max_c \delta_c(\phi) \tag{3.9}$$

$$\delta_c(\phi) = \phi^\top \Sigma^{-1} \mu_c - \frac{1}{2} \mu_c^\top \Sigma^{-1} \mu_c + log(p_c) \tag{3.10}$$

Where $\mu_c = \frac{1}{N_c} \sum \phi_c$ is the empirical mean calculated from training samples of class c and $\Sigma = \frac{1}{C} \sum_{c=1}^{C} \Sigma_c$ is the pooled feature covariance matrix. The a-priori-probability p_c is assumed to be equal for all classes: $p_c = \frac{1}{C}$.

Even if the assumption of equal covariance matrices for all classes is often violated for EMG data-sets, it was found that multiclass-LDA performs equally well as other, more complex classifiers [Englehart and Hudgins, 2003]. Also in a pilot analysis for this study quadratic discriminant analysis (QDA), which considers the individual covariances of all classes did not perform better than LDA. Since the dimensionality of the feature space can become relatively large depending on the number of selected components and the type of CSP multiclass extension, the robustness of the empirical covariance estimation can become problematic due to the limited amount of available training data. Therefore, a shrinkage regularized version of LDA was applied in which the pooled covariance matrix was replaced by a regularized version with decreased off-diagonal elements [Blankertz et al., 2011]. The regularization parameter was automatically selected solely based on the training set as proposed by [Ledoit and Wolf, 2004]. All arm positions were included in

both training and test sets. For extensive investigations on training strategies for position robust control with reduced amount of training data see [Fougner et al., 2011].

For a practical application as the control of hand prostheses, it is not suitable to use too many channels. The power consumption and the production costs would be too high for a clinical application. Therefore, the classification performance was investigated with a reduced set of 22 channels, located in two rows with a distance of 16 mm. Within each row the channels were equally spaced and formed a ring around the forearm. All classification results were obtained from the reduced channel set. For the derivation in the baseline method, the bipolar couples were formed by opposite channels of both rows.

3.4.5 Cross-validation Results

(a)   (b)
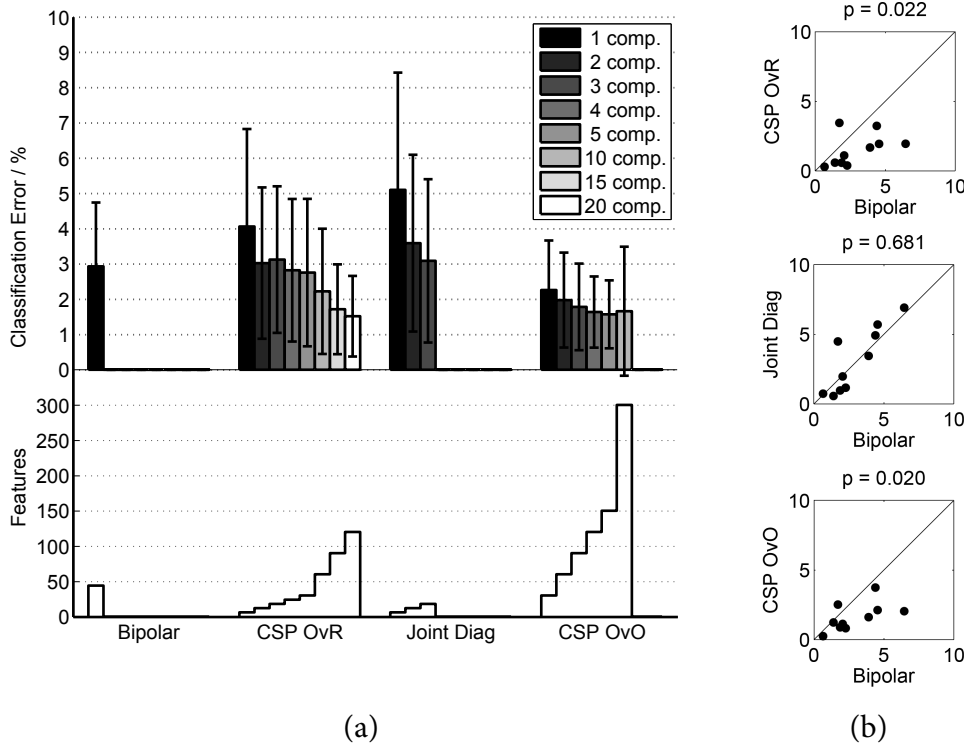
Figure 3.7: Cross-validation results for a six-class classification task. (a): Classification error for the baseline method and all investigated CSP-extensions (mean and standard-deviation across subjects). The gray-level indicates the number of components used per combination and the curve bellow the total number of components that corresponds to the dimensionality in feature-space. (b): Direct comparison of the classification errors with the baseline method *bipolar* for each subject and p-values for t-test

The cross-validation error is reported for all CSP extensions and various numbers of components (Fig. 3.7). Choosing more components within each of the proposed CSP extensions generally improved the performance. Even when the total number of components became larger than the number of raw signals, the performance increased further. If a sufficiently high number of components was selected, *CSP OvR* and *CSP OvO* perform better than the reference method *Bipolar*. Both extensions had approximately the same error rates for the same number of total components. The error increased again slightly, for the highest number of investigated components at *CSP OvO*. This might be caused by overfitting, due to the high dimensional feature space and the limited amount of available training data. For *Joint Diagonalization*, it is not possible to select more components than raw signals. With the highest choice of three components per class this method did not perform better than the baseline method.

In figure 3.7(b), all CSP methods are directly compared with the reference method *bipolar* for each subject individually. For each method only a fixed number of components is shown. The total number of components was 18 in case of *Joint Diagonalization* (3 components × 6 classes), 120 for *CSP OvR* (20 components × 6 combinations) and 120 for *CSP OvO* (8 components × 15 combinations). Above each plot the t-test significance value is shown for that comparison. *CSP OvR* and *CSP OvO* performed better than the baseline method for all but one subject and the differences were significant. *Joint Diagonalization* performed for four subjects better, for four worse and for two similar as the baseline method. There were no significant differences.
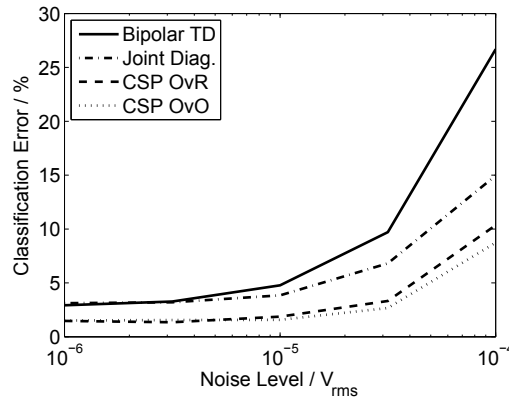
3.4.6 Robustness to Sensor-noise

Figure 3.8: Evaluation of the robustness to artificially added sensor-noise. All CSP multiclass extensions are less affected by the noise than the baseline method without optimized spatial filters.

Due to the low electrode-skin impedances of the wet Ag/AgCl electrodes used in this study and the high-quality biosignal amplifiers (very high input impedance and common mode rejection ratio), the noise level of the signals is very low. For a practical application in prosthetics, dry electrodes are needed, which can increase the noise level significantly depending on the skin conditions. Therefore, the robustness of all methods to an increased noise level is investigated. Uncorrelated white Gaussian noise was added to all monopolar signals (training and test data). The noise was filtered in the same way as the EMG, so only the frequency components within the pass bands of the temporal filters affected the signals. Five different noise-levels are investigated with a post-filter-amplitude of $1 - 100\mu V_{rms}$. This corresponds to the range of noise levels that are common for dry electrodes, depending on the skin conditions and the level of electromagnetic interference.

The degradation of classification error depending on the level of added noise is shown in figure 3.8. The number of components is the same as for the significance tests (totally 120 for *CSP OvO* and *CSP OvR*, 18 for *Joint Diagonalization*). For all methods, the classification error is monotonically increasing with increasing noise level. The increase in error is strongest in the case of bipolar derivation while all CSP extensions are affected less by the decreasing signal quality. *CSP OvR* and *CSP OvO* that performed already best without additional noise show also the lowest error under noisy conditions.

3.4.7 Interpretation of Spatial Filters

Each spatial filter as introduced in equation 3.1 is defined by its weights w and characterizes a linear mapping from sensor space in a component with certain properties — in case of CSP optimal class-separation. An analysis of the learned filter weights w can be useful to understand its behavior and draw conclusions to the underlying physiology. As worked out in [Haufe et al., 2014], a direct spatial interpretation of the filter-coefficients is not meaningful. Sensors with large filter coefficients do not necessarily contain the underlying physiological signal, but may instead provide information about the noise that corrupts other sensors with the signal of interest [Parra et al., 2005]. Instead, the filter weights w, which correspond to a (data-driven) *backward model* to some hidden components can be transferred into a *forward model* a, which is well interpretable:

$$\boldsymbol{x}(t) = \boldsymbol{a}^\top s(t) \tag{3.11}$$

The entries of the activation pattern a_i describe the strength and direction with that the i'th component $s_i(t)$ is represented in each individual channel. This allows for localizing the origin of the component and can give insights into its underlying physiology. In case of CSP, where the full squared filter matrix $\boldsymbol{W} \in \mathbb{R}^{D \times D}$ is available, the transformation from a backward into a forward model is given by the transpose of its inverse: $\boldsymbol{A} = (\boldsymbol{W}^{-1})^\top$.
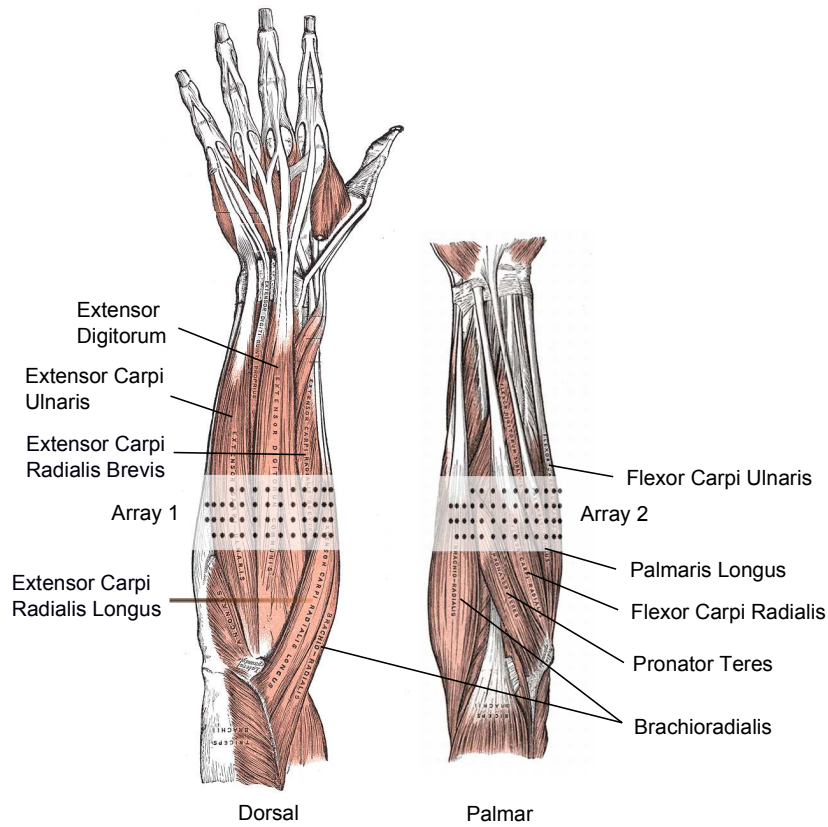
Figure 3.9: Anatomy of the forearm with approximated electrode position (modified from [Gray, 1918]).

In the graphical representations (Fig. 3.11, 3.12 and 3.13) blue represents negative entries of the forward coefficients a, red positive entries and white values close to zero. Each dot corresponds to the position of one sensor and the values in between are obtained by cubic interpolation. The first patterns are of particular interest (for OvO also last patterns), since they show the sources of the most discriminative components. In order to relate the patterns with the underlying muscle activity they are compared with the variance patterns which show the distribution of EMG activity over the arrays (Fig. 3.10). The approximate position of the arrays in relation to the muscles is given in figure 3.9.

Patterns of CSP One vs. Rest and Joint Diagonalization

Since the patterns of *CSP OvR* (Fig. 3.11) and *joint diagonalization* (Fig.3.12) are very similar, they are analyzed together. In some cases the signs are flipped, but this is of less interest, as CSP is invariant with respect to the signs which have no influence on the variances
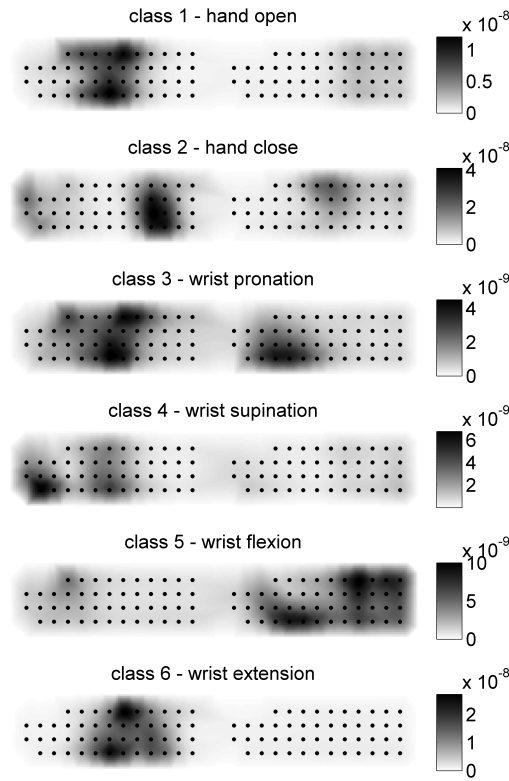
Figure 3.10: Variance patterns of the raw, temporal filtered signals. Since the range of variances is quite different for different classes, each plot is scaled individually. White corresponds to no activity and black to the variance of the strongest channel.

of the corresponding components. The reason for the similarity between the patterns of both methods can be found in the optimization criteria of these two approaches, which are actually not so different. Even if *CSP OvR* does not diagonalize each of the individual covariance matrices of the "rest classes" explicitly, in both methods a component with maximal variance for one class has a minimized sum of variances over all other classes.

Class 1 – Hand Open   The variance pattern shows EMG activity mainly above musculus extensor digitorum, which is responsible for extension of the fingers and wrist. The first three CSP patterns focus in the same region which is physiologically meaningful, as this muscle is responsible for extending the fingers when opening the hand.

Class 2 – Hand Close   The variance pattern shows activity above a wide region including Extensor Carpi Radialis Brevis and Longus, Extensor Carpi Ulnaris and Flexor Carpi Radialis which can be explained by the fact the subject made a fist for that many muscles contract to stabilize wrist and hand. The CSP patterns focus mainly in regions
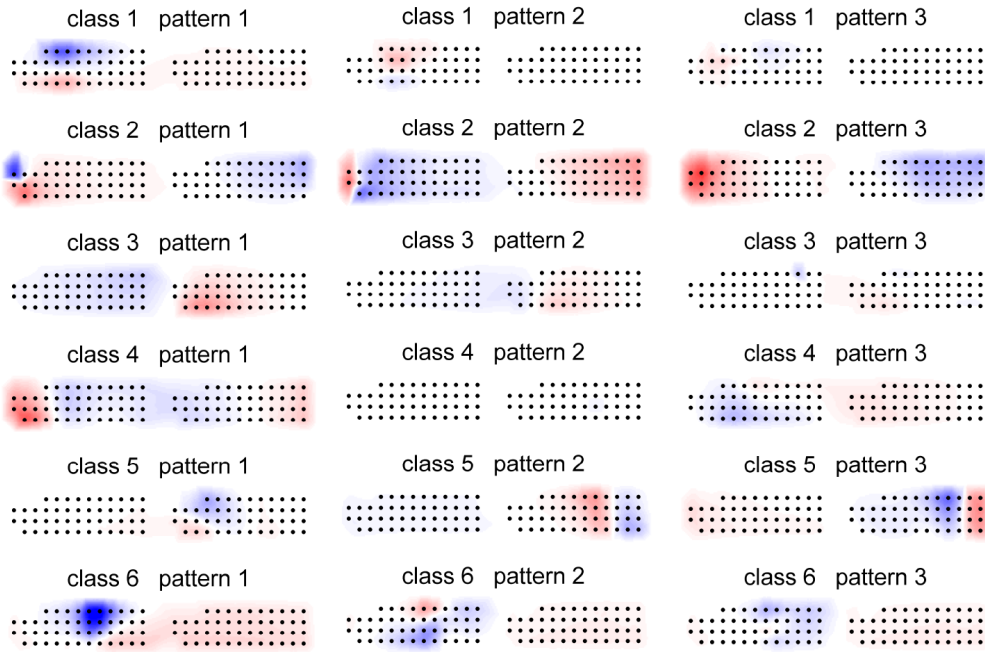
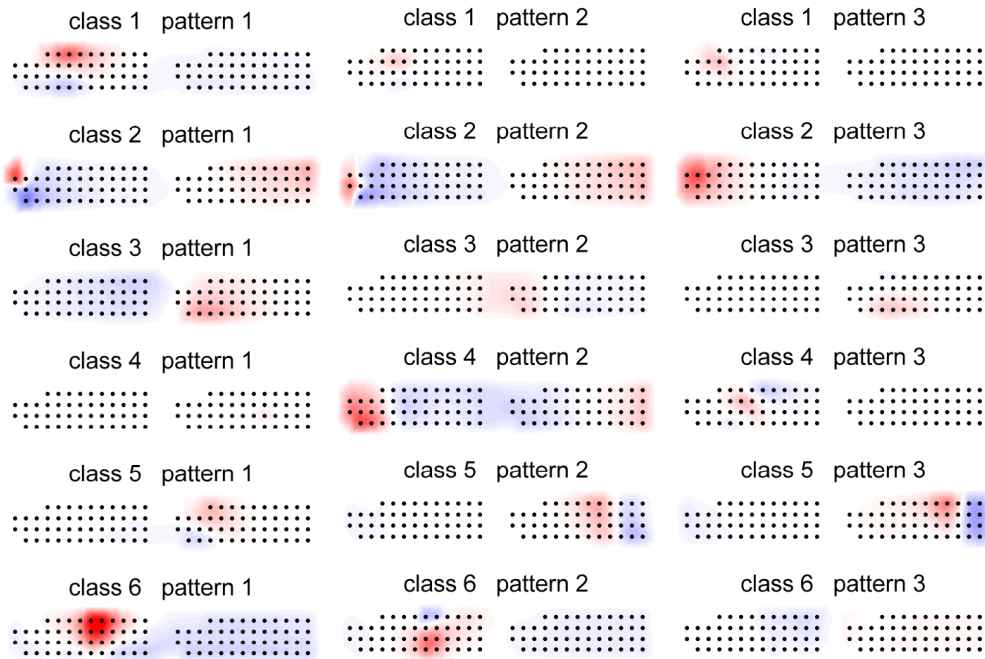Figure 3.11: First three patterns for each class of **CSP one vs. rest**

Figure 3.12: First three patterns for each class of **CSP joint diagonalization**

with moderate variance but interestingly the region with maximal variance above Extensor Carpi Radialis Brevis and Longus is completely left out in the CSP patterns.

Class 3 – Pronation   The variance pattern shows two regions of strong activation. One is located above Pronator Teres, which is the most important muscle for the pronation of the wrist. The second region is located above Extensor Digitorum, which may be co-activated in strong pronations. The CSP patterns focus mainly above a physiologically meaningful area above Pronator Teres but a light and smooth activity above Brachioradialis, Carpi Radialis Longus and Carpi Radialis Brevis is observed. The latter might come from some spillover of Pronator Teres through the other muscles.

Class 4 – Supination   The principal muscle for supination in the region of the electrodes is Musculus Supinator, which is a relatively small and deep muscle, covered by the extensors. For that reason no strong signals can be expected and indeed the variance is quite low, as the scaling of the variance pattern shows. There are two active spots in the region of Extensor Carpi Ulnaris and the left (ulnar) side of Extensor Digitorum. The CSP pattern focus mainly in the same region as the variance pattern but additionally a light contribution over large regions of both arrays is observed. Likely, the algorithm focused on co-activated finger-extensions, which if consistently activated during supination may provide more discriminative information in the surface EMG than the deep Musculus Supinator.

Class 5 – Wrist Flexion   The variance pattern shows activity above Flexor Carpi Radialis and Palmaris Longus which is physiologically meaningful for wrist flexion. Additionally there is activity in the region of Pronator Teres. Either this muscle is co-activated for stabilization, or the activity comes from another muscle like Brachioradialis, which overlaps Pronator Teres partly. The second and third CSP pattern focus only in the anatomical plausible regions of Flexor Carpi Radialis and Palmaris Longus. The other activity above Pronator Teres and Brachioradialis is captured in the first CSP-component. This is an interesting example, which demonstrates that often more than one component per class is needed to capture all relevant information.

Class 6 – Wrist Extension   The variance pattern shows high activity mainly above Extensor Digitorum, similar as for the class hand open. The CSP patterns focus in the same region plus in a second region, above Extensor Carpi Radialis Brevis and Longus, which are also involved in the extension of the wrist.

Summary   For *hand open* and *wrist flexion* the CSP patterns focus in the same regions as the variance patterns. For *pronation*, *supination* and *wrist extension* the CSP-patterns focus partly in the regions with high variance, but additional discriminative regions are

found that are not visible in the variance patterns. For *hand close* the best discriminative regions are found in areas completely distinct from those with highest signal power. This shows that the regions with strongest muscle activity are not necessarily the regions with most discriminative information.

Patterns of CSP One vs. One
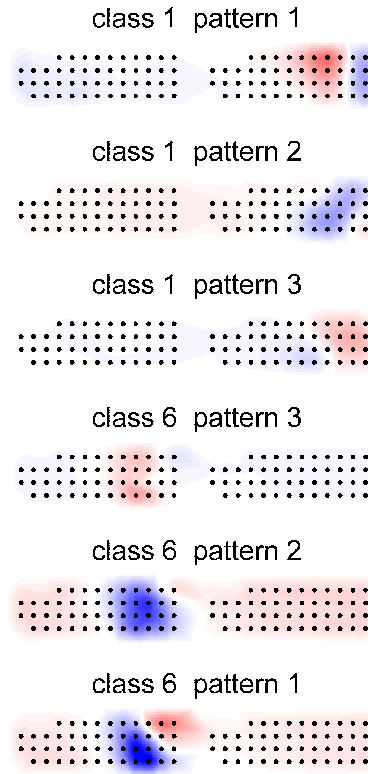
Figure 3.13: Example of CSP patterns of the **one vs. one** extension for the class combination *hand open* and *wrist extension*

Due to the high number of combinations for the *one vs. one* extension only an interesting example is shown, which involves a combination of two classes that corresponds to similar muscle activation, namely *hand open* and *wrist extension*. The similarity is seen in the variance patterns (Fig. 3.10 class one and six), which reveal activity in similar regions, overlapping each other partly. Figure 3.13 shows the first and last three patterns of the CSP filter that separate the chosen classes. The lower three patterns correspond to the components with high output for the class *wrist extension* and focus in a region with high EMG activity for that class. A careful comparison of the CSP patterns with the variance patterns shows that the focus of the CSP patterns is on the very right side

of the region with high variance for that class. In this region the other class *hand open* is less active, since its variance pattern is located slightly more to the left. The upper three patterns correspond to the class *hand open*. They focus in a region on the second array, far beside the region of maximal variance. The region is rather in a location, where *hand open* has moderate activity, while the other class is not active at all. This demonstrates how CSP can extract highly separable components, by utilizing also EMG activity from less active regions, which potentially originates from synergistically activated muscles.

3.5 Discussion

3.5.1 Impact

The results of this analysis show the off-line performance for static contractions, which cannot be put on a level with the performance in a real-world application. But by mixing different arm positions and adding artificial noise, the analysis included two important factors that can degrade the performance in a real-world application. This does not render online-tests in out-of-lab conditions redundant, but it brings the off-line analysis closer to the real-world scenario. It was shown that with a sufficiently high number of CSP-components the classification error can be almost halved compared to the baseline method. Under noisy conditions this significant advantage is even larger. These results indicate that the proposed methods can significantly increase the reliability of a myoelectric control system.

3.5.2 Pattern Interpretation

In contrast to many other methods, CSP allows for a physiological interpretation of the results. EMG signals have a very good SNR and the variance patterns provide already a good overview about the regions with muscle activation for each movement. As one would expect, many CSP patterns focus in regions with high variance. But since the goal of CSP is an optimal separability, the most important patterns do not necessarily coincide with the regions of largest signal amplitude. Instead, other regions with weaker signals, which may be related to smaller, deeper or synergistically activated muscles, are in many cases equally important to distinguish the movements. This is consistent with previous findings on heuristic channel selections [Hahne et al., 2010].

In future work, channel-selection techniques based on the CSP patterns could be developed to efficiently determine good electrode configurations for clinical applications.

3.5.3 Limitations

Even though it was shown that six different contraction patterns could be reliably classified, the study in this chapter has certain limitations. The classification approach does not provide an estimation of the muscle force that could be used to control the velocity or the grip-force when applied in prosthetics. The approach is also limited to a fixed set of pre-defined patterns. Even if additional classes of combined movements could be integrated, more complex movements would still require to be split into different submovements that need to be executed sequentially. Thus, despite the great improvements compared to the current state of the art used in prosthetics, the approach does not allow for natural and fluent movements. Further, this study was done with able-bodied subjects only. It remains to be shown that a sufficient accuracy can be reached for subjects with amputation or congenital limb deficiency who are potential users of the methods. These shortcomings will be addressed in the following chapters.

4 Regression-based Control

4.1 Introduction

To increase the functionality of myoelectric control, research has focused in the past decades mainly on classification-based approaches. Reviews on this development are provided by [Zecca et al., 2002, Oskoei and Hu, 2007, Scheme and Englehart, 2011]. Since a classifier only decides which movement is activated but does not allow for controlling the speed or the force of a prosthesis, classification-based approaches can be combined with a force estimation. Typically the mean amplitude of all EMG channels is used for that. Since this value differs significantly between different types of movements, individual scaling factors for each class are applied, which are obtained by analyzing maximum voluntary contractions. One problem with this approach is that classification errors can lead to very strong false activations, since in case of classification errors also the wrong scaling factor is applied.

In contrast to the clinical state of the art described in section 2.3.1, classification-based approaches allow to directly access all functions of the prosthesis without time-consuming mode-switching. However, since only one function can be activated at a time, complex movement still have to be split into several sub-tasks, which have to be executed sequentially as in the clinical state of the art. Recent efforts have extended the classifiers by combined motion classes [Buerkle et al., 2006, Geng et al., 2012, Young et al., 2013, Ortiz-Catalan et al., 2014]. This allows to activate two functions at the same time, but still limits the diversity of possible movements because the speed of the related DOFs cannot be controlled independently.

Instead, regression techniques can be applied to achieve an *independent* proportional and simultaneous control [Fougner et al., 2012]. The major difference to classification is that a regressor does not decide for a certain class, but instead a continuous (proportional) output value is estimated for each DOF. This can facilitate a very fluent and natural control. Lacking of this natural control is indeed one of the main limitations of the current myoelectric control approach based on classification [Jiang et al., 2012a]. Relative little work has been done on regression in the context of myoelectric control, mostly focusing on multilayer perceptrons (MLPs) [Nielsen et al., 2011, Muceli and Farina, 2012, Jiang et al., 2012b, Ameri et al., 2014c].

The study described in this chapter aims at a comprehensive and systematic comparison of state-of-the-art regression methods for independent proportional and simultaneous myoelectric control of multiple DOFs. Simple linear models are compared with

state-of-the-art non-linear and non-parametric machine learning methods. For a clinical application, a method should require little user training, be computationally efficient and also perform well with few electrodes. Those aspects are addressed as well in the present study by reducing the amount of training data, reducing the number of EMG channels and by evaluating the processing times of the algorithms.

Previous studies on simultaneous myoelectric control explored different feature-sets, such as the variance of the EMG (also denoted as mean square value) [Jiang et al., 2009, Jiang et al., 2012b] or, similarly, the lowpass-filtered, down-sampled squared raw EMG-signal [Muceli et al., 2014] and various time-domain and frequency domain features [Nielsen et al., 2011]. Differences in performance have been reported for different features, but the reasons for these differences where not fully discovered. In this study it is demonstrated that the relationship between the variance of the EMG and the wrist angle is highly non-linear and that simple transformations in feature space can simplify the problem. This allows to use linear methods, which are computationally very efficient. Four linear and non-linear regression techniques, namely linear regression (LR), mixture of linear experts (ME), multilayer perceptrons (MLPs) and kernel ridge regression (KRR) are compared. This provides an evaluation of the potential use of EMG for simultaneous and proportional control and indications on the main factors of influence for regression performance.

This chapter is based on previous publications, in particular [Hahne et al., 2012b], [Hahne et al., 2014a] and [Hahne et al., 2014b].

4.2 Regression Techniques

A regressor predicts continuous target variables $\boldsymbol{y}$ from continuous input features $\boldsymbol{\phi}$. In general both the input and the target variable can be multivariate. It is important to choose a suitable complexity for the regression model to fit the underlying problem. If the complexity is too low, the target variable cannot be approximated properly. If the complexity off the model is too high, there is an increased risk of overfitting to the training-samples. Thus the complexity class should be chosen high enough to model the underlying problem but not larger. To reduce the complexity within one model class, regularization techniques can be applied.

Let $\boldsymbol{\Phi} \in \mathbb{R}^{D_{\boldsymbol{\Phi}} \times N_{\boldsymbol{\Phi}}}$ denote the set of $D_{\boldsymbol{\Phi}}$ dimensional feature vectors for $N_{\boldsymbol{\Phi}}$ time instances (feature-samples), and $\boldsymbol{Y} \in \mathbb{R}^{D_Y \times N_{\boldsymbol{\Phi}}}$ contain the corresponding wrist angles for D_Y DOFs as data labels. The goal of all regression techniques is to find a mapping $\widehat{\boldsymbol{Y}} = f(\boldsymbol{\Phi})$, where $\widehat{\boldsymbol{Y}}$ is an approximation of $\boldsymbol{Y}$.

4.2.1 Linear Regression

In linear regression (LR) [Bishop, 2007] the mapping function is linear:

$$\widehat{\boldsymbol{Y}} = \boldsymbol{W}^\top \boldsymbol{\Phi} + \boldsymbol{w}_0 \tag{4.1}$$

$\boldsymbol{W} \in \mathbb{R}^{D_\Phi \times D_Y}$ contains the weight vectors and $\boldsymbol{w}_0$ the bias that can compensate for possible offsets. By convention $\boldsymbol{w}_0$ can be included in $\boldsymbol{W}$ by extending $\boldsymbol{\Phi}$ by an additional dimension with N_Φ ones. Under the assumption of Gaussian noise, the maximum likelihood solution for $\boldsymbol{W}$ is obtained by minimizing the sum-of-squares error function:

$$E(\boldsymbol{W}) = \frac{1}{2} \sum_{d=1}^{D_Y} (\boldsymbol{y}_d - \boldsymbol{w}_d^\top \boldsymbol{\Phi})^2 \tag{4.2}$$

The solution can be derived easily and is given in a closed form by:

$$\boldsymbol{W} = (\boldsymbol{\Phi}\boldsymbol{\Phi}^\top)^{-1}\boldsymbol{\Phi}\boldsymbol{Y}^\top \tag{4.3}$$

The term $(\boldsymbol{\Phi}\boldsymbol{\Phi}^\top)^{-1}\boldsymbol{\Phi}$ is known as the *Moore-Penrose pseudo-inverse*. Especially when little amount of training data is available, there is a risk of overfitting the model to the training samples, which can be reduced by regularization. The complexity of the model is decreased by penalizing large entries in $\boldsymbol{W}$. This is done by extending the error function with a regularization term that includes a particular norm of $\boldsymbol{W}$ (eq. 4.4). For the L_2 norm large entries are penalized strongly while the model is less impaired for smaller coefficients. In opposition to other norms the solution remains in a closed form and extends to:

$$E_2(\boldsymbol{W}) = \frac{1}{2} \sum_{d=1}^{D_Y} (\boldsymbol{y}_d - \boldsymbol{w}_d^\top \boldsymbol{\Phi})^2 + \frac{1}{2}\lambda \sum_{d=1}^{D_Y} \boldsymbol{w}_d^2 \tag{4.4}$$

$$\boldsymbol{W} = (\boldsymbol{\Phi}\boldsymbol{\Phi}^\top + \lambda\boldsymbol{I})^{-1}\boldsymbol{\Phi}\boldsymbol{Y}^\top \tag{4.5}$$

$\boldsymbol{I}$ is the identity matrix and the regularization constant λ can be determined using grid-search techniques in a nested cross-validation. Note that other norms can be used for different regularization goals. E.g. the L_1 norm leads to sparse solutions and can thus be used for feature or channel selection [Hwang et al., 2014a].

4.2.2 Mixture of Linear Experts (ME)

In LR each column vector $\boldsymbol{w}_d$ of $\boldsymbol{W}$ is responsible for the mapping from $\boldsymbol{\Phi}$ to one DOF in $\hat{\boldsymbol{Y}}$. This means that in LR the same coefficients are used for both antagonistic wrist movements (positive and negative labels of the same DOF), which is physiologically not reasonable, since the antagonistic movements involve different muscles.

Therefore, an extension of LR is proposed, which uses two different weight vectors, $\boldsymbol{w}_{d+}$ and $\boldsymbol{w}_{d-}$, for each DOF d that are individually trained using only time intervals with positive or negative labels, respectively. The outputs of both filters are combined smoothly according to the probability to which direction the current feature sample belongs to, estimated by logistic regression [Parra et al., 2005, Bishop, 2007]:

$$\hat{y}(t) = \begin{bmatrix} \boldsymbol{w}_+ \\ \boldsymbol{w}_- \end{bmatrix}^\top \begin{bmatrix} \boldsymbol{\phi}(t) \; p(c = 1|\boldsymbol{\phi}(t)) \\ \boldsymbol{\phi}(t) \; p(c = -1|\boldsymbol{\phi}(t)) \end{bmatrix} \tag{4.6}$$

It is assumed that the data, when projected onto one coordinate, follows a logistic distribution. I.e. the likelihood that a sample $\boldsymbol{\phi}(t)$ belongs to the positive class, c = 1, follows:

$$p(c = 1|\boldsymbol{\phi}(t)) = \sigma(s) = \frac{1}{1 + e^{-s}} = \frac{1}{1 + e^{(\boldsymbol{\beta}^\top \boldsymbol{\phi}(t) + \beta_0)}} \tag{4.7}$$

This likelihood is parameterized by the coefficients $\boldsymbol{\beta}$ and a bias β_0. For the negative class it is defined as $p(c = -1|\boldsymbol{\phi}(t)) = 1 - \sigma(s)$. The parameters ($\beta_0$ can be integrated in $\boldsymbol{\beta}$) are obtained by maximizing the likelihood for a set of training samples:

$$\boldsymbol{\beta} = arg \min_{\boldsymbol{\beta}} \; L(\boldsymbol{\beta}) \tag{4.8}$$

with the negative log-likelihood, defined as:

$$L(\boldsymbol{\beta}) = -\sum_t log \; p(c_t|\boldsymbol{\phi}(t)) \tag{4.9}$$

There exists no closed-form solution for this problem, but the optimization can be done efficiently with an algorithm based on iterative reweighted least squares:

$$\boldsymbol{\beta_d}^{(k+1)} = \boldsymbol{\beta_d}^{(k)} - E\left[\frac{\partial^2 L(\boldsymbol{\beta_d})}{\partial\boldsymbol{\beta_d}\partial\boldsymbol{\beta_d}^\top}\right]^{-1} \frac{\partial L(\boldsymbol{\beta_d})}{\partial\boldsymbol{\beta_d}} \tag{4.10}$$

ME can be seen as piece-wise linear with a smooth transition between two linear regions per DOF.

4.2.3 Multilayer Perceptrons (MLPs)

MLPs constitute a class of artificial neuronal networks that have been widely used in the context of myoelectric control for classification [Kelly et al., 1990, Hudgins et al., 1993] and recently also for regression [Nielsen et al., 2011, Muceli and Farina, 2012]. MLPs consist of units (perceptrons), which are arranged in several layers (Fig. 4.1). The input layer is followed by one or more hidden layers and an output layer. The output of each unit is a linear combination of all outputs from the previous layer, filtered by a potentially non-linear activation function φ. Each unit in the input layer represents one input signal, i.e. the number of input units is defined by the dimensionality of the feature space D_Φ. The number of units in the output layer corresponds to the number of values to be estimated by the network. Typically one output unit per class is chosen in architectures for classification. For regression, one output unit is needed per DOF that is to be estimated by the MLP. The number of units in the hidden layer(s) is typically determined empirically.

It has been shown that an MLP with one hidden layer with sigmoidal activation function and a linear activation function in the output layer, can approximate any continuous mapping function $\boldsymbol{f} : \mathbb{R}^n \to \mathbb{R}^m$, given that sufficiently high number of units in the hidden layer are provided [Funahashi, 1989, Hornik et al., 1989]. Mathematically the output of an MLP with that structure can be described as follows:

$$\hat{\boldsymbol{y}}(t) = \boldsymbol{W^{(2)}}^\top(\varphi(\boldsymbol{W^{(1)}}^\top\boldsymbol{\phi}(t) + \boldsymbol{w}_0^{(1)})) + \boldsymbol{w}_0^{(2)} \tag{4.11}$$

$\varphi(x)$ is the sigmoid function and $\boldsymbol{W^{(1)}}$ and $\boldsymbol{W^{(2)}}$ are linear mappings from the input to the hidden and from the hidden to the output layer, respectively. $\boldsymbol{w}_0^{(1)}$ and $\boldsymbol{w}_0^{(2)}$ are bias vectors of the corresponding mappings. To train the MLP network, the coefficients are initialized randomly and outputs $\hat{\boldsymbol{y}}(t)$ are generated for a certain set of training samples $\boldsymbol{\phi}(t)$ with known labels $\boldsymbol{y}(t)$. The squared error over these training samples is computed at the output of the network:

$$\boldsymbol{E}_{MSE} = \frac{1}{2}\frac{1}{N_\Phi}\sum_{t=1}^{N_\Phi}(\hat{\boldsymbol{y}}(t) - \boldsymbol{y}(t))^2 \tag{4.12}$$

With the Levenberg-Marquardt backpropagation algorithm, the partial derivatives of the error with respect to the parameters are computed for all layers of the network. The coefficients are then updated by standard gradient decent techniques and the procedure is repeated until the weights converge [Bishop, 2007]. To reduce the problem of over-fitting, the error function is extended by a regularization term, which penalizes large entries in the coefficients $\boldsymbol{W}$:

$$\boldsymbol{E} = (1 - \lambda)\boldsymbol{E}_{MSE} + \lambda \|\boldsymbol{W}\|_2 \tag{4.13}$$

The optimal regularization parameter λ is determined in a nested cross-validation.
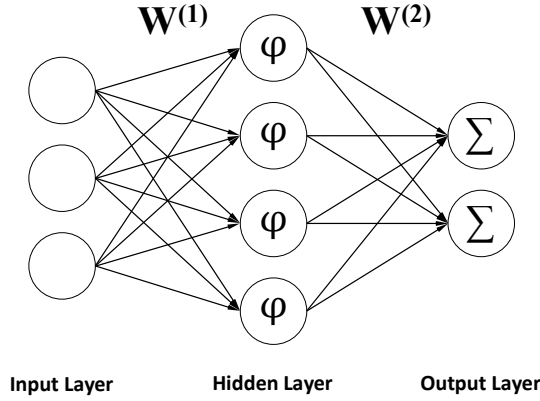

Figure 4.1: Schematic visualization of an MLP network structure with one hidden layer with sigmoidal activation function and a linear activation function in the output layer.

In this work, an individual network was applied for each DOF with the structure described above and only one output unit, as suggested previously for myoelectric control [Muceli and Farina, 2012]. All MLP computations including training with the back-propagation algorithm were implemented with the MATLAB neural network toolbox. A grid search on a range between one and 20 hidden neurons showed that the performance did not increase when more than three neurons per MLP were used, independently of the number of features. When too many neurons were used, the performance decreased again, as the amount of training data needed to properly train the network increases with its complexity. Thus, the size of the hidden neurons was fixed to three units per MLP. Similar results were also reported by other studies [Nielsen et al., 2011, Muceli and Farina, 2012]. An alternative approach with a single MLP and two output units for estimating both DOFs by the same network led to similar results, when twice as many neurons were applied in the hidden layer. But due to the reduced complexity, the first approach with two individual networks was more stable and faster to train.

In some previous studies, where MLPs were applied with a high-dimensional feature-sets, the number of network inputs was reduced by principal component analysis (PCA) [Muceli and Farina, 2012, Hahne et al., 2012b]. The number of PCA components was defined by a threshold on the fraction of variance, captured by those components. This can speed up the training, but may lead to a reduced performance. For a fair comparison with the other methods no dimensionality reduction was applied here.

4.2.4 Kernel Ridge Regression (KRR)

A simple but very powerful non-linear regression method is *kernel ridge regression*. The key idea of KRR is to map the data from feature space through a potentially non-linear

kernel function h into an M dimensional kernel space. In kernel space $h(\phi)$ the problem is solved linearly (eq. 4.14) using the same regularized optimization function as for LR.

$$\hat{y} = \sum_{m=1}^{M} \beta_m h_m(\phi) = \boldsymbol{\beta}^\top \boldsymbol{H} \qquad (4.14)$$

The essence of the kernel trick [Müller et al., 2001, Schölkopf et al., 1998, Müller et al., 2003, Schölkopf and Smola, 2002] is that one can obtain the estimate $\hat{\boldsymbol{y}}$ instead also as a linear combination of the inner products between the test feature sample ϕ and all training feature samples ϕ_i in kernel space (eq. 4.15). Therefore, the representation of the features in kernel space $\boldsymbol{H} \in \mathbb{R}^{M \times N_\Phi}$ does not need to be known explicitly. Instead only the inner product in kernel space $k(\phi_i, \phi_j) = < h(\phi_i), \mathrm{h}(\phi_j) >_h$ is needed. This inner product can be seen as a measure of similarity between feature samples.

$$\hat{y} = \sum_{i=1}^{N_\Phi} \alpha_i k(\phi, \phi_i) \qquad (4.15)$$

The L_2 regularized least mean squares solution of eq. 4.14 can be brought into a form satisfying eq. 4.15. The dual coefficients $\boldsymbol{\alpha}$ are then given by eq. 4.16, where $\boldsymbol{K} = \boldsymbol{H}^\top \boldsymbol{H}$ is the kernel matrix. Again the representations of features in kernel space are not explicitly needed, since $\boldsymbol{K}$ consists only of inner products in kernel space $\boldsymbol{K}_{i,j} = k(\phi_i, \phi_j)$; $i, j = 1..N_\Phi$. Note that KRR scales easily up to multidimensional outputs corresponding to several DOFs, by changing the dimensionality of $\boldsymbol{Y}$ in eq. 4.16.

$$\boldsymbol{\alpha} = (\boldsymbol{K} + \lambda \boldsymbol{I})^{-1} \boldsymbol{Y}^\top \qquad (4.16)$$

In this work the Gaussian kernel function with width σ is used:

$$k(\phi_i, \phi_j) = exp(-\frac{1}{2\sigma^2}(\phi_i - \phi_j)^2), \qquad (4.17)$$

A proper choice of the hyper-parameters σ and λ is essential, as KRR is very sensitive to overfitting to the training data. In this work, they were optimized by a logarithmic grid-search in a nested cross-validation. As the number of elements in the kernel matrix is growing quadratically with the number of training-samples N_Φ, KRR can become computationally challenging and requires a significant amount of memory for large training-sets. There exist approaches to address this problem [Rahimi and Recht, 2008]. For a detailed review of KRR see [Hastie et al., 2003, Shawe-Taylor and Cristianini, 2004].

4.3 Experiments

4.3.1 Setup

This study involved ten able bodied subjects (3 females, 7 males, age 19 - 30) and one person with congenital upper limb deficiency (male, age 39) performing a series of wrist movements. Accurate data labels were gained by recording the wrist angles with a motion tracking system (Xsens with MTx sensors, Fig. 4.2(b)). EMG was recorded with a high density 192-channel electrode grid (ELSCH064NM 3-3, OT Bioelettronica, 8 x 24 channels, 10 mm inter-electrode-distance) in a monopolar configuration. The electrode array was placed on the proximal portion of the left forearm.
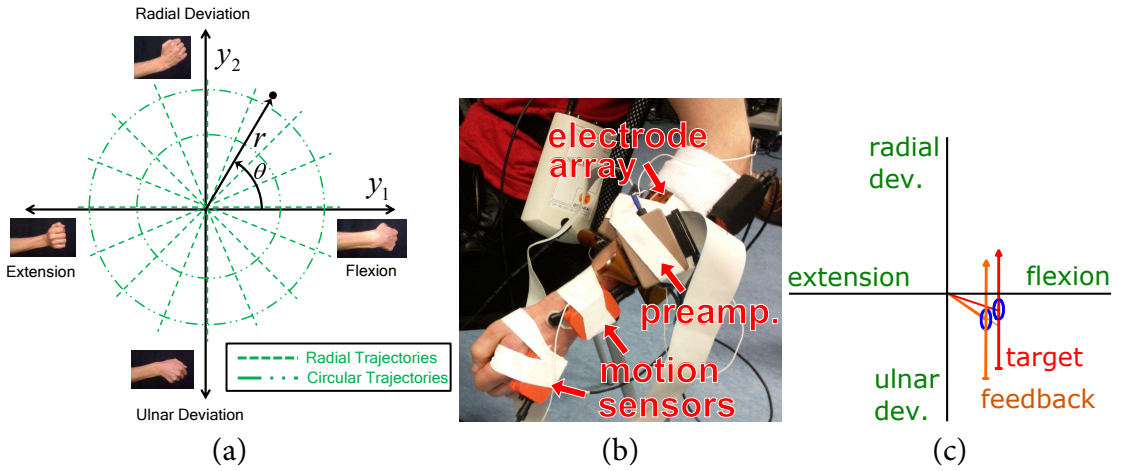

Figure 4.2: Experimental setup: (a) Radial and circular target trajectories the subjects were instructed to follow (dashed and dash-doted lines). Labels y spanned by the two wrist angles in Cartesian and in polar coordinates (r and θ). (b) Placement of electrodes and motion sensors. (c) Visual feedback during recording.

The biosignal amplifier was a 12 bit "OT Bioelettronica EMGUSB-2", configured to a sampling rate of 2048Hz. The reference electrode was a disposable Ag/AgCl electrode placed on the elbow. Ground was formed by an electrode band placed at the distal end of the forearm. Synchronization between kinematic and EMG signals was performed offline via a square-wave synchronization signal provided by the motion tracking system that was recorded as an additional (auxiliary) channel.

4.3.2 Paradigm

This study will focus only on two DOFs, wrist flexion/extension and radial/ulnar deviation (Fig. 4.2(a)). This restriction helped to prevent long recording times and difficulties with recording stability. Rotation, the third DOF of the wrist, causes the muscles to shift
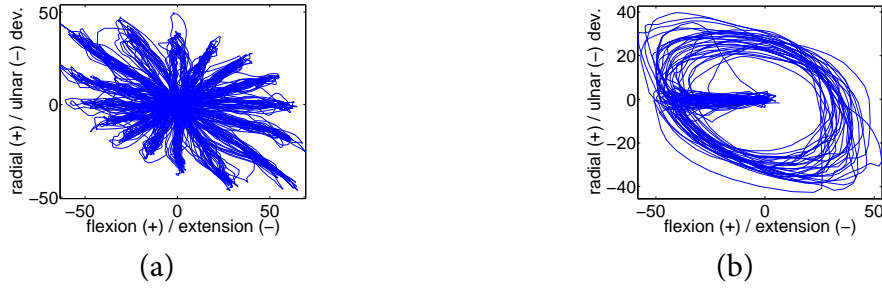
Figure 4.3: Motion traces obtained by the motion tracking system (in degree) for (a): radial trajectories and (b): circular trajectories. The motion signals form the data labels $y(t)$ used to train and test the regressors.

relative to the skin in able-bodied subjects and it is not clear if this complication occurs also at persons with limb deficiency.

The target movement trajectories (Fig. 4.2(a)) included moving the wrist in 16 (radial) directions and drawing circles of two different diameters (each clockwise and counterclockwise). Subjects were instructed to keep the fingers in a relaxed position and not to rotate the wrist (keeping the thumb pointing upwards). At the beginning of each session, the individual range of motion in both DOFs of the subject was measured. The experimental paradigm was calibrated in such a way that the radial trajectories would start at the center (rest position) and reach the maximal range of motion for each direction. The time from the center position to the maximal position was 3 s, followed by 2 s at the maximal position and 3 s for returning to the center position. Circular trajectories were located at 90% and 60% of the maximal range of motion and had a duration of 10 s. The completion of one trajectory will be referred in the following as a trial. The experiment was divided into several runs, where each run contained each type of trajectory (16 radial and 4 circular trials) exactly once. During the recordings, the target wrist angles were displayed on a computer screen together with the actual angles obtained by the motion tracking system (Fig. 4.2(c)). This online feedback assisted subjects in better matching the target trajectories. Six able bodied subjects and the subject with congenital deficiency performed 15 runs and 4 subjects stopped after 10 runs because of fatigue. The time to record one session with 15 runs was about one hour plus another hour for placing the electrodes and motion sensors and familiarizing with the system.

To investigate the transferability of the results to the contra-lateral training strategy, for five out of the ten able bodied subjects, motion data was recorded from both sides, while the subjects performed bilateral mirrored movements [Nielsen et al., 2011]. This allowed for comparing the performance of ipsi-lateral training (motion data from the EMG side were used as training labels) with contra-lateral training (motion data from the other side were used as training labels). The contra-lateral training is relevant, particularly for

future applications in uni-lateral amputees, where motion data can only be obtained from the intact side. The kinematic feedback for all able bodied subjects was provided for the side of EMG recordings. An example of the recorded motion data is shown in figure 4.3.

To prove that the applied methods are also suitable for users of upper limb prostheses, one subject with congenital limb deficiency was included. The subject's forearm terminates at the wrist level. This subject performed also bilateral mirrored contractions. The EMG signals were recorded from the side with deficiency (right side) and motion data were obtained from the contra-lateral side with intact limb. All experiments were in accordance with the Declaration of Helsinki and were approved by the local ethics commission. (Ethikkommission d. Med. Fak. Göttingen, approval number 8/2/11)

4.3.3 Preprocessing and Feature Extraction

The data were filtered using a 4th order Butterworth highpass filter ($f_c = 20Hz$) to remove movement artifacts, a lowpass ($f_c = 500Hz$) to remove high frequency noise and a 50 Hz comb filter to remove power-line interference, including harmonics. Sample-wise common mean subtraction was performed to remove correlated noise and distortion that might be caused by activity at the reference electrode.

Features were extracted from non-overlapping intervals of 200 ms. This window duration is within the acceptable time delay between user command and prosthesis action [Farrell and Weir, 2007, Smith et al., 2011]. To obtain good estimation results when using linear methods the relationship between the features and the target labels (i.e. the motion data) should be as linear as possible. As the first feature the *variance* is used, which was frequently used for simultaneous myoelectric control [Jiang et al., 2009, Muceli and Farina, 2012]:

$$\phi_{VAR}(t) = \frac{1}{N-1} \sum_{i \in \boldsymbol{b}_t} \boldsymbol{x}(i)^2 \tag{4.18}$$

$\boldsymbol{b}_t$ contains all N (raw-data) sample-indices of the t'th block. It will be shown in section 4.3.5 that the variance is increasing monotonically with the deflection of the wrist in any direction, but the relationship between deflection and variance is not linear (see Fig. 4.4(a)). Two simple non-linear transformations of the variance features are tested that result in features denoted by *RMS* and *LOG-VAR*, to linearize the relationship:

$$\phi_{RMS} = \sqrt{\phi_{VAR}} \tag{4.19}$$

$$\phi_{LOG-VAR} = log(\phi_{VAR}) \tag{4.20}$$

Commercially available myoprostheses use active electrode modules, which provide the mean absolute value (MAV) of the EMG. This is very similar to the RMS, but easier to generate in analog circuits. For the sake of completeness and to demonstrate practical relevance, the MAV is also included in the following investigations:

$$\phi_{MAV}(t) = \frac{1}{N} \sum_{i \in \boldsymbol{b}_t} |\boldsymbol{x}(i)| \qquad (4.21)$$

All dimensions in feature space are normalized to have on average unit variance. This is useful for methods with parameters that depend on the numerical range of the features, such as the kernel width for KRR. The scaling factors are calculated based on the training data sets only.

4.3.4 Performance Evaluation and Parameter Optimization

To evaluate the performance, a five-fold cross-validation is applied. The folds are formed by entire runs. This is done in order to keep training and test set not only disjoint but as independent as possible [Lemm et al., 2011] and to guarantee a balanced appearance of movements within both sets. As a performance metric the r-square value is used:

$$r^2 = 1 - \frac{\sum_d \mathrm{Var}(y_d - \hat{y}_d)}{\sum_d \mathrm{Var}(y_d)} \qquad (4.22)$$

y_d is the wrist deflection angle of the dth DOF, measured by the motion tracking system, and $\hat{y}_d$ its estimate, predicted by the regression models. The numerator is the mean squared error, which is normalized by the variance of the correct labels in the denominator. Thus, the r-square value is not influenced by the numerical range of the labels. The maximal r-square value at perfect estimation is one. Note that also negative r-square values are possible for estimation errors larger than the variance of the targets.

For optimizing parameters such as the regularization constants, a nested cross-validation is applied. I.e. with the training set of each fold, a second (inner) cross-validation is done to determine the performance for a certain parameter configuration. This inner cross-validation is repeated for a number of parameter configurations and the best configuration is used to train the algorithm for the outer cross-validation [Müller et al., 2001,Lemm et al., 2011]. The reported performance is measured on the test sets of the outer cross-validation, which is not used to determine the parameters. Simply repeating a normal cross-validation with different parameter settings would lead to a wrong performance estimation, since the parameters would over-fit to the test data sets. A typical session in this study with 15 runs contains 14700 feature samples whereof 11760 are used in each outer fold for training and parameter optimization and 2940 for testing. For the investigations in section 4.3.8 the training sets are reduced while the test-sets are kept unchanged.
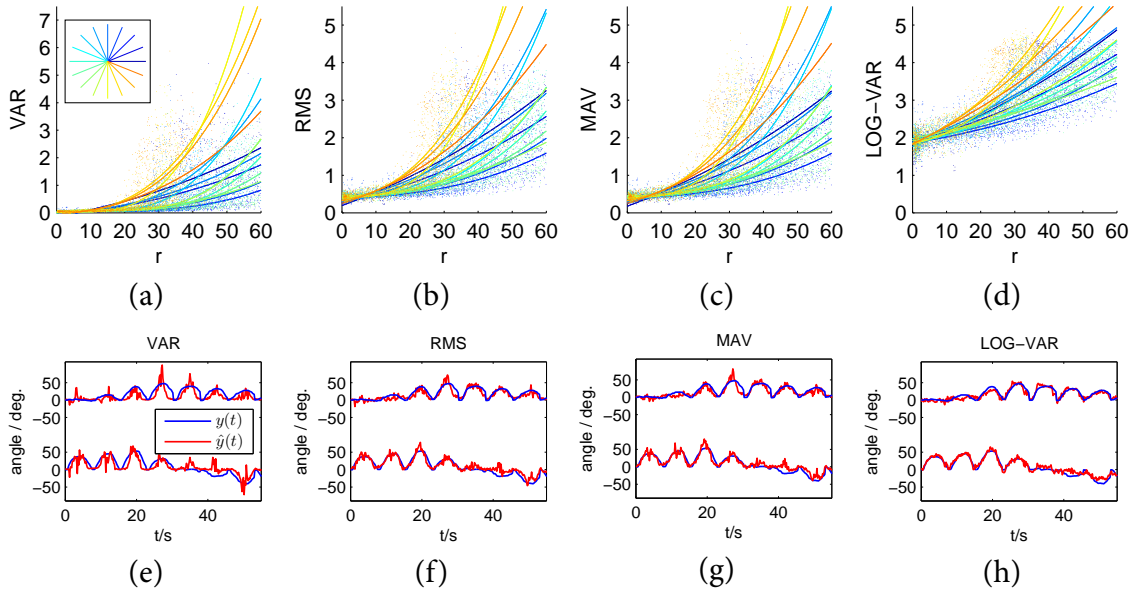
4.3.5 Effect of Feature Transformations

Figure 4.4: Visualization of feature intensity (features averaged over all channels) vs. wrist inclination r for radial trajectories in polar coordinates (a-d). Each line was obtained by polynomial fitting of the intensities for one direction of wrist inclination θ. For this illustration, only radial trajectories were used and the color of each curve indicates the direction of the trajectory as illustrated in the legend in panel a. The lower panels (e-h) show an example of the estimations $\hat{y}$ by linear regression and the true labels y for all features. The lower curves show the DOF flexion/extension and the upper curves show ulnar/radial deviation. For the LOG-VAR feature the relationship between the wrist inclination and the feature intensity is almost linear (a), which results in the best estimation (h).

This section presents a qualitative analysis of the chosen feature-type and its influence to the prediction with a linear method. Quantitative results based on cross-validation will follow in section 4.3.6 and 4.3.10. Figure 4.4 illustrates the linearization of the problem by simple transformations in feature-space. Since it is impossible to visualize the relationship between the labels and the features in full dimension, the features are averaged over all channels. Although this "feature intensity" does not contain enough information for the regression task, it can give insights to the complexity of the underlying relationship. The top row (a-c) illustrates the relationship between the wrist inclination r and the EMG feature intensity. Several trials of the radial trajectories are plotted. The x-axis shows the distance from center position, the y-axis shows feature intensity, and different target di-

rections are distinguished by different colors. The curves are obtained by polynomial fitting with a model complexity limited to third order.

Prediction with variance features   Plot (a) in figure 4.4 illustrates the non-linear relationship between EMG variance and wrist inclination. When estimating the labels with LR, the predicted wrist angles cannot be modeled well, as depicted in figure 4.4(e). For wrist angles close to the origin, the predicted angle is *underestimated* while at wrist angles far from the origin, the predicted angles tend to be *overestimated*.

Prediction with RMS features   The panels in the second column of figure 4.4 show data and results for the square root of the variance features. Panel (b) illustrates that the non-linearity between wrist inclination and EMG features is not as pronounced as in the case of the variance features in panel (a). This leads to a better prediction, as visualized in figure 4.4(f).

Prediction with MAV features   For the MAV features both the relationship between wrist angles and feature intensity in panel (c) and the linear estimation in panel (g) are very similar to the ones related to RMS. This emphasizes the similarity of the two features.

Prediction with LOG-VAR features   The results obtained when taking the logarithm of the EMG variance are depicted in the panels in the right column of figure 4.4. In contrast to the other features, the relationship between wrist angles and EMG LOG-VAR is almost linear, as illustrated in panel (d). This leads to a significantly better prediction with less under- or overestimation at small or large targets as shown qualitatively in figure 4.4(h).

4.3.6 Regression Performance

The effect of linearization is also seen in the cross-validation performance, quantified by the r-square value (Fig. 4.5). To check for statistical significance 3-way ANOVA ($p = 0.05$) was performed. The three factors were regressor, feature and subject. Subjects 8 and 9 had large negative r-square values (at LR with VAR, < -10) and were excluded from the test as outliers. The full model ANOVA (with all two-way interactions and the three-way interaction) revealed no significant three-way interaction ($p = 0.99$), and two-way interactions including subject ($p = 0.36$) with regressor and $p = 0.58$ with feature, respectively. These interaction terms were pooled to perform a three-way ANOVA with only the two-way interaction between regressor and feature. Significant interaction was detected ($p < 10^{-3}$).

Subsequently, compartmentalized two-way ANOVA tests were performed by fixing the level of one of the two interacting factors. When the level of regressor was fixed

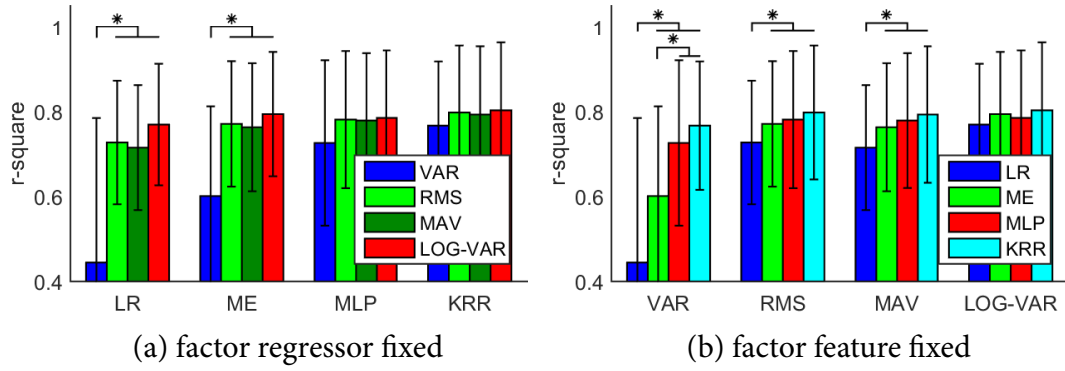(a) factor regressor fixed   (b) factor feature fixed

Figure 4.5: Mean cross-validation performance of ipsi-lateral training for all features and regressors. Factor regressor (a) and factor feature (b) fixed for statistical comparison. The error bars indicate standard deviation and the lines with stars above the bars mark cases that are significantly different ($p = 0.05$).
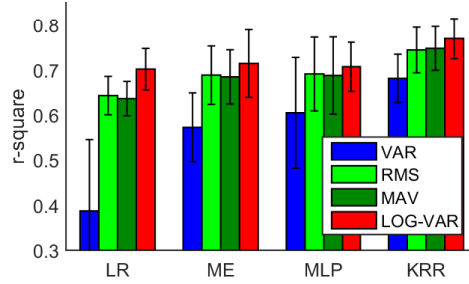

Figure 4.6: Cross-validation performance for a subject with congenital deficiency, trained with contra-lateral motion data. Error bars indicate inter-fold standard deviation. The effect of feature transformations is the same as for able-bodied subjects: RMS and MAV lead to better and LOG-VAR to best results for all regressors and the effect was stronger for linear methods.

at LR, ME, MLP, and KRR, the 2-way ANOVA tests found that the factor feature was significant ($p < 10^{-3}$) for LR and ME and not significant for MLP and KRR ($p = 0.08$ and $p = 0.07$ respectively). Post-hoc Tukey-Kramer tests showed that only VAR features performed significantly worse than all other features for LR and ME (Fig. 4.5(a)).

When the level of features was fixed at VAR, RMS, MAV, and LOG-VAR, the 2-way ANOVA tests found that regressor was not significant for LOG-VAR ($p = 0.15$), while it was significant for VAR, RMS and MAV ($p < 10^{-3}$ for all cases). Post-hoc Tukey-Kramer tests showed that, for the VAR feature, LR was significantly worse than the other three regressors, ME was significant worse than MLP and KRR, while there was no significant difference between MLP and KRR. For the RMS and the MAV features, LR was

significantly different from ME, MLP and KRR, and no other significant different pairs were found. For LOG-VAR features, no significant differences were found among all the regressors (Fig. 4.5(b)).

All in all the linear or piecewise linear methods LR and ME performed significantly worse than non-linear methods with variance features. When transformed with a logarithm into LOG-VAR features, all regressors performed similar. For the features RMS and MAV, only the linear regressor performed slightly worse than the other regressors. For the non-linear regressors MLP and KRR all features performed similar. The extension of LR by ME to two linear regions for antagonistic movements led to significant improvements for all features except LOG-VAR.

For the subject with congenital limb deficiency the effect of feature transformation was similar to able-bodied subjects (Fig. 4.6). With the LOG-VAR feature the r-square value was 0.7 to 0.8, which is almost as good as the average of able-bodied subjects. Because for LOG-VAR features all regressors perform equally well, the following investigations (except section 4.3.10) are based on this feature only.
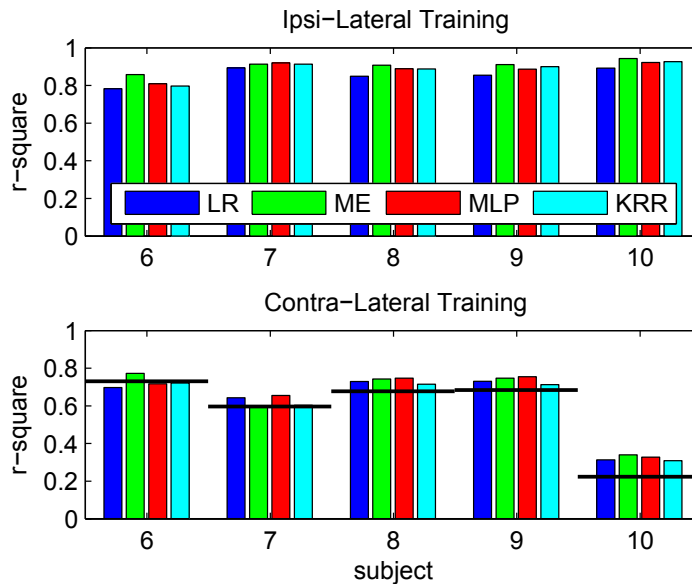

Figure 4.7: Cross-validation performance for ipsi- (u.) and contra-lateral training (d.); the decrease in performance from ipsi- to contra-lateral training is approximately proportional to the ability of the subjects to copy the movements from left and right wrist as indicated by the black horizontal lines.

4.3.7 Contra-lateral Training

In order to assess the ability of all investigated methods to be applied to uni-lateral amputees, each model was trained with the contra-lateral and tested with the ipsi-lateral labels (available for five subjects, Fig. 4.7). The performance decreased from approximately 0.8 - 0.9 (ipsi-lateral training, upper panel) to 0.6 - 0.7 (contra-lateral training, lower panel) for four subjects and to 0.3 - 0.4 for one subject. This is to be compared to the accuracy of matching between the kinematics of the left and the right hand (black lines in Fig. 4.7, lower panel). The fact that the performance of the contra-lateral training is approximately proportional to this accuracy reveals that the performance drop is largely a result of the inability of the subject to perform exact mirror movements.

4.3.8 Influence of Amount and Diversity of Training Data
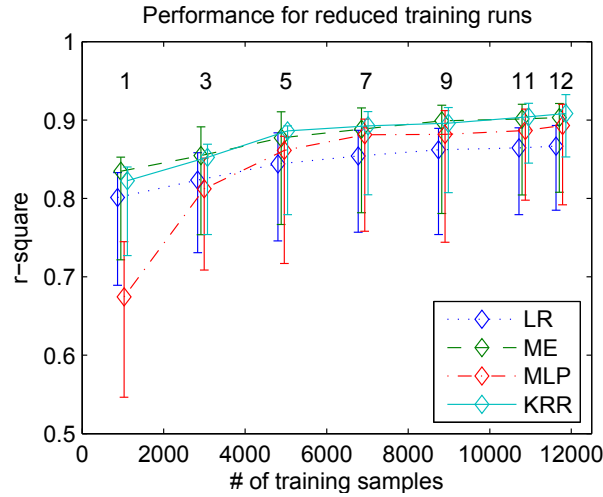

Figure 4.8: Cross-validation performance with reduced training data. Curves indicate median across subjects and whiskers show 25/75 percentiles. The numbers above the curves indicate the number of runs used for training. 1000 feature-samples correspond to 200 s of data. ME, KRR and LR are less influenced by the reduction of training data as compared to MLP.

For a clinical application a regressor should be calibrated with as few training data as possible and generalize well from a small number of training trajectories to all possible combinations of co-activated DOFs. This includes also regions where two DOFs are activated in a different proportion. The generalization performance of all regressors is quantified by successively reducing the amount and the diversity of the training data. These results are based on the six able-bodied subjects for whom 15 runs are available.
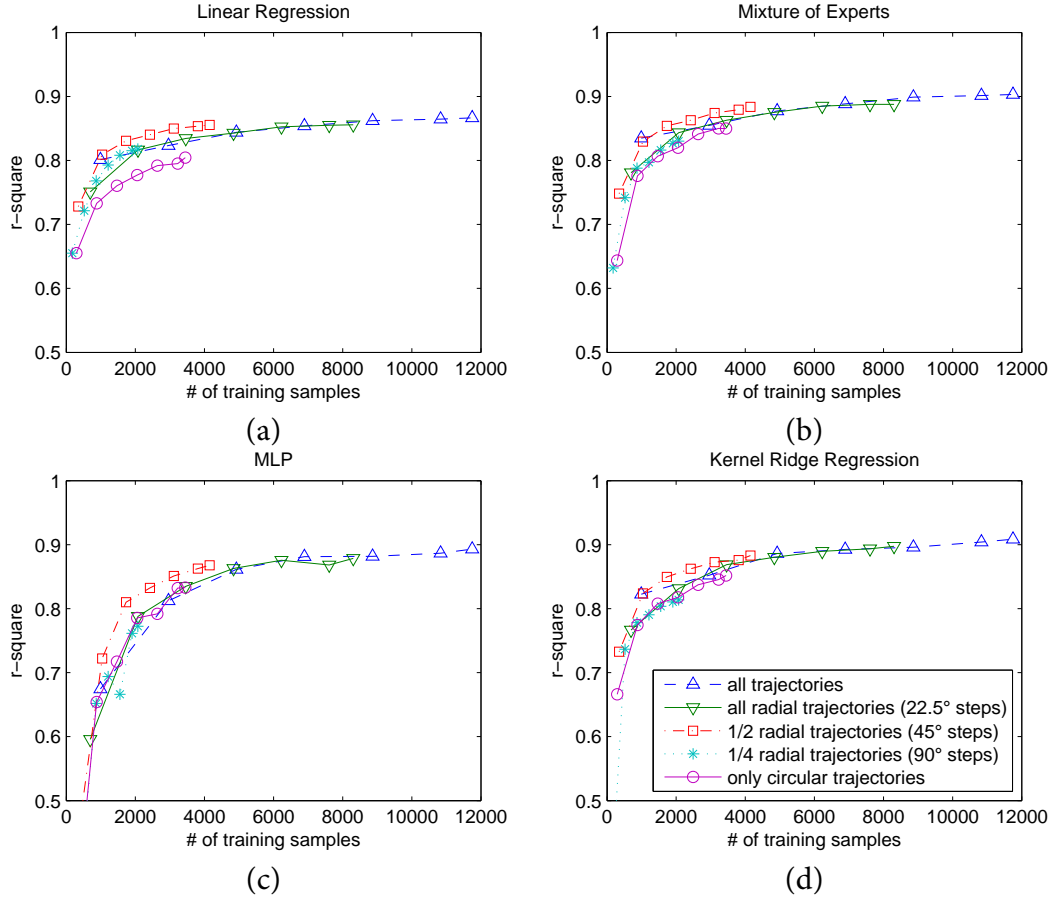
Figure 4.9: Cross-validation performance for a combined reduction training trajectories and runs. The curves indicate median across subjects and whiskers show 25/75 percentiles. For all regressors the performance increases with increasing number of training samples nearly independently of the specific choice of trajectories.

First all 20 trajectories are used in the training-sets and only the amount of training data is reduced by successively excluding entire runs from the training-sets in the cross-validation. The test-sets remain unchanged. As expected, the performance decreases when the amount of training data is reduced (Fig. 4.8). KRR, ME and LR are relatively robust to a reduction of training data, the performance remains above 0.8, even if only one run is used. In contrast, MLP require a larger set of training examples.

Second a combined reduction of the diversity and the amount of training data is performed. The aim of this investigation is to assess whether it is better to reduce the density of combined training movements or to reduce the number of repetitions if the time for collecting training data is limited. For the diversity reduction the following subsets of trajectories are defined:

1) all trajectories (20 trials per run)

2) all radial trajectories ($22.5°$ steps, 16 trials per run)

3) half of radial trajectories ($45°$ steps, 8 trials per run)

4) quarter of radial trajectories ($90°$ steps, 4 trials per run)

5) all circular trajectories (4 trials per run)

Again, the results are shown in dependence of the amount of training samples, which corresponds to the time that would be needed to record the data (Fig. 4.9). The performance depends mainly on the total amount of training samples and the curves of all trajectory subsets are located in relative narrow corridors. Whether the same number of samples is obtained by using a higher diversity and less repetitions or the other way around has almost no influence. As long as enough training samples are used (e.g. more than 1500), different trajectory subsets perform almost equally well. Even if only single activations of individual DOFs are used for training ("1/4 radial trajectories"), all methods performed still very well on the test data, which included all combined movements. This indicates that all four regressors can generalize from a relatively small set of co-activations to all regions in y. Only in the case where just circular trajectories are used, LR performs slightly worse and the case with 1/2 radial trajectories seems to perform slightly better for MLP. These results show only the testing performance averaged over all regions of y. A more detailed view will be provided in section 4.3.10.

4.3.9 Computational Costs

As an indication of the computational load of the algorithms, the processing time for training is measured (Fig. 4.10(a)). All processing is done in MATLAB 64 bit, running on a system with a 2.67 GHz processor and 8 GB of memory. Evidently LR is exceedingly fast (100 ms with all data included). In contrast, the MLP can take substantial amount of time for training (up to 5 minutes). ME and KRR require moderate training times of less than one minute with all data included.

The computational cost for applying the methods is shown in figure 4.10(b). The time to apply LR, ME and MLP does not depend on the amount of training data and is very fast (LR:5 ms, ME:40 ms and MLP:100 ms for the entire test data of 3000 samples or 600 seconds of EMG data). KRR is a non-parametric model and needs to access all training data samples during testing. Testing time for KRR thus increases with increased training-set and reaches around 2.5 s for the largest training set (10ms per sample).
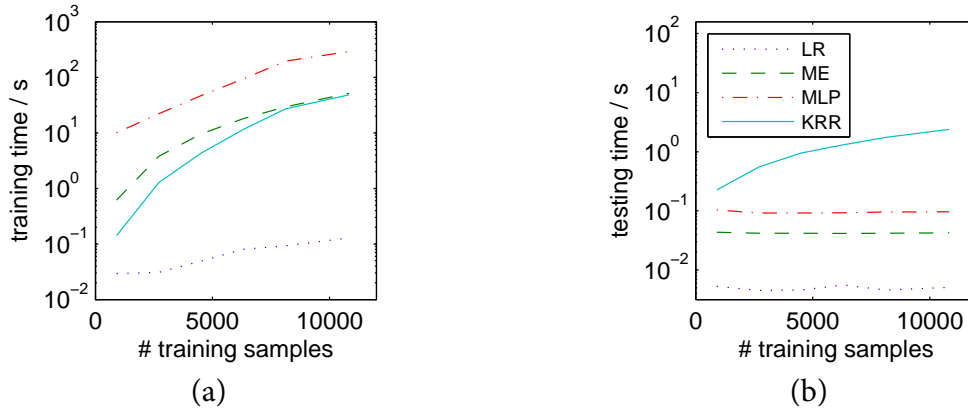
(a)   (b)

Figure 4.10: Computational costs, empirically investigated by measuring (a) the training and (b) the testing time as functions of the training set size.

4.3.10 Linear Separability

To investigate the influence of the features and the training trajectories in more detail, the performance of LR is visualized for all regions of y individually (Fig. 4.11). Since the r-square value is not usable as a performance metric for single feature samples, the absolute estimation error in degrees is used as another intuitive metric. The error is computed on the testing-sets of all radial trajectories and interpolated for the regions in between. To exclude the influence of the training set size, the same amount of data is used in all three training modalities (3 trials with 16 trajectories, 6 trials with 8 trajectories and 12 trials with 4 trajectories).

Figure 4.4 indicated that the features VAR, RMS and MAV are not linearly related to the wrist angles and over-shoots were observed for large angles. This indication is confirmed by figure 4.11. For variance-features, the estimation error is relatively small for small angles and increases dramatically for wrist angles above 20-30 degrees. For RMS and MAV features the region of accurate estimation is increased, but still large estimation errors are observed for wrist angles close to the maximal range of motion. With LOG-VAR features almost all regions are estimated equally well.

Figure 4.9 indicated that for the overall performance it is not needed to include combined movements in the training. Figure 4.11 shows explicitly that the selection of training trajectories has also little influence on the distribution of the error in the output space y. For LOG-VAR features the wrist angels are estimated with an error mostly below 12 degrees. Moreover, the estimation error is almost uniform over the entire range of motion, independently of the diversity of training trajectories. The fact that the error is almost uniform, even if only non-combined movements are used for training, underlines the generalization abilities of the linear regressor and shows that the investigated DOFs are separable. I.e. they can be trained individually and superimpose linearly.
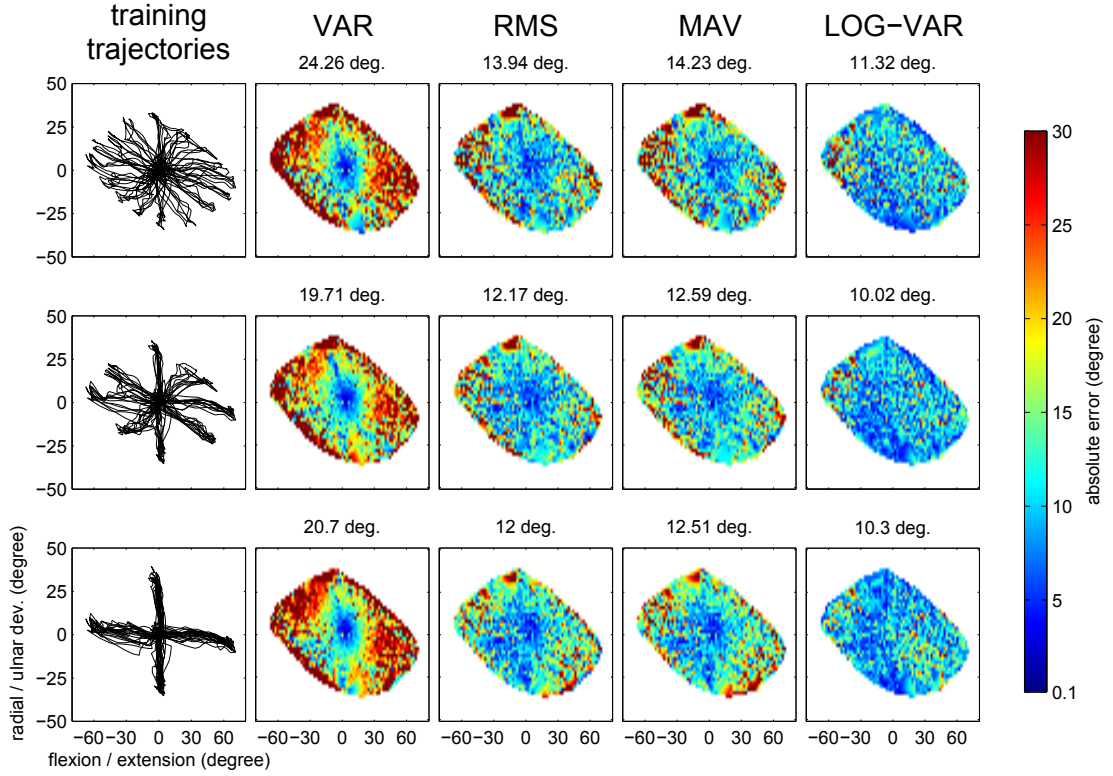
Figure 4.11: Estimation error for all regions of y for LR and one representative subject. The left column shows the training trajectories used in this row and the other columns the absolute interpolated estimation error (in degrees) for the features VAR, RMS, MAV and LOG-VAR. The titles indicate the average errors of the corresponding plots. For VAR, RMS and MAV the error is large mainly in the outer regions. With LOG-VAR the wrist angels are estimated well in all regions. The used training trajectory subset has almost no influence on the distribution of the error. Even if only single DOFs are active for training (lower row), the estimation error is low, also in regions of combined movements.

4.3.11 Channel Reduction

For this study data was recorded with 192 channels. Cost and power consumption will set limits on the number of channels that can be used in a clinical prosthetic system. Therefore, the performances of the algorithms are also investigated for reduced sets of 96, 48, 24, 16, 12 and 6 channels with a regular spacing (Fig. 4.12).

For all methods the performance increases with increasing number of channels and saturates at half of the available channels. When the number of channels is reduced below approximately 12 to 16, the performance drops abruptly. KRR performs best in all cases and achieves an r-square value of 0.8 with only 12 monopolar channels. However,

Performance with reduced number of channles

(a)

Subject with congenital limb deficiency

(b)

| 6 | 12 | 16 | 24 | 48 | 96 |

(c)
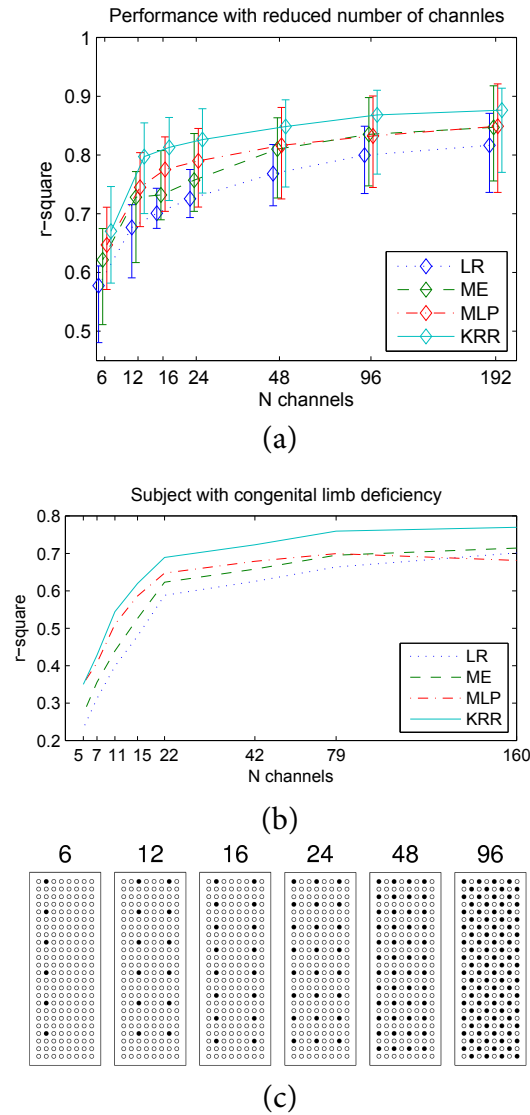
Figure 4.12: Reduced channel-sets: (a) Cross-validation performance with reduced channel-sets for able-bodied subjects (median and 25/75 percentiles across subjects). The performance decreased with decreasing number of channels and dropped abruptly when fewer than 12 to 16 channels were used. (b) Cross-validation performance with reduced channel-sets for the subject with congenital deficiency. The results were similar to those from the able-bodied subjects, but the performance drop occurred when fewer than 22 channels were used. (c) Definition of the regular spaced channel subsets.

the differences between the methods are rather small. E.g. the computational cheaper method ME has with the same number of channels still a performance of 0.73.

Similar results are obtained for the subject with congenital deficiency (Fig. 4.12 (b)). The number of channels differs from figure 4.12(c) because the electrode array had to be cut to fit the size of the residual limb without overlap. Again, KRR performance is best and a drop in performance below a certain number of channels is observed (22 channels in this case).

4.4 Discussion

This chapter presented a systematic comparison of EMG features and regression techniques for simultaneous and proportional control of multiple DOFs. The evaluation scenarios, in which the methods are compared, have targeted aspects that are important for clinical applications.

4.4.1 Feature Representation

Previous studies on simultaneous and proportional control have often used variance-features to capture EMG activity [Jiang et al., 2009, Jiang et al., 2012b, Muceli and Farina, 2012]. However, the variance increases disproportionately to the wrist angles as force increases to achieve extreme wrist inclinations. A simple non-linear transformation (logarithm) can account for this non linearity and thus improves the performance for all methods tested. This is particularly true for the linear and step wise linear methods (LR and ME), which obtained with this simple modification a performance closer to the more complex non-linear algorithms. For opposite directions there are used different muscles, which leads to an additional non-linearity of the problem. The goal of the mixture of expert technique proposed here is to break the linear trajectory into two regressors, each specializing into antagonistic movements for each DOF. With this modification the remaining non-linearity is largely addressed and the performance increases to levels comparable to state-of-the-art non-linear regression algorithms.

A major advantage of linear methods is the dramatically reduced computational demand for training and evaluation; both LR and the ME model are convex problems that can be solved very efficiently. Moreover, linear methods are less prone to overfitting than non-linear methods. LR and ME can be easily realized on a very simple and cheap microcontroller with little power consumption and are readily modified for real-time adaptation. In contrast to linear methods, non-parametric models like KRR suffer from large memory requirements and significantly longer evaluation times for large calibration data sets. Parametric non-linear models such as artificial neural networks on the other hand do not require as much memory and are relatively fast during evaluation, but training can be slow and they require longer calibration sessions.

4.4.2 Clinical Applicability

Separability of movements

It was demonstrated that combined movements of the investigated DOFs flexion/extension and radial/ulnar deviation are almost equally well estimated with linear methods as non-combined movements, even if not included in training. This indicates that the individual DOFs are separable, i.e. the features superimpose linearly from non-combined movements. For the clinical application this is of very high value, as individuals with upper limb deficiencies have often problems to produce precise combined contractions. Moreover, accurate data labels which would render a precise execution of the movements redundant cannot be obtained for those persons as motion tracking is limited to the contra lateral side. Future work should investigate, if this separability is also given for other DOFs.

Amount of calibration data

In clinical practice it is desirable that the controller requires as little calibration data as possible to reduce the temporal effort for fitting. With approximately 2000 feature samples (less than seven minutes training data) the ME algorithm performs already reasonably well. Increasing the recording time beyond this point provides diminishing returns. With the current implementation of MLP about 5000 training samples (more than 15 minutes) are needed to avoid a substantial drop in performance. However, there exist techniques that could increase the performance for small training sets [Montavon et al., 2012].

In most previous studies on myoelectric control an arbitrary amount of training samples was recorded. The investigations in this work demonstrated the strong effect of the amount of training data on the performance. It is suggested to consider this in the design of future training protocols.

Computational costs

The current clinical standard for fitting the prosthetic device involves a computer to visualize the EMG signals and configure the parameter settings. Thus, the computational cost of training is of lesser concern. However, future devices may aim to adaptively calibrate the device in real-time, in which case efficient learning algorithms are a key requirement. The training times for LR is negligible and the algorithm is readily converted into a real-time setting. For the full data set ME and KRR needed almost a minute. But assuming a reduced data set of 2000 samples, which would still lead to a reasonable performance, ME and KRR could be trained in less than 5 seconds. To train MLP with 5000 samples requires approximately 60 seconds, which would preclude real-time adaptation.

This could perhaps be mitigated by reducing the number of channels and more efficient implementations.

The computational costs during execution is critical because they need to fulfill real-time requirements on an embedded system with little computational power. The time to evaluate one test sample must not exceed a few milliseconds. Therefore, the processing times measured on the machine described in section 4.3.8 can only give a rough assessment. The processing for LR consists only of a single matrix-vector multiplication and is negligible. ME and MLP consist of several matrix-vector multiplications and evaluations of sigmoid functions. This is also possible on a relatively simple system. The application of KRR involves evaluating the kernel-function for the test sample with all training data points and a matrix-vector multiplication with the dual coefficients. The processing costs and the memory requirements are growing with the number of training samples and are relatively high already for medium training data sets. The substantially larger computational costs in the application phase and the larger memory requirements make KRR less attractive for an application in prosthetics, where minimal hardware resources are required. Note that there exist techniques to reduce the memory requirements and computational costs of KRR (see e.g. [Seeger, 2008], [Rahimi and Recht, 2008]).

Number of channels

Because of costs, power consumption and reliability, the number of electrodes for a clinical application should be as small as possible. Reducing the number of channels leads to a reduced performance for all investigated methods. But even with 12 channels the regressors were still able to estimate the wrist position with an r-square value of 0.7 to 0.8. For the subject with congenital deficiency, 22 channels were sufficient to reach an r-square value of 0.6 to 0.7. The number of needed channels may vary significantly for subjects with limb deficiency depending on the individual anatomy and capabilities. The channels were selected arbitrarily with a regular spacing. With automatic channel-selection methods a higher performance can be reached with even fewer channels [Hahne et al., 2010, Hwang et al., 2014a]. This is important particularly for potential users of myoprostheses.

Transfer to individuals with upper limb deficiency

It was demonstrated for one subject with congenital limb deficiency that the algorithms work also for potential users of prosthetic devices. The performance was only slightly below that of able-bodied subjects and the main findings, including the positive effect of the feature transformations, were valid also for this subject. This indicates that the findings may transfer to potential users of myoelectric prostheses and emphasizes the relevance of this work.

For subjects with uni-lateral limb deficiency, contra-lateral motion tracking is one possibility to train the algorithms, which was also investigated in this study. The performance in this case depends on both the ability of the user to execute the contractions with the disabled side and the ability to copy the movements from the intact side. As shown in section 4.3.7, the capability to precisely mirror movements has a large variability, even for able-bodied subjects. The subject with congenital limb deficiency who participated in this study performed relatively good, which may be caused in parts by his long residual limb. Excluding combined movements from the training protocol as discussed in section 4.4.2 may be one step to simplify training and enable simultaneous and proportional control to a larger group of prosthetic users.

The experiments in this study are based on two DOFs, namely flexion/extension and radial/ulnar deviation of the wrist, where the latter is not available in current prosthesis hardware. Muscles active for those movements are located close to the skin leading to good EMG signals and less problems due to skin-muscle-shifts are expected compared to pronation/supination. These problems might be a minor issue when applied to amputees because of different anatomy. However, the control signals from radial/ulnar deviation can also be used to control the rotation unit of the prosthesis if this leads to more stable results.

4.4.3 Limitations

The methods described in this chapter would allow for a significantly improved and more natural control in comparison with the classification approach and the study focused on clinically relevant factors. However, there are still issues that need to be addressed. The used semi-disposable Ag/AgCl electrodes that are applied with electrode-gel provide a very good signal quality with high SNR, but they are not suitable for a use in prosthetics. Preparation time, costs and long-term stability would not fulfill the constraints of this application, where dry electrodes are required. The motion-tracking-system used in this study provides accurate labels for training the algorithms, but its costs would exceed clinical requirements and it cannot be used for bi-lateral amputees who would benefit most from advanced control-techniques.

The evaluation should be done in a closed-loop real-time system to allow the user to correct for shortcomings of the algorithm. Also user-training needs to be addressed, especially for subjects with amputation or congenital limb deficiency, who may need to (re-)learn the execution of muscle-contractions which they usually do not perform in their daily life. Static regression models as used in this study may limit potential development of the user. These issues will be addressed in the next chapter.

5 Real-time Control and Co-Adaptive Learning

5.1 Introduction

Most studies on myoelectric control including those described in the previous chapters are done offline with pre-recorded data. While this is very useful to compare different algorithms and to optimize parameters, it allows only for limited conclusions on the usability in a final application. Offline metrics do not necessarily correlate with the performance in a real-time application [Jiang et al., 2014b]. If the user receives real-time feedback, he/she can adapt the muscle-contractions to optimize the performance. In such a closed loop-control both user related errors caused by variations in the execution of the contractions and algorithm-related errors, may be corrected by user-adaptation. Moreover, the user can learn to generate EMG patterns that are more suitable for myoelectric control (e.g. stronger, better separable or more consistent).

Other real-time studies on myoelectric control typically work with static models, i.e. the model is trained once based on calibration data and is not changed during the application phase [Ameri et al., 2014c, Jiang et al., 2014a, Wurth and Hargrove, 2014, Fougner et al., 2014]. This allows for a more realistic performance evaluation compared to offline studies. However, due to the fixed machine learning model the user will adapt in a direction that gives optimal results for that particular model, learning of the user is therefore restricted and only possible within a certain range.

Several studies have investigated adaptation in the context of myoelectric control. Most of them focused on the classification-based approach [Nishikawa et al., 2001, Sensinger et al., 2009, He et al., 2012, Zhang et al., 2013, Chen et al., 2013] and employed adaptation with the goal to compensate for non-stationarities [Vidovic et al., 2015]. In classification, unsupervised adaptation is possible by using the classifier-output as adaptation target and considering only classifier decisions with high confidence. It was shown offline that this can reduce the impact of slowly changing signal conditions, but there is the risk that false labels are used for adaptation. This can cause a destructive avalanche effect, as it increases the likelihood of further fail-adaptations [He et al., 2012]. Therefore, supervised adaptation, which requires explicit user-interaction is more robust [Sensinger et al., 2009].

For regression approaches the confidence-based unsupervised adaptation is not applicable because no discrete states are given, which could be used as adaptation targets.

However, since the user gets a direct real-time feedback in regression-based control, which reacts direction-dependent on all changes in the EMG (and not just if a classification boundary is crossed) he/she can intuitively compensate for undesired drifts of the output caused by non-stationarities. Gijsberts et al. proposed a supervised adaptation approach for regression-based control, but investigated the adaptation only offline [Gijsberts et al., 2014].

[Powell et al., 2014] demonstrated the great importance of user-training for classification-based myoelectric control. They used a strategy based on alternating offline calibration of the classifier and real-time evaluation with a virtual prosthesis. With the support of confusion matrices and measures for quantifying inter-class distances and within-class-consistencies [Bunderson et al., 2012], problematic movements were identified manually and improved by a targeted user-training.

[Pilarski et al., 2011] explored the possibility to use actor-critic reinforcement learning for training and adaptation of a myoelectric controller. This is a very interesting approach as it allows for adaptation based on a single, binary reward signal only. However, the approach was tested on one able-bodied subject only and included only two contraction patterns. Thus, it remains to be seen if this strategy can also efficiently be used to control more than one DOF with free activation ratios, as required for independent proportional control.

The aim of the study described in this chapter is to investigate the benefits of interactive real-time learning for regression-based myoelectric control as a complement to commonly performed offline calibration. In real-time experiments the behavior of a closed loop system consisting of the user and the controller was analyzed while both user and algorithm were adapting towards the common goal to reach optimal performance. This concept of mutual (or co-adaptive) learning has been proven to be highly efficient in the context of brain-computer-interfaces [Vidaurre et al., 2011b, Vidaurre et al., 2011a, Lemm et al., 2011]. A co-adaptive system of this type is influenced by the speed with that both learners, the human and the machine, are adapting [Vidaurre et al., 2011a]. While the learning speed of the human is not known and may vary between subjects, the adaptation speed of the machine can be controlled via hyper-parameters of the algorithm.

A real-time-learning algorithm, namely Recursive Least Squares is applied in an experiment with ten able-bodied subjects and two individuals with congenital limb deficiency. The influence of the algorithms adaptation speed is investigated and the real-time performance of the adapted models is compared with several control-conditions based on offline calibration. It will be shown that co-adaptive real-time learning is beneficial compared to offline-calibration and that the optimal learning speed of the algorithm is consistent between able bodied subjects and the potential users in prosthetic application.

This chapter is based on previous publications, in particular [Hahne et al., 2015a] and [Hahne et al., 2015b].

5.2 Recursive Least Squares

A linear regression model can be trained offline using a batch algorithm, as shown in the last chapter. Typically the least mean-squares solution [Bishop, 2007] is applied:

$$\boldsymbol{W} = (\boldsymbol{\Phi}\boldsymbol{\Phi}^\top)^{-1}\boldsymbol{\Phi}\boldsymbol{Y}^\top \tag{5.1}$$

In the supervised, co-adaptive learning paradigm that will be described in more detail in section 5.3, the regression model is to be continuously updated. In cases like this, on-line learning algorithms are more efficient than repeated batch training with increasing training sets. Here, the exponential Recursive Least Squares (RLS) algorithm was chosen, which is an efficient and stable extension of the batch algorithm [Hayes, 1996]. RLS minimizes the following cost function:

$$\boldsymbol{E}(t) = \sum_{i=0}^{t} \lambda^{t-i} e^2(i) \tag{5.2}$$

$e^2(i)$ is the squared error and $0 < \lambda \leq 1$ an exponential weighting constant that determines the influence of new data-samples and thus the speed of adaptation. Based on an adaptive Wiener filter with this cost function the following set of update equations can be derived:

$$\begin{aligned}
\boldsymbol{\alpha}(t) &= \boldsymbol{y}(t)^\top - \boldsymbol{\phi}(t)^\top \boldsymbol{W}(t-1) & (5.3)\\
\boldsymbol{g}(t) &= \boldsymbol{P}(t-1)\boldsymbol{\phi}(t)\left(\lambda + \boldsymbol{\phi}(t)^\top \boldsymbol{P}(t-1)\boldsymbol{\phi}(t)\right)^{-1} & (5.4)\\
\boldsymbol{P}(t) &= \lambda^{-1}\boldsymbol{P}(t-1) - \boldsymbol{g}(t)\boldsymbol{\phi}(t)^\top \lambda^{-1}\boldsymbol{P}(t-1) & (5.5)\\
\boldsymbol{W}(t) &= \boldsymbol{W}(t-1) + \boldsymbol{\alpha}(t)\boldsymbol{g}(t) & (5.6)
\end{aligned}$$

$\boldsymbol{\alpha}(t)$ is the error with that the model from the previous update step would predict a new incoming data-sample at time instance t. $\boldsymbol{P}(t)$ is the inverse of the exponentially weighted deterministic covariance matrix and $\boldsymbol{g}(t)$ is the gain vector. Small values for λ cause a relatively fast adaptation and larger values (close to one) cause slower adaptation. For $\lambda = 1$ the algorithm becomes the *growing window RLS*, which gives equal weight to all samples and results in exactly the same solution as the batch algorithm trained with all collected data points. A detailed introduction on RLS is found in [Hayes, 1996].

In the following experiments, the model is initialized with the conventional batch algorithm ($\boldsymbol{W}(0)$ as Eq. (5.1) and $\boldsymbol{P}(0) = (\boldsymbol{X}\boldsymbol{X}^\top)^{-1}$) based on some calibration data. This approach can be seen as a two-stage procedure: calibration with growing window RLS followed by real-time adaptation with exponentially weighted RLS. This scheme was chosen to give equal weight to all calibration samples and to start with the same condition for all learning constants to be investigated. In the experiments, the influence of the adaptation speed, determined by the learning constant λ, is investigated.

5.3 Experimental Evaluation
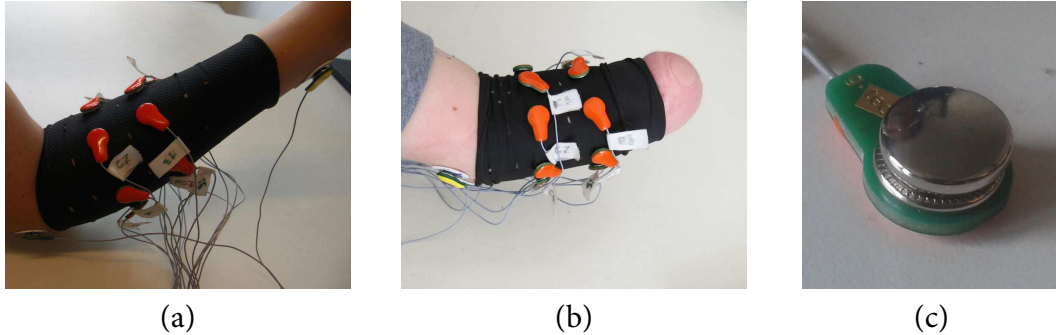
5.3.1 Experimental Setup

Figure 5.1: EMG acquisition setup including the textile hose with integrated dry EMG electrodes. (a) Setup mounted on an able-bodied subject. (b) Setup mounted on a subject with transradial amputation. (c) Custom-made dry EMG electrode mounted on preamplifier.

The experimental setup comprised a 24 bit, 16 channel biosignal amplifier with an extension for dry electrodes (g.tec USBamp + g.tec Sahara), 16 custom-made dry, monopolar steel electrodes with 12 mm diameter that were integrated into a custom made stretchable textile hose (Fig. 5.1). The signals were sampled at 1200 Hz and frequencies above the Nyquist criterion were removed with internal low pass filters provided by the amplifier. All further processing and visualization were performed in MATLAB 12a 64 bit running on a 2.67 Ghz, dual-core computer with 8 GB RAM. An overview on the signal processing chain is given in figure 5.2.

The electrodes were equally distributed on two circles with a distance of 35 mm to each other and the circumference of the textile hose adapted to the arm of the subject. The hose was placed on the dominant forearm, such that the electrodes were located approximately above the region with largest diameter. Ground and reference electrodes were placed on bony sections of the wrist and the Olecranon with little EMG activity. All experiments were in accordance with the Declaration of Helsinki and were approved by the local ethics commission (Ethikkommison Charité Berlin, approval number EA4/085/11).

5.3.2 Pre-processing and Feature Extraction

The data were acquired and processed in blocks of 40 ms, corresponding to the update rate of the system ($f_{update} = 25\ Hz$). Sample-wise common mean subtraction was performed to remove correlated noise and distortion that may be introduced by activity at
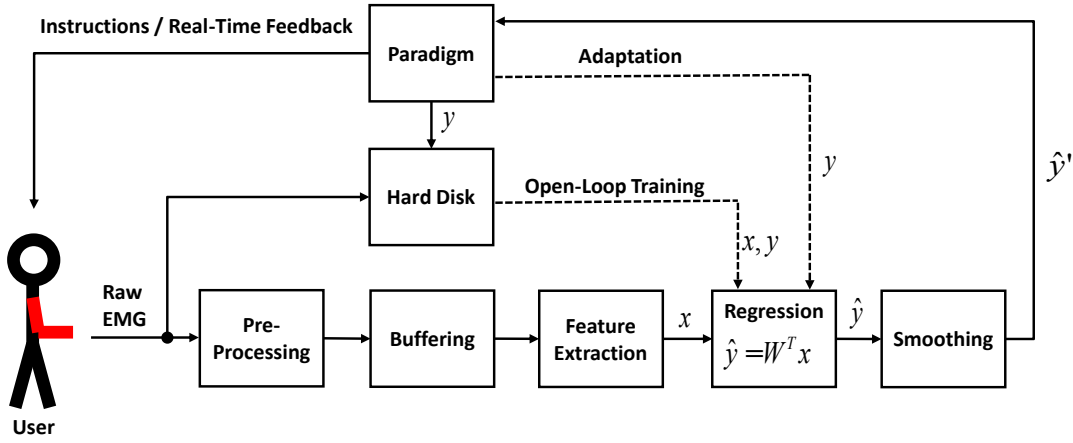
Figure 5.2: Schematic overview on the signal processing chain. In conventional open-loop training the user receives fixed instructions when training data is collected. In the proposed real-time training, the loop is closed via feedback provided to the user, while the regression coefficients are updated with RLS. Pre-processing and feature extraction blocks were omitted in the open-loop training path for sake of readability.

the reference electrode and 50 Hz comb filters were applied to remove power-line interferences, including its harmonics. To reduce movement artifacts and maximize the signal-to-noise-ratio, the data were further filtered by 4th order Butterworth band-pass filters with a pass band between 30 and 300 Hz. After pre-processing, the data were written into a queue buffer so that the last 12 s of data were available for feature extraction and real-time visualization.

As shown in chapter 4, the LOG-VAR of the band-pass filtered EMG is approximately linear related to the joint angle and thus allows for using the computationally very efficient linear regression approach. Therefore, this feature was extracted for each channel, resulting in a 16-dimensional feature-vector $\phi(t)$. The feature extraction was based on blocks of 200 ms with an increment of 40 ms, equivalent to the update rate of the system. This window duration is within the acceptable time delay between user command and prosthesis reaction [Englehart and Hudgins, 2003], [Farrell and Weir, 2007].

5.3.3 Regression and Post-Processing

To estimate the wrist angles from EMG features an instantaneous, linear regression model was applied:

$$\widehat{\boldsymbol{y}}(t) = \boldsymbol{W}^\top \boldsymbol{\phi}(t) \qquad (5.7)$$

Each dimension in $\hat{\boldsymbol{y}}(t)$ corresponds to one estimated joint angle and the feature-vector $\boldsymbol{\phi}(t)$ is extended for each time instance by the constant 1 to incorporate a bias compensation in $\boldsymbol{W}$. Here, the weight matrix $\boldsymbol{W}$, which characterizes the regression model, is therefore of size $< 17 \times 2 >$.

Since the instantaneous regression output $\hat{\boldsymbol{y}}(t)$ contains undesired high-frequency components caused by the stochastic nature of the EMG signal, an exponential moving-average filter (EMA) was applied to obtain a smooth controller output $\widehat{\boldsymbol{y}\prime}(t)$. The advantage of an EMA filter in comparison with a commonly used Butterworth post-processing filter is that it reacts relatively fast and does not introduce a systematic overshoot in its step-response. These are important properties in real-time control tasks. The EMA filter is defined as:

$$\widehat{\boldsymbol{y}\prime}(t) = \gamma \widehat{\boldsymbol{y}\prime}(t-1) + (1-\gamma)\widehat{\boldsymbol{y}}(t) \tag{5.8}$$

The filter-constant γ determines the amount of smoothing, which is a trade-off between stability and speed. It was determined empirically to $\gamma = 24/25$, which gave a relative stable output without causing any significant delays, so that the subjects had the feeling of an immediate response.

5.3.4 Experimental Paradigm
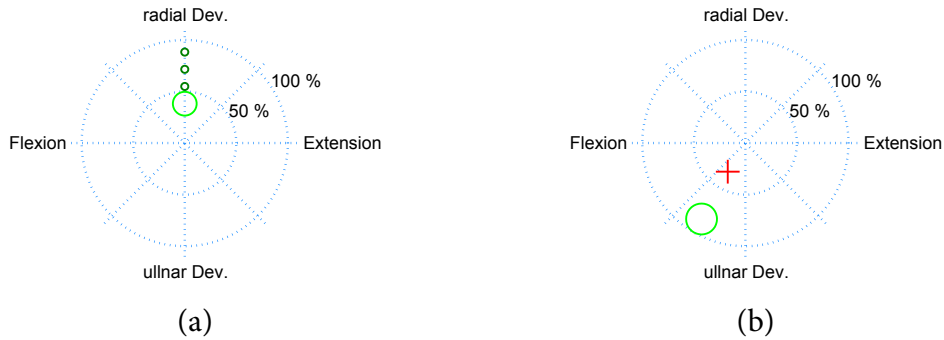
Figure 5.3: Experimental paradigm. (a) Display presented to the subject during calibration phase without feedback. A green "target-cursor" moves along pre-defined trajectories and the subject is asked to follow this cursor with wrist deflections. The upcoming target location is indicated with three small dark green circles to minimize delays between the instruction and user-reaction. (b) Display presented to the subject during performance evaluation and adaptation phases. The subject controls the red cross with muscle contractions and tries to hit the green circle, i.e. remain within the stationary target circle for one second without leaving it.

Figure 5.4: Experimental setup during real-time control performed by a subject with congenital limb deficiency.

This study involved simultaneous movements of the two wrist DOFs flexion/extension and radial/ulnar deviation, which were already investigated offline in the previous chapter. The relative wrist angles were visualized on a user screen by a two dimensional coordinate system, in which the horizontal axis corresponds to flexion/extension and the vertical axis to radial/ulnar deviation (Fig. 5.3). The center corresponds to the rest position and all points on the outer circle (100%) to a full inclination of the wrist into the corresponding direction. This control scheme is referred to as position-control and provides a direct view on the capabilities of the regressor [Ameri et al., 2014b]. Figure 5.4 shows the entire setup during the experiment with one of the subjects with congenital limb-deficiency.

Calibration Runs

For people with limb deficiency who are the potential users of the proposed method it is very difficult to perform accurate combined movements without the intrinsic feedback of the limb. In the offline-study, described in the previous chapter, it was found that even when trained with individually activated DOFs only, combined movements of the two wrist DOFs investigated here can be estimated with relatively high accuracy, even by a linear regressor. Therefore, the calibration runs in this study are composed of single DOF activations only. In this study the motion-tracking system is omitted and visual cues are used as training targets for an initial offline calibration and the control conditions. The

subjects were instructed to follow a target that moved along predefined trajectories with their wrists angles and the subjects with congenital limb deficiency were asked to perform equivalent contractions. The trajectories were defined as follows: three seconds movement from rest position to maximal inclination, two seconds remaining in this position and three seconds returning to rest position. In each calibration-run this was repeated once for all four directions (Fig. 5.3 (a)).

Evaluation Runs

For real-time evaluation, the current wrist position estimated from the EMG was visualized on an user screen by a red cursor. Circles with a radius of 0.15 units appeared within the coordinate system and the subject was asked to hit the stationary targets by moving the red cursor into the circle and remaining there for one second without leaving it. To allow for a fair and systematic comparison, the circle-positions were taken in randomized order from a pre-defined list that consisted of 8 equally spaced circles with a center-to-origin distance of 0.5 units and 16 circles at 0.85 units. The circle-positions are shown in figure 5.6. In order to approach each target from the rest-position and thus avoid possible influences of the randomized order (e.g. when two circles appear close to each other), before each regular target, an additional "rest-target" was placed at the origin of the coordinate system. Thus, one evaluation run consisted of 24 regular targets and 24 "rest-targets". The latter ones were not counted for the performance-evaluation. If a circle was not hit within ten seconds, a time-out took effect and the run continued with the next target.

The metrics used to evaluate the performance (completion rate, completion time, overshoot ratio and path efficiency) are explained in table 5.1. All hit and missed targets were included in the performance evaluation in order to avoid the potential bias caused by easier targets closer to the origin that were hit more frequently.

Table 5.1: Performance Metrics

Metric	Description
Completion Rate	Ratio of successfully hit targets and total number of targets
Completion Time	Average time to hit a target, for missed targets the time-out is counted (10 s)
Overshoot Ratio	Number of times a target was left before 1 s dwell time, normalized by the total number of targets
Path Efficiency	Average ratio of shortest path to reach the target and actually traveled path-length

Adaptation Runs

A similar paradigm as in the evaluation runs was applied for real-time adaptation. In order to adapt the model only for problematic regions, the adaptation started when a circle was not hit within the first five seconds after its appearance and stopped when the target was hit or the ten second time-out occurred. The subjects were informed by an auditory signal about the start of the adaptation phase and were instructed to keep trying to hit the target. During the adaptation-phase the current feature vector was used to adapt the regression model towards the circle position by one RLS-iteration in each system update circle. This usually improved the regression model for the region of the current target. Since the target position is known to the algorithm during adaptation, a fair evaluation of the performance during these runs is not possible. Thus, the adaptation-runs were not taken into account for performance evaluation.

Study Design

The goal of this study was to explore co-adaptive real-time-learning as a tool to train regression algorithms for myoelectric control and to investigate the influence of the adaptation speed within the two-learners problem consisting of human and machine. To compare the results of co-adaptive learning with those of conventional offline training and determine to which extend improvements may be caused by pure user-learning, four control conditions were included which will be explained below in more detail. Ten able-bodied subjects (five females, five males, age 21-53) and two individuals with congenital limb-deficiency (congenital 1: female, age 36, residual limb length approximately 1/3 of the normal forearm; congenital 2: male, age 41, residual limb until wrist-level) were recruited to participate in this study. A chronological overview of the experiment is provided in table 5.2.

In the beginning of the session the signal quality was checked by visual inspection of the filtered EMG during rest and contraction. The experimenter explained the paradigm to the subject and demonstrated the wrist movements, which were copied by the subject for training purpose. A real-time visualization of the EMG-amplitudes was used for the subjects with congenital limb-deficiency, to verify that they generated different contraction patterns for the four non-combined movements of the two DOFs used in this study. After one demo run that was rejected and only done for familiarization purposes with the paradigm, four calibration runs were recorded and used to generate a regression model by conventional offline training using the batch algorithm (Eq. 5.1). This model was tested with one evaluation run as a baseline condition denoted by "init 1".

In the following phase co-adaptive real-time-learning was investigated. For each adaptation-speed, two runs were performed: One adaptation run and one evaluation run. For each adaptation run the RLS algorithm was initialized as described in section 5.2, based on the first three calibration runs. This was done to utilize approximately the same

amount of data for obtaining the adapted model as in the baseline condition. After completing each adaptation run, the adapted model was tested in one evaluation run. This was repeated for each learning speed determined by λ. The values for λ to be tested (0.96 - 1) were selected empirically. In order to avoid a bias due to user-learning without confusing the subjects, the values of lambda were for half of the subjects in ascending and the other half in descending order.

To evaluate learning effects of the user in an isolated way, the same model as for the baseline condition was tested a second time, when the user obtained more experience with the paradigm and the control ("init 2"). Since a major shortcoming of the baseline-condition was in many cases a limited range of motion, another control-condition ("up-scale") was tested, where the output was upscaled by a factor that was determined for each subject individually, such that all regions of the output space could be reached.

As a final control condition, four additional calibration runs were recorded in the end of the session and used to train a regression model as in the baseline condition. This was done to test, if re-calibration after obtaining experience with the control could improve the performance in a final evaluation run ("re-calibration").

Table 5.2: Chronological overview of the runs performed in this study

run	type	init with run	description
1 - 4	cal		calibration
5	eval	1 - 4	init 1
6,8,10,12,14	adapt	1 - 3	adaptation with different λ
7,9,11,13,15	eval		evaluation of adapted models
16	eval	1 - 4	init 2
17	eval	1 - 4	test upscaling
18 - 21	cal		re-calibration
22	eval	18 - 21	test re-calibration

5.3.5 Quantitative Performance

For all subjects the real-time performance was evaluated in four control conditions and after real-time-learning with five different adaptation speeds (Fig. 5.5 (a) - (d)). To test for statistical differences for the ten able bodied subjects, one-way repeated-measure (RM)-ANOVA was conducted using SPSS. The significance threshold was set to 0.05. Since RM-ANOVA assumes equal variances for all conditions, Mauchly's Test of Sphericity was conducted. A significant difference between the variances of each condition was found for *path efficiency*, therefore Greenhouse-Geisser correction [Greenhouse and
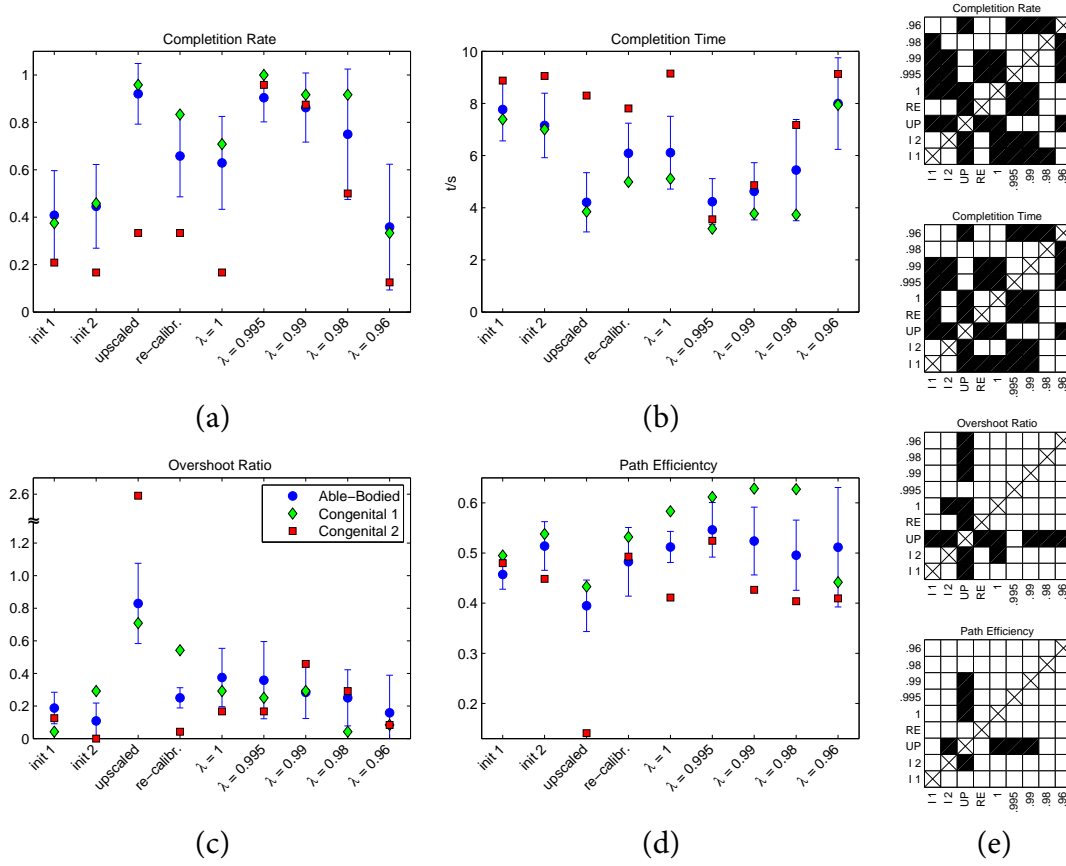
Figure 5.5: Real-time evaluation results for the four control conditions and after adaptation with different λ (not in chronological order). Blue circles and error bars show mean and standard deviation across all able bodied subjects, the red squares and green diamonds indicate the performances of the two congenital subjects. Panel (a) - (d) show completion rate, completion time, overshoot ratio and path efficiency. The plots in panel (e) show the RM-ANOVA results, black fields indicate statistically significant differences between the corresponding conditions ($p < 0.05$). The best performance across all metrics is obtained after adaptation with $\lambda = 0.995$. Completion rate and time show similar results for the upscaled condition but the poor overshoot ratio and path efficiency obtained with the upscaled model indicate a drop in stability. The subjects with congenital limb deficiency show the same trends as able-bodied subjects and reach a similar performance after co-adaptive real-time learning.

Geisser, 1959] was done for this metric. For all four performance metrics, significant differences were found (completion rate: $F(8,72) = 24.378$, $p < 0.001$; completion time: $F(8,72) = 23.018$, $p < 0.001$; overshoot-ratio: $F(8,72) = 13.625$, $p < 0.001$, path efficiency: $F(2.66, 23.98) = 4.664$, $p = 0.013$). To identify the conditions with significant differences, a Bonferroni multiple comparison test was performed. The results of this comparison are visualized in figure 5.5 (e).

For co-adaptive learning, the test related to $\lambda = 0.995$ showed the best performance with the highest completion rate, lowest completion time and highest path efficiency. Completion rate and completion time significantly improved compared to the baseline condition "init 1", while overshoot ratio and path efficiency did not show any significant difference to the baseline. The control condition "init 2", in which the same regression model as in the model as in "init 1" was tested a 2nd time to investigate isolated user-learning effects, showed a slight trend of improvement in all metrics compared to "init 1", but none of these differences were significant. A similar trend was observed for the re-calibration condition. Here only completion time showed significant improvements. Note that the slightly improved performances for "init 2" and "re-calibration" in terms of completion rate and completion time were still significantly lower than the ones of the best adapted model ($\lambda = 0.995$).

The upscaled model showed improvements in the completion rate and completion time that were statistical significant, similar as real-time learning with optimal adaptation speed. However, the control became rather unstable. This is seen in the overshoot ratio, which worsened significantly and showed the lowest performance among all conditions. The difference to the best adaptation condition is marginally significant (p = 0.052) and statistically significant to the other conditions. The upscaled condition showed also the lowest path efficiency, which was significantly worse than for "init 2" and the adapted model with suitable λ.

For the two subjects with congenital limb deficiency, similar trends as for the able-bodied subjects were observed, except that "congenital 2" performed relatively poor in all control conditions. Especially the condition "upscaled" showed very low performance in all metrics and the very high overshoot ratio and very low path efficiency confirmed that the control was rather unstable. After co-adaptive learning with suitable adaptation speed, both subjects with congenital limb deficiency performed as good as the able-bodied subjects. Moreover, the optimal learning constant was consistent between able-bodied subjects and those with limb deficiency ($\lambda = 0.995$).

5.3.6 Qualitative Observations

The cursor-traces and target hit maps for two representative able-bodied subjects and the two subjects with congenital limb deficiency are presented in figure 5.6. In the baseline condition ("I1") the black traces and the missed targets indicate that certain regions could not be reached. The accessible range remained almost unchanged in the second test of
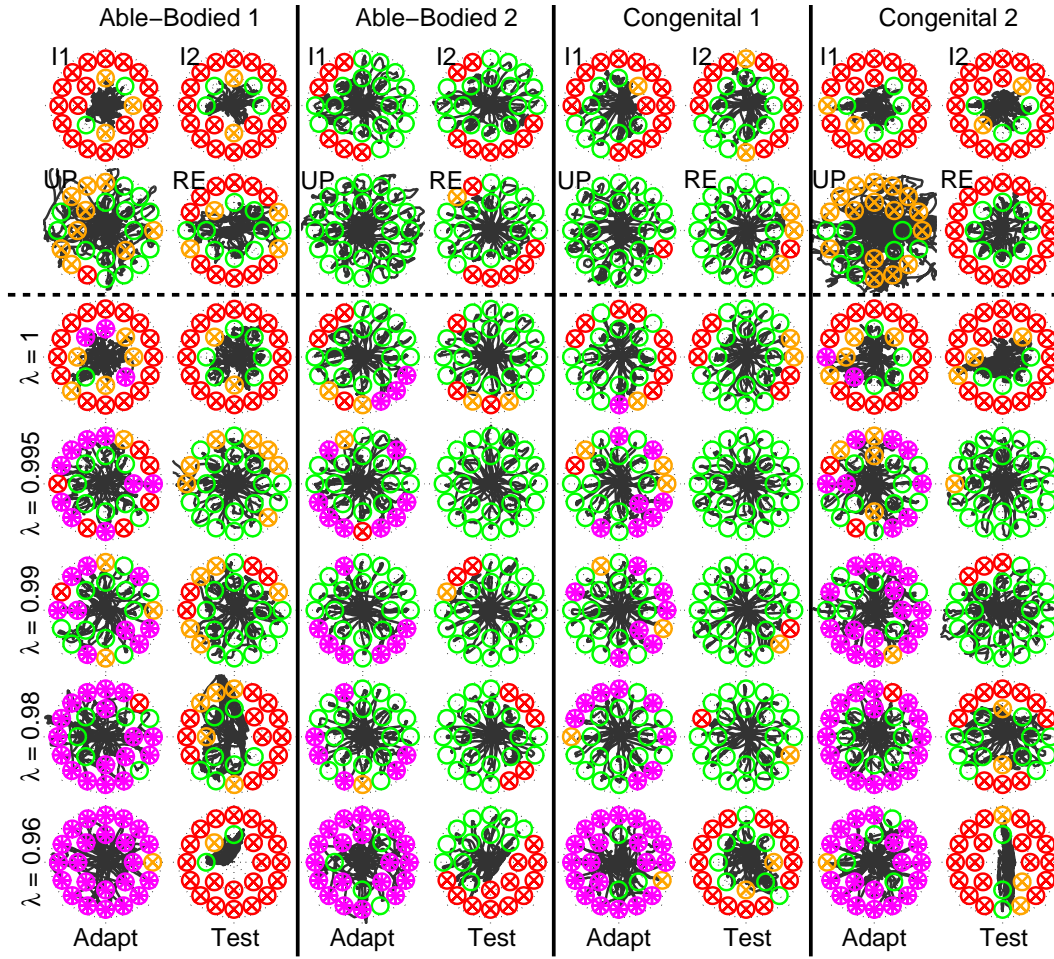
Figure 5.6: Representative qualitative visualization of control performance for two able-bodied subjects with relatively low (able-bodied 1) and high (able-bodied 2) initial performance and for the two subjects with congenital limb deficiency. The black curves show the traces of the control cursor, green circles represent successfully hit targets, red circles missed targets and orange circles targets that were entered but not hit because of insufficient dwell time. For the adaptation runs green circles represent targets that were hit before adaptation started, violet circles targets that were hit during the adaptation phase and red circles targets that were missed despite adaptation. Above the dashed line the four control conditions are presented: Initial model tested in the beginning (I1) and towards the end of the session (I2), upscaled output (UP) and re-calibrated (RE). Below the adaptation runs with different learning constants λ are shown (Adapt) next to the evaluation runs to test the adapted models (Test). Best results were obtained after adaptation with $\lambda = 0.995$. The range became more uniform and covered in most cases the entire unit circle, while the control-stability was maintained.

the initial regression model, after the subject gained more experience with the control ("I2"). The repeated offline learning with new calibration runs recorded at the end of the session ("RE") could slightly improve the accessible range in some cases, but never solved that issue fully.

In the evaluation runs after real-time learning with $\lambda = 0.995$ the range improved for all subjects and became also more uniform, so that most targets could be hit or at least shortly entered (for able-bodied 1). For slower adaptation ($\lambda = 1$) the range increased only slightly, while too fast adaptation ($\lambda \geq 0.99$) led also to suboptimal ranges. The fastest adaptation speed ($\lambda = 0.96$) caused a poor and often very asymmetrical range. This indicates that the regressor overfitted to the last recent adaptation targets and "forgot" the relation between EMG features and output-space for other regions. Checking the (randomized) order in which the targets in these particular cases appeared confirmed that the accessible range was indeed formed by the last adaptation targets only.

Upscaling of the regression output ("UP") caused by definition an extended range of motion, so that all targets came into the accessible range. However, even if almost all targets could be entered at least once after upscaling, in many cases the user did not succeed in keeping the cursor within the target for one second, as required by the test. This indicates that the controllability was dramatically decreased and became much worse than in the tests after real-time learning with optimal adaptation speed. While the straight traces after real-time learning indicate that the subjects could approach the targets directly and with high confidence, the trace in the upscaled condition reveal that there were strong overshoots and that the subjects often had to correct the direction. No qualitative difference is observed between able-bodied subjects and those with congenital limb deficiency.

5.4 Demonstration in Prosthetic Application

To demonstrate that the methods described above are transferable into clinical practice, an embedded system for prosthetic control was developed. In the design of the embedded system, attention was payed to fulfill clinical and commercial requirements. I.e., the size, power-consumption and costs were minimized. An overview on the hardware and software components is given in figure 5.7.

5.4.1 Hardware

To match clinical requirements, simplify the integration of the electrodes to a prosthetic socket, and to ensure robustness against electromagnetic interferences and patient-safety [Webster, 2007], certified, commercially available electrodes (Otto Bock, 13E200) were used. These active, bipolar electrode modules incorporate amplifiers with adjustable gain, temporal filters and a rectification and low-pass filtering of the signals. Thus, the provided outputs form the mean absolute values (MAV) of the EMG signal, which can be directly
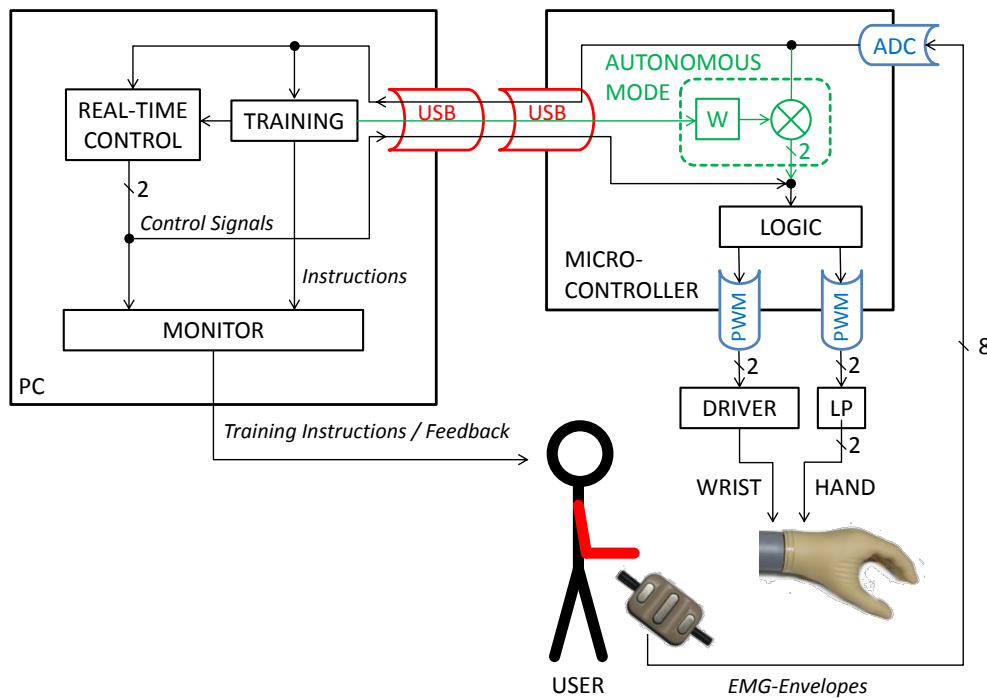
Figure 5.7: Block diagram of the embedded system for simultaneous and proportional real-time control of a prosthetic hand with two DOFs. After training with the support of a PC, the system run fully autonomously.

used as a feature for regression. As shown offline in the previous chapter, MAV features do not perform significantly worse than LOG-VAR features with a linear regressor.

A commercially available, certified prosthetic hand (Otto Bock, DMC Hand Plus) was used, in combination with a rotation unit (Otto Bock, Electric Wrist Rotator). The rechargeable 7.2 V, 900 mAh lithium-ion battery of the prosthetic hand was also used to power the embedded system.

An ATMEL ATXMEGA32-A4U was selected as microcontroller (MC). This 8 bit device can be operated with up to 32 MHz and has already most required components included, such as analog to digital converters (ADC), pulse-width modulated (PWM) outputs, a hardware multiplier, a calibrated R/C-oscillator, flash, EEPROM and SRAM memory and a USB-interface. A linear voltage regulator (Texas Instruments, TPS7233) was used with regulated output of 3.3 V, to transfer the prosthesis battery voltage into the operation range of the MC.

Two electrode signals were emulated for opening and closing, which are normally used as control-inputs in the standard clinical application (see section 2.3.1). This was done to control the prosthetic hand without any modifications on the device. The two required
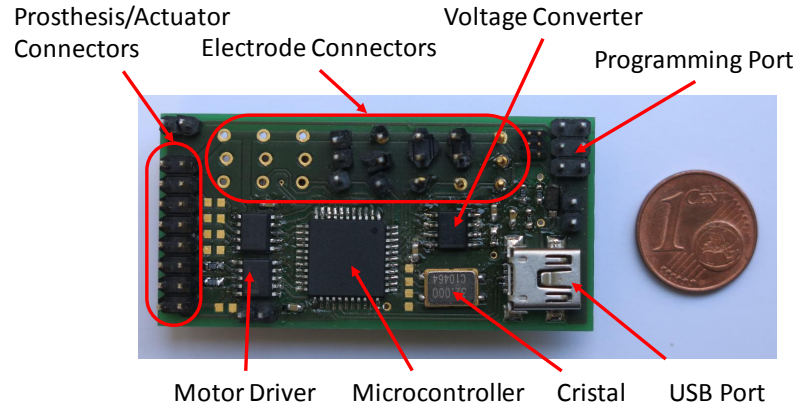
Figure 5.8: Miniaturized version of the embedded system

analog signals were generated by smoothing two PWM signals with passive RC low-pass filters. The rotation unit is driven proportionally by a motor driver IC (ON Semiconductor, LV8548MC), which is controlled by PWM signals and provides the required currents for the rotation motor.

A picture of the assembled printed circuit board of the embedded system is shown in figure 5.8. With a size of $56 \times 28 \times 15$ mm and a weight of 10 g it can be easily integrated into a prosthetic socket. The costs are approximately 10 € and the power consumption at 7.2 V is 15 mA plus 650 μA for each electrode module.

5.4.2 Software

As training of the machine (and the user) is significantly easier with the visualization possibilities offered by a computer screen, in the chosen design this is still done with the support of a PC. This complies with the clinical practice, which for many prosthetic devices supports or even requires the use of a PC.

The same MATLAB framework is used for training as in the experiments described in section 5.3. The two DOFs are mapped into the two functions of the prosthesis, hand open/close and rotation. The software framework was extended by another data-acquisition class, which allows to use the embedded system as input device. In this way, all tools, including the co-adaptive learning paradigm are available also in combination with the embedded system. Once, a linear regression model has been trained, it can be tested with the prosthesis by sending control signals via USB to the prosthesis. When training is finished, the regression coefficients are transmitted to the embedded system and stored permanently in the EEPROM. Then the embedded system is disconnected from the PC and runs in an autonomous mode. The acquired electrode signals are directly mapped into control signals for the prosthesis. All operations were implemented in 16 bit fixed-point operations with an update rate of 25 Hz. In the power-on sequence of the firmware
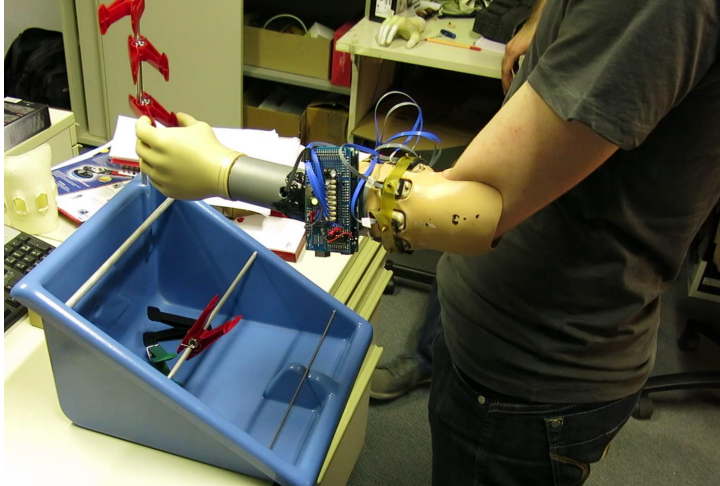
Figure 5.9: Evaluation of the first prototype of the embedded system on a subject with transradial amputation in the standardized "clothes-pin test" that requires the use of both DOFs. The subject was able to quickly and safely replace the pins from the vertical to the horizontal bar and vice versa and the movements appeared very smooth and natural.

the stored regression model is automatically loaded from EEPROM and the autonomous mode is started. Therefore, the device can be used as simple as a conventional prosthesis, once it is configured and intermediately switched off to recharge the battery without any need for a PC.

5.4.3 Evaluation on subject with transradial amputation

A prototype of the system was tested on one subject with transradial hand amputation (male, 25 years). Eight electrodes were integrated into a customized socket on which the prosthesis was mounted. After a short training period that involved three calibration runs and one adaption run with $\lambda = 0.995$ in neutral arm position (arm down), the user could accurately control the speed for both DOFs of the prosthesis simultaneously and independently. As a smooth transition between the activation of both DOFs was possible, the movements appeared very fluent and natural. Also single activations of both DOFs were possible in both directions, without unintended simultaneous activations. No decrease in performance was observed when the arm position was changed, during walking, after donning and doffing the socket, or using the trained model on another day.

In a preliminary evaluation with the standardized clothes pin test [Kuiken et al., 2004], in which the subject was asked to pick up three clothes pins from a horizontal bar, rotate them and place them on a vertical bar he required 10.6 s $\pm$ 0.6 s (mean $\pm$ std) — a result that compares very competitively to the literature [Amsuess et al., 2014a].

5.5 Discussion

In this chapter, it was shown that by using computationally efficient linear regression techniques, two degrees of freedom could be controlled in real-time by all tested able bodied subjects and two individuals with upper limb deficiency. A novel co-adaptive learning based paradigm was introduced, which proved to be efficient and beneficial compared to conventional offline calibration. In this approach both the human and the machine learner are provided with a common target and real-time feedback of the estimated position in 2D. The paradigm was defined such, that machine adaptation was limited to problematic targets, resulting in improvements particularly for those regions. In conventional training approaches, any improvement of the machine learning model require a retraining with new calibration data [Simon et al., 2012]. When feedback is provided only in the testing phase, and not during the collection of training samples, the learning of the users and the algorithm are interleaved and the user can only very slowly adjust his contraction patterns. Thus, many iterations of sequential user and machine adaptation may be required until the performance converges on a satisfying level. In the presented adaptation paradigm the machine learning model is updated at the same time as the user learns to adjust muscle contractions to reach the desired target. The experiment demonstrated that this co-adaptive learning approach leads in most cases within very short time to a well performing and stable control.

5.5.1 Learning Speed

A crucial trade-off in co-adaptive learning is that between stability and speed of adaptation [Vidaurre et al., 2011a]. If the machine learner is adapting too fast, the system may become instable. If it is adapting too slow, only little improvements may be achieved within a given time. In the presented study this trade-off was regulated by the learning constant of the recursive least-squares algorithm. It was found that all subjects (able-bodied and with congenital limb-deficiency) achieved best performance with a similar learning constant, suggesting that this parameter is fundamentally the same and should be applicable to most individuals. This means that the time-consuming parameter optimization could be omitted, which would make the suggested approach very efficient. Within very short time the human and the machine can concurrently learn and a good regression model is obtained as an outcome.

5.5.2 Alternative Approaches

The co-adaptive learning strategy was compared with several alternative approaches. The same conventionally open-loop trained model as in the baseline condition "init 1" was tested a second time towards the end of the experiment to evaluate effects of pure user-learning. As each of the five adaptation runs started with this model, the user had rela-

tively large amount of time to learn how to overcome the limitations of the initial regression model, by adapting the muscle contractions. The fact, that no significant improvements were found in this test, showed that limitations of the initial regression-model could not be compensated by the user within the investigated time. With the repeated open-loop calibration, one iteration of interleaved user and machine adaptation was executed. This resulted only in relatively small improvements, which were not significant for most performance metrics. Repeating this interleaved adaptation procedure several times, as previously suggested [Powell et al., 2014], may lead to further improvements, but is a very time-consuming procedure. In contrast, the proposed co-adaptive learning approach required only one run of concurrent user and machine adaptation to converge in a good performance.

One of the major problems in the open loop trained model was a limited range of motion (30% to 80% of the maximal range for some directions). This may be at least partly caused by inaccurate data-labels, due to the abandonment of a motion tracking system, which would not be applicable to bilateral amputees. A heuristic compensation approach was tested by upscaling of the regression output with an individually determined factor to reach all regions of the unit circle, in which the targets appeared. This did not solve the problem, as it resulted in a loose of fine-control. This means that the extended range was acquired with the price of reduced stability. In contrast, subsequent co-adaptation compensated for the initial miss-calibration and led typically to an extended motion-range while maintaining the possibility of fine-control.

5.5.3 Clinical Applicability

Attention was paid in the design of the experiments, desribed in section 5.3, to fulfill clinical requirements. Even if gel-electrodes provide a better signal quality [Clancy et al., 2002], a dry electrode system was selected, as only dry electrodes are suitable for an application in prosthetics. Further, a motion tracking system was omitted, which aside of concerns about cost, is not applicable to bilateral amputees, who stand to benefit the most from advanced hand prostheses. Finally, very efficient linear processing techniques were used that provide minimal latency and can be readily implemented in low-power and low-cost digital hardware required for a clinical application [Jiang et al., 2012a].

Section 5.4 demonstrated the usability of the presented approach in a prosthetic application. Miniaturized EMG electrode modules from conventional myoprostheses were used, which can be integrated into a prosthetic socket, instead of the 24 bit low noise desktop biosignal amplifier. The computations, that are required for the control, were reduced to 16 bit fixed-point operations in order to be executed on a miniaturized embedded system with a low-power, low-cost 8 bit microcontroller that fulfills clinical requirements. It has been shown previously in real-world tasks with a physical prosthetic device, that for 90 % of the users an additional processing delay of 100 - 125 ms has no influence on the performance [Farrell and Weir, 2007]. The additional reaction time of the presented em-

bedded system compared to the conventional control is around 40 ms in the autonomous mode, which is clearly within the acceptable range and was not noticed by the user.

In the preliminary tests a robust control was possible even when disturbing factors such as altered arm position, the weight of the prosthesis or donning and doffing of the socket were introduced. If these initial results will be confirmed also in permanent use, this critical clinical requirement is fulfilled.

One of the major complains of powered hand prostheses is weight [Kejlaa, 1993]. Therefore, many amputees and persons with congenital limb deficiency prefer to use a significantly lighter cosmetic prosthesis without any active functionality or refuse to use a prosthesis completely. Depending on the model and size, the weight of a commercially available prosthetic hand is in the range of 350-600 g [Belter et al., 2013]. Additionally 200-400 g have to be counted for the socket with integrated electrodes and 50-150 g for the rechargeable battery. The battery is usually dimensioned to operate the device for an entire day and the majority of the power is consumed by the motors that actuate the prosthesis. With only 10 g, the additional weight of the embedded system is negligible. Due to the low power-consumption and the possibility to supply the system with the prosthesis battery, also indirect weight increase due the need for additional batteries is avoided.

Once the locations for EMG detection are defined and the electrodes are integrated into the socket, the system can be worn and used as a conventional myoelectric prosthesis, i.e. the complexity for the user is sufficiently low for a clinical application. The fitting process with the presented system on the other hand is significantly more complex as for a conventional myoelectric prosthesis. The identification of suitable electrode locations, user-training and algorithmic calibration may become challenging when the methods would be used clinically in a larger scale. In future work this procedure should be automatized as far as possible to reduce the likelihood of fitting problems. Channel-selection algorithms in combination with a high density electrode grid such as the one proposed in [Hwang et al., 2014a] could support this process.

5.5.4 Limitations and Future Work

It was shown that co-adaptive learning can be used as an efficient tool to let the human and a regression model converge in a common, well performing control strategy. However, this was demonstrated for the two DOFs flexion/extension and radial/ulnar deviation only. It remains to be investigated if the linear approach is also sufficient for other movements and when the number of DOFs is increased. E.g. a rotation of the wrist, which is still possible for many amputees and individuals with congenital limb deficiency, can cause a re-orientation of the forearm muscles. This may result in a non-linear interaction between individual DOFs when simultaneously activated. Therefore, non-linear regression methods may be required. But integrating this into the presented framework is straight-forward, since real-time learning algorithms are available also for many non-linear regression techniques [Nishikawa et al., 2001, Gijsberts et al., 2014]. With increas-

ing number of DOFs the presented strategy to adapt explicitly for problematic regions is expected to be particularly efficient, as the amount of combined movements grows exponentially with the number of DOFs, making it practically impossible to collect training data for all combinations.

To prove that the system is reliable enough for a daily use, long-term tests with more subjects under real-world conditions and a systematical investigation of the robustness are required: The influence of some of the disturbing factors such as altered arm positions and electrode shifts should be quantified in specially designed laboratory experiments. However, additional factors like sweat, variations of the stump-volume or other, yet unknown factors, may show up outside the laboratory and during long-term use only. Also a judgment of the users is required after long term tests and a careful comparison with the clinical state of the art .

6 Summary and Conclusion

The concept of using EMG signals to control powered upper limb prostheses was introduced 1948 by Reiter and the proposed technique, based on two bipolar electrodes that allows for controlling only one function at a time, is still the clinical state of the art. Several decades of research on more advanced control systems had relatively little impact on the clinical practice because most proposed techniques failed under realistic conditions. Many studies have been conducted fully offline, did not consider clinically important factors and were done on able-bodied subjects only. The aim of the work presented in this thesis is to develop robust machine learning based control techniques that fulfill the clinical requirements and are therefore clinically applicable.

Classification-based approaches, that have been the focus of research since many decades, achieved very high performance under stable conditions but often collapsed when disturbing factors were introduced, which occur under real-worlds conditions. The work presented in chapter 3 aimed to increase the robustness of the classification-based control approach. Optimized spatial filters, which maximize the difference in variance between classes in raw-signal domain, were introduced to myoelectric control. In particular three multiclass extensions were investigated, namely *one vs. one*, *one vs. rest* and *joint diagonalization* of the common spatial pattern algorithm.

The accuracy and robustness against two important factors, that impair the performance in real-world conditions, were investigated on experimental data with particularly introduced variations of the arm position and artificially added noise. The *one vs. one* and the *one vs. rest* extension led to a significantly improved performance and a higher robustness against noise compared to the conventional approach without spatial filters.

Moreover, by transferring the backward models of the spatial filters into forward models, the locations of underlying components, that are most relevant for classification, are discovered and allow for a physiological interpretation of the learned filter coefficients. It was found that the regions of best discrimination do not necessarily coincide with the regions of strongest muscle-activity. Instead, other regions, possibly related to smaller, deeper, or synergistically activated muscles provide in some cases better information to distinguishes the movements.

Chapter 4 provided a detailed and thorough comparison of regression techniques, which allows for simultaneous and proportional control of multiple DOFs. It was demonstrated that the relationship between wrist angles and the EMG variance is rather non-linear, which requires computationally expensive non-linear regression techniques like neuronal networks or kernel ridge regression. By transforming the variance-features with

simple non-linear transformations, like the square-root or a logarithmic function, the relationship between features and wrist-angles can be linearized, which allows for using computationally very efficient linear regression techniques. A mixture of linear experts was introduced, to compensate for additional non-linearities that are caused by the fact that for antagonistic movements within the same DOF different muscles are required. This is an extension of linear regression, which splits the problem into two linear sections per DOF. The results were consistent between able-bodied subjects and an individual with congenital limb deficiency.

A special focus was given to the analysis of practical relevant factors. For the first time a systematic investigation regarding the amount and the diversity of data was provided, which is needed to train regression-based myoelectric controllers. It was found that the absolute amount of training samples investigated within a practical meaningful range has a strong influence on the performance, but that the diversity of the training movements has almost no influence. Even if only individual movements were used in the training, most combined movements were estimated well even with linear methods. This shows that the two investigated wrist-DOFs are separable, i.e. they can be trained individually and superimpose linearly. Since potential users of myoelectric prostheses are often not able to execute precise combined movements without the intrinsic feedback of the missing limb, this finding is of very high practical relevance.

A real-time system for simultaneous and proportional control was developed, based on these results, and presented in chapter 5. After calibrating the system in a way that is also suitable for most prosthetic users, based on individual movements and without using motion tracking, most subjects were able to simultaneously control 2 degrees of freedom, but certain regions could often not be reached. A novel real-time learning paradigm was introduced, in which the regression model is adapted in a supervised manner while the regression output is provided as visual feedback to the user. As the user immediately reacts on the provided feedback, this leads to a co-adaptation between the controller and the user. When a proper adaptation speed is chosen, the control significantly improves within short time. Moreover, the optimal range for the critical choice of the learning constant was consistent between most able-bodied subjects and the two individuals with congenital limb-deficiency.

An embedded system was developed for a prosthetic hand with two degrees of freedom, to prove that the presented techniques for simultaneous and proportional control are clinically applicable. A test was conducted on a user with transradial amputation and a physical hand prosthesis, mounted to a prosthetic socket with integrated electrodes. He was able to control the two functions, open/close and wrist rotation independently and reliably, also during walking, in altered arm positions and when using the same regression model on a second day without retraining.

In conclusion, a simple and efficient machine learning based system was developed for independent simultaneous and proportional myoelectric control of two DOFs, which is practical applicable. It can be used in combination with commercially available prosthetic

components and provides great improvements compared to the clinical state of the art. In combination with the presented learning strategy it is expected to be useful for a large number of end-users.

Bibliography

[Al-Faiz and Al-Mashhadany, 2009] Al-Faiz, M. and Al-Mashhadany, Y. (2009). Human arm movements recognition based on emg signal. *MASAUM Journal Of Basic and Applied Sciences (MJBAS)*, 1(2):164–171.

[Al-Timemy et al., 2013] Al-Timemy, A., Bugmann, G., Escudero, J., and Outram, N. (2013). A preliminary investigation of the effect of force variation for myoelectric control of hand prosthesis. In *Engineering in Medicine and Biology Society (EMBC), 2013 35th Annual International Conference of the IEEE*, pages 5758–5761.

[Almström et al., 1981] Almström, C., Herberts, P., and Körner, L. (1981). Experience with swedish multifunctional prosthetic hands controlled by pattern recognition of multiple myoelectric signals. *International Orthopaedics*, 5(1):15–21.

[Ameri et al., 2014a] Ameri, A., Kamavuako, E. N., Scheme, E. J., Englehart, K. B., Parker, P., et al. (2014a). Support vector regression for improved real-time, simultaneous myoelectric control. *Neural Systems and Rehabilitation Engineering, IEEE Transactions on*, 22(6):1198–1209.

[Ameri et al., 2014b] Ameri, A., Kamavuako, E. N., Scheme, E. J., Englehart, K. B., and Parker, P. A. (2014b). Real-time, simultaneous myoelectric control using visual target-based training paradigm. *Biomedical Signal Processing and Control*, 13:8–14.

[Ameri et al., 2014c] Ameri, A., Scheme, E., Kamavuako, E., Englehart, K., and Parker, P. (2014c). Real-time, simultaneous myoelectric control using force and position-based training paradigms. *Biomedical Engineering, IEEE Transactions on*, 61(2):279–287.

[Amsuess et al., 2014a] Amsuess, S., Gobel, P., Graimann, B., and Farina, D. (2014a). A multi-class proportional myocontrol algorithm for upper limb prosthesis control: Validation in real-life scenarios on amputees. *Neural Systems and Rehabilitation Engineering, IEEE Transactions on*, 23(5):827–836.

[Amsuess et al., 2014b] Amsuess, S., Goebel, P., Graimann, B., and Farina, D. (2014b). Extending mode switching to multiple degrees of freedom in hand prosthesis control is not efficient. In *Engineering in Medicine and Biology Society (EMBC), 2014 36th Annual International Conference of the IEEE*, pages 658–661.

[Amsuss et al., 2013] Amsuss, S., Paredes, L. P., Rudigkeit, N., Graimann, B., Herrmann, M. J., and Farina, D. (2013). Long term stability of surface emg pattern classification for prosthetic control. In *Engineering in Medicine and Biology Society (EMBC), 2013 35th Annual International Conference of the IEEE*, pages 3622–3625. IEEE.

[Baker et al., 2010] Baker, J., Scheme, E., Englehart, K., Hutchinson, D., and Greger, B. (2010). Continuous detection and decoding of dexterous finger flexions with implantable MyoElectric sensors. *Neural Systems and Rehabilitation Engineering, IEEE Transactions on*, 18(4):424–432.

[Belter et al., 2013] Belter, J. T., Segil, J. L., Dollar, A. M., and Weir, R. F. (2013). Mechanical design and performance specifications of anthropomorphic prosthetic hands: a review. *Journal of rehabilitation research and development*, 50(5):599–618.

[Berlichingen-Rossach, 1861] Berlichingen-Rossach, F. W. G. (1861). *Geschichte des Ritters Götz von Berlichingen mit der eisernen Hand und seiner Familie.* FA Brockhaus.

[Berning et al., 2014] Berning, K., Cohick, S., Johnson, R., Miller, L. A., and Sensinger, J. W. (2014). Comparison of body-powered voluntary opening and voluntary closing prehensor for activities of daily life. *Journal of Rehabilitation Research and Development*, 51(2):253–261.

[Bishop, 2007] Bishop, C. M. (2007). *Pattern Recognition and Machine Learning (Information Science and Statistics).* Springer.

[Blankertz et al., 2011] Blankertz, B., Lemm, S., Treder, M., Haufe, S., and Müller, K.-R. (2011). Single-trial analysis and classification of ERP components–a tutorial. *NeuroImage*, 56(2):814–825.

[Blankertz et al., 2008] Blankertz, B., Tomioka, R., Lemm, S., Kawanabe, M., and Müller, K.-R. (2008). Optimizing spatial filters for robust EEG Single-Trial analysis. *Signal Processing Magazine, IEEE*, 25(1):41–56.

[Buchthal and Schmalbruch, 1980] Buchthal, F. and Schmalbruch, H. (1980). Motor unit of mammalian muscle. *Physiol Rev*, 60(1):90–142.

[Buerkle et al., 2006] Buerkle, V. R., Englehart, K., and Hudgins, B. (2006). Pattern recognition of single and combined motions from the shoulder complex. In *Engineering in Medicine and Biology Society (EMBC), 2006 28th Annual International Conference of the IEEE*, pages 3419–3422.

[Bunderson et al., 2012] Bunderson, N. E., Kuiken, T., et al. (2012). Quantification of feature space changes with experience during electromyogram pattern recognition control. *Neural Systems and Rehabilitation Engineering, IEEE Transactions on*, 20(3):239–246.

[Castellini et al., 2009] Castellini, C., Gruppioni, E., Davalli, A., and Sandini, G. (2009). Fine detection of grasp force and posture by amputees via surface electromyography. *Journal of Physiology, Paris*, 103(3):255–262.

[Castellini and van der Smagt, 2009] Castellini, C. and van der Smagt, P. (2009). Surface EMG in advanced hand prosthetics. *Biological Cybernetics*, 100(1):35–47.

[Chen et al., 2013] Chen, X., Zhang, D., and Zhu, X. (2013). Application of a self-enhancing classification method to electromyography pattern recognition for multifunctional prosthesis control. *Journal of NeuroEngineering and Rehabilitation*, 10(1):44.

[Chi et al., 2010] Chi, Y. M., Jung, T.-P., and Cauwenberghs, G. (2010). Dry-contact and noncontact biopotential electrodes: methodological review. *Biomedical Engineering, IEEE Reviews in*, 3:106–119.

[Chu et al., 2006] Chu, J. U., Moon, I., and Mun, M. S. (2006). A real-time EMG pattern recognition system based on linear-nonlinear feature projection for a multifunction myoelectric hand. *Biomedical Engineering, IEEE Transactions on*, 53(11):2232–2239.

[Cipriani et al., 2011a] Cipriani, C., Controzzi, M., and Carrozza, M. C. (2011a). The SmartHand transradial prosthesis. *Journal of NeuroEngineering and Rehabilitation*, 8(1):29.

[Cipriani et al., 2011b] Cipriani, C., Sassu, R., Controzzi, M., and Carrozza, M. C. (2011b). Influence of the weight actions of the hand prosthesis on the performance of pattern recognition based myoelectric control: Preliminary study. In *Engineering in Medicine and Biology Society (EMBC), 2011 33th Annual International Conference of the IEEE*, pages 1620–1623. IEEE.

[Clancy et al., 2002] Clancy, E. A., Morin, E. L., and Merletti, R. (2002). Sampling, noise-reduction and amplitude estimation issues in surface electromyography. *Journal of Electromyography and Kinesiology*, 12(1):1–16.

[Coapt-LLC, 2015] Coapt-LLC (2015). Coapt - complete control. Available Online: http://coaptengineering.com, Accessed: Apr 21, 2015.

[Despopoulos and Silbernagl, 2003] Despopoulos, A. and Silbernagl, S. (2003). *Color atlas of physiology*. Thieme.

[Dillingham et al., 1998] Dillingham, T. R., Pezzin, L. E., and MacKenzie, E. J. (1998). Incidence, acute care length of stay, and discharge to rehabilitation of traumatic amputee patients: an epidemiologic study. *Archives of physical medicine and rehabilitation*, 79(3):279–287.

[Disselhorst-Klug et al., 1997] Disselhorst-Klug, C., Silny, J., and Rau, G. (1997). Improvement of spatial resolution in surface-EMG: a theoretical and experimental comparison of different spatial filters. *Biomedical Engineering, IEEE Transactions on*, 44(7):567–574.

[Dornhege et al., 2004] Dornhege, G., Blankertz, B., Curio, G., and Müller, K.-R. (2004). Boosting bit rates in noninvasive EEG single-trial classifications by feature combination and multiclass paradigms. *Biomedical Engineering, IEEE Transactions on*, 51(6):993–1002.

[Dornhege et al., 2007] Dornhege, G., del R. Millán, J., Hinterberger, T., McFarland, D. J., and Müller, K.-R. (2007). *Toward Brain-Computer Interfacing*, pages 207–233. Cambridge: The MIT Press.

[Englehart et al., 2001] Englehart, K., Hudgin, B., and Parker, P. A. (2001). A wavelet-based continuous classification scheme for multifunction myoelectric control. *Biomedical Engineering, IEEE Transactions on*, 48(3):302–311.

[Englehart and Hudgins, 2003] Englehart, K. and Hudgins, B. (2003). A robust, real-time control scheme for multifunction myoelectric control. *Biomedical Engineering, IEEE Transactions on*, 50(7):848–854.

[Farina et al., 2003] Farina, D., Arendt-Nielsen, L., Merletti, R., Indino, B., and Graven-Nielsen, T. (2003). Selectivity of spatial filters for surface EMG detection from the tibialis anterior muscle. *Biomedical Engineering, IEEE Transactions on*, 50(3):354–364.

[Farina et al., 2014] Farina, D., Jiang, N., Rehbaum, H., Holobar, A., Graimann, B., Dietl, H., and Aszmann, O. (2014). The extraction of neural information from the surface EMG for the control of upper-limb prostheses: Emerging avenues and challenges. *Neural Systems and Rehabilitation Engineering, IEEE Transactions on*, 22(4):797–809.

[Farrell and Weir, 2007] Farrell, T. R. and Weir, R. F. (2007). The optimal controller delay for myoelectric prostheses. *Neural Systems and Rehabilitation Engineering, IEEE Transactions on*, 15(1):111–118.

[Fite et al., 2008] Fite, K., Withrow, T., Shen, X., Wait, K., Mitchell, J., and Goldfarb, M. (2008). A gas-actuated anthropomorphic prosthesis for transhumeral amputees. *IEEE Transactions on Robotics*, 24(1):159–169.

[Fougner et al., 2011] Fougner, A., Scheme, E., Chan, A., Englehart, K., and Stavdahl, O. (2011). Resolving the limb position effect in myoelectric pattern recognition. *Neural Systems and Rehabilitation Engineering, IEEE Transactions on*, 9(6):644–651.

[Fougner et al., 2012] Fougner, A., Stavdahl, O., Kyberd, P., Losier, Y., and Parker, P. (2012). Control of upper limb prostheses: Terminology and proportional myoelectric control #x2014;a review. *Neural Systems and Rehabilitation Engineering, IEEE Transactions on*, 20(5):663–677.

[Fougner et al., 2014] Fougner, A. L., Stavdahl, Ø., and Kyberd, P. J. (2014). System training and assessment in simultaneous proportional myoelectric prosthesis control. *Journal of neuroengineering and rehabilitation*, 11(1):75.

[Funahashi, 1989] Funahashi, K.-I. (1989). On the approximate realization of continuous mappings by neural networks. *Neural networks*, 2(3):183–192.

[Geng et al., 2012] Geng, Y., Tao, D., Chen, L., and Li, G. (2012). Recognition of combined arm motions using support vector machine. In *Informatics in Control, Automation and Robotics*, number 133 in Lecture Notes in Electrical Engineering, pages 807–814. Springer.

[Gijsberts et al., 2014] Gijsberts, A., Bohra, R., González, D. S., Werner, A., Nowak, M., Caputo, B., Roa, M. A., and Castellini, C. (2014). Stable myoelectric control of a hand prosthesis using non-linear incremental learning. *Frontiers in neurorobotics*, 8(1):1–8.

[Glaser et al., 2013] Glaser, V., Holobar, A., and Zazula, D. (2013). Real-time motor unit identification from high-density surface emg. *Neural Systems and Rehabilitation Engineering, IEEE Transactions on*, 21(6):949–958.

[Graupe and Cline, 1975] Graupe, D. and Cline, W. K. (1975). Functional separation of emg signals via arma identification methods for prosthesis control purposes. *Systems, Man and Cybernetics, IEEE Transactions on*, (2):252–259.

[Gray, 1918] Gray, H. (1918). *Anatomy of the human body*, chapter 4, pages 1821–1865. Philadelphia: Lea & Febiger.

[Greenhouse and Geisser, 1959] Greenhouse, S. W. and Geisser, S. (1959). On methods in the analysis of profile data. *Psychometrika*, 24(2):95–112.

[Hahne et al., 2014a] Hahne, J. M., Biessmann, F., Jiang, N., Rehbaum, H., Meinecke, F., Müller, K.-R., Farina, D., and Parra, L. (2014a). Linear and non-linear regression techniques for simultaneous and proportional myoelectric control. *Neural Systems and Rehabilitation Engineering, IEEE Transactions on*, 22(2):269–279.

[Hahne et al., 2014b] Hahne, J. M., Dahne, S., Farina, D., Parra, L., and Müller, K.-R. (2014b). Separability of wrist motions in simultaneous and proportional myoelectric control. In *Bernstein Conference, Göttingen, 2015*.

[Hahne et al., 2015a] Hahne, J. M., Dahne, S., Hwang, H.-J., Müller, K.-R., and Parra, L. (2015a). Concurrent adaptation of human and machine improves simultaneous and proportional myoelectric control. *Neural Systems and Rehabilitation Engineering, IEEE Transactions on*, 23(4):618–627.

[Hahne et al., 2012a] Hahne, J. M., Graimann, B., and Müller, K.-R. (2012a). Spatial filtering for robust myoelectric control. *Biomedical Engineering, IEEE Transactions on*, 59(5):1436–1443.

[Hahne et al., 2010] Hahne, J. M., Herrmann, M., Hofmann, D., Paulus, M., and Graimann, B. (2010). Electrode configuration for multifunctional myoprostheses. In *The 18th Congress of the International Society of Electrophysiology and Kinesiology*, Aalborg, Denmark.

[Hahne et al., 2015b] Hahne, J. M., Müller, K.-R., and Farina, D. (2015b). An embedded system for simultaneous and proportional myoelectric control of upper limb prostheses. In *Engineering in Medicine and Biology Society (EMBC), 2015 37th Annual International Conference of the IEEE*.

[Hahne et al., 2012b] Hahne, J. M., Rehbaum, H., Biessmann, F., Meinecke, F., Müller, K.-R., Jiang, N., Farina, D., and Parra, L. (2012b). Simultaneous and proportional control of 2D wrist movements with myoelectric signals. In *2012 IEEE International Workshop on Machine Learning for Signal Processing (MLSP)*.

[Hannaford and Lehman, 1986] Hannaford, B. and Lehman, S. (1986). Short time fourier analysis of the electromyogram: fast movements and constant contraction. *Biomedical Engineering, IEEE Transactions on*, (12):1173–1181.

[Hargrove et al., 2008] Hargrove, L., Englehart, K., and Hudgins, B. (2008). A training strategy to reduce classification degradation due to electrode displacements in pattern recognition based myoelectric control. *Biomedical Signal Processing and Control*, 3(2):175–180.

[Hastie et al., 2003] Hastie, T., Tibshirani, R., and Friedman, J. H. (2003). *The Elements of Statistical Learning*, chapter 7, pages 241–245. New York: Springer, corrected edition.

[Haufe et al., 2014] Haufe, S., Meinecke, F., Görgen, K., Dähne, S., Haynes, J.-D., Blankertz, B., and Biessmann, F. (2014). On the interpretation of weight vectors of linear models in multivariate neuroimaging. *NeuroImage*, 87:96–110.

[Hayes, 1996] Hayes, M. H. (1996). *Statistical digital signal processing and modeling*, pages 541–553. John Wiley & Sons, New York.

[He et al., 2015] He, J., Zhang, D., Jiang, N., Sheng, X., Farina, D., and Zhu, X. (2015). User adaptation in long-term, open-loop myoelectric training: implications for EMG pattern recognition in prosthesis control. *Journal of Neural Engineering*, 12(4):046005.

[He et al., 2012] He, J., Zhang, D., and Zhu, X. (2012). Adaptive pattern recognition of myoelectric signal towards practical multifunctional prosthesis control. In *Intelligent Robotics and Applications*, number 7506 in Lecture Notes in Computer Science, pages 518–525. Springer Berlin Heidelberg.

[Herberts et al., 1968] Herberts, P., Kadefors, R., Kaiser, E., and PetersÃľn, I. (1968). Implantation of micro-circuits for myo-electric control of prostheses. *The Journal of Bone and Joint Surgery. British Volume*, 50(4):780–91.

[Holobar et al., 2010] Holobar, A., Minetto, M. A., Botter, A., Negro, F., and Farina, D. (2010). Experimental analysis of accuracy in the identification of motor unit spike trains from high-density surface EMG. *Neural Systems and Rehabilitation Engineering, IEEE Transactions on*, 18(3):221–229.

[Hornik et al., 1989] Hornik, K., Stinchcombe, M., and White, H. (1989). Multilayer feedforward networks are universal approximators. *Neural networks*, 2(5):359–366.

[Huang et al., 2005] Huang, Y., Englehart, K. B., Hudgins, B., and Chan, A. D. C. (2005). A gaussian mixture model based classification scheme for myoelectric control of powered upper limb prostheses. *Biomedical Engineering, IEEE Transactions on*, 52(11):1801–1811.

[Hudgins et al., 1993] Hudgins, B., Parker, P., and Scott, R. N. (1993). A new strategy for multifunction myoelectric control. *Biomedical Engineering, IEEE Transactions on*, 40(1):82–94.

[Hwang et al., 2014a] Hwang, H.-J., Hahne, J. M., and Müller, K.-R. (2014a). Channel selection for simultaneous and proportional myoelectric prosthesis control of multiple degrees-of-freedom. *Journal of Neural Engineering*, 11(5):056008.

[Hwang et al., 2014b] Hwang, H.-J., Hahne, J. M., and Müller, K.-R. (2014b). Impact of arm position change on the performance of simultaneous and proportional myoelectric control. In *International BioMedical Engineering Conference (IBEC)*.

[James and Luff, 2006] James, J. and Luff, R. (2006). The amputee statistical database for the united kingdom. *National Amputee Statistical Database*, page 12.

[Jiang et al., 2012a] Jiang, N., Dosen, S., Müller, K.-R., and Farina, D. (2012a). Myoelectric control of artificial limbs; is there a need to change focus? *IEEE Signal Processing Magazine*, 29(5):149–152.

[Jiang et al., 2009] Jiang, N., Englehart, K. B., and Parker, P. A. (2009). Extracting simultaneous and proportional neural control information for multiple-DOF prostheses from the surface electromyographic signal. *IEEE Transactions on Bio-Medical Engineering*, 56(4):1070–1080.

[Jiang et al., 2014a] Jiang, N., Rehbaum, H., Vujaklija, I., Graimann, B., and Farina, D. (2014a). Intuitive, online, simultaneous and proportional myoelectric control over two degrees of freedom in upper limb amputees. *Neural Systems and Rehabilitation Engineering, IEEE Transactions on*, 22(3):501–510.

[Jiang et al., 2012b] Jiang, N., Vest-Nielsen, J. L., Muceli, S., and Farina, D. (2012b). EMG-based simultaneous and proportional estimation of wrist/hand dynamics in uni-lateral trans-radial amputees. *Journal of NeuroEngineering and Rehabilitation*, 9(1):42.

[Jiang et al., 2014b] Jiang, N., Vujaklija, I., Rehbaum, H., Graimann, B., and Farina, D. (2014b). Is accurate mapping of EMG signals on kinematics needed for precise online myoelectric control? *Neural Systems and Rehabilitation Engineering, IEEE Transactions on*, 22(3):549–558.

[Kejlaa, 1993] Kejlaa, G. (1993). Consumer concerns and the functional value of prostheses to upper limb amputees. *Prosthetics and orthotics international*, 17(3):157–163.

[Kelly et al., 1990] Kelly, M., Parker, P., and Scott, R. (1990). The application of neural networks to myoelectric signal analysis: a preliminary study. *Biomedical Engineering, IEEE Transactions on*, 37(3):221–230.

[Kuiken et al., 2004] Kuiken, T. A., Dumanian, G., Lipschutz, R., Miller, L., and Stubblefield, K. (2004). The use of targeted muscle reinnervation for improved myoelectric prosthesis control in a bilateral shoulder disarticulation amputee. *Prosthetics and Orthotics International*, 28(3):245–253.

[Kutzenberger and Hackl, 2006] Kutzenberger, E. and Hackl, P. (2006). *Jahrbuch der Gesundheitsstatistik: 2004*. Statistik österreich, 1st edition.

[Ledoit and Wolf, 2004] Ledoit, O. and Wolf, M. (2004). A well-conditioned estimator for large-dimensional covariance matrices. *Journal of Multivariate Analysis*, 88(2):365–411.

[Lemm et al., 2011] Lemm, S., Blankertz, B., Dickhaus, T., and Müller, K.-R. (2011). Introduction to machine learning for brain imaging. *Neuroimage*, 56(2):387–399.

[Lewis et al., 2013] Lewis, S., Russold, M., Dietl, H., Ruff, R., Audi, J., Hoffmann, K.-P., Abu-Saleh, L., Schroeder, D., Krautschneider, W., Westendorff, S., Gail, A., Meiners,

T., and Kaniusas, E. (2013). Fully implantable multi-channel measurement system for acquisition of muscle activity. *IEEE Transactions on Instrumentation and Measurement*, 62(7):1972–1981.

[Lorrain et al., 2011] Lorrain, T., Jiang, N., and Farina, D. (2011). Influence of the training set on the accuracy of surface EMG classification in dynamic contractions for the control of multifunction prostheses. *Journal of Neuroengineering and Rehabilitation*, 25(8):1–8.

[Marieb and Hoehn, 2013] Marieb, E. N. and Hoehn, K. (2013). *Human anatomy and physiology*. Pearson Education, 9th edition edition.

[Merletti et al., 2009] Merletti, R., Botter, A., Troiano, A., Merlo, E., and Minetto, M. A. (2009). Technology and instrumentation for detection and conditioning of the surface electromyographic signal: state of the art. *Clinical Biomechanics*, 24(2):122–134.

[Miguelez, 2011] Miguelez, J. M. (2011). Clinical experiences with the michelangelo hand, a four-year review. In *MyoElectric Controls/Powered Prosthetics Symposium, Fredericton, New Brunswick, Canada*.

[Montavon et al., 2012] Montavon, G., Orr, G. B., and Müller, K.-R. (2012). *Neural Networks: Tricks of the Trade, Reloaded*, volume 7700 of *Lecture Notes in Computer Science (LNCS)*. Springer, 2nd edition.

[Muceli and Farina, 2012] Muceli, S. and Farina, D. (2012). Simultaneous and proportional estimation of handkinematics from emg during mirrored movements at multipledegrees-of-freedom. *Neural Systems and Rehabilitation Engineering, IEEE Transactions on*, 20(3):371–378.

[Muceli et al., 2014] Muceli, S., Jiang, N., and Farina, D. (2014). Extracting signals robust to electrode number and shift for online simultaneous and proportional myoelectric control by factorization algorithms. *Neural Systems and Rehabilitation Engineering, IEEE Transactions on*, 22(3):623–633.

[Müller et al., 2003] Müller, K.-R., Anderson, C. W., and Birch, G. E. (2003). Linear and non-linear methods for brain-computer interfaces. *Neural Systems and Rehabilitation Engineering, IEEE Transactions on*, 11(2):165–169.

[Müller et al., 2001] Müller, K.-R., Mika, S., Ratsch, G., Tsuda, K., and Schölkopf, B. B. (2001). An introduction to kernel-based learning algorithms. *Neural Networks, IEEE Transactions on*, 12(2):181–201.

[Muzumdar, 2004] Muzumdar, A. (2004). *Powered upper limb prostheses: control, implementation and clinical application*. Springer.

[Nielsen et al., 2011] Nielsen, J. L., Holmgaard, S., Jiang, N., Englehart, K. B., Farina, D., and Parker, P. A. (2011). Simultaneous and proportional force estimation for multi-function myoelectric prostheses using mirrored bilateral training. *Biomedical Engineering, IEEE Transactions on*, 58(3):681–688.

[Nishikawa et al., 2001] Nishikawa, D., Yu, W., Yokoi, H., and Kakazu, Y. (2001). Online learning method for EMG prosthetic hand control. *Electronics and Communications in Japan (Part III: Fundamental Electronic Science)*, 84(10):35–46.

[Ortiz-Catalan et al., 2014] Ortiz-Catalan, M., Hakansson, B., and Branemark, R. (2014). Real-time and simultaneous control of artificial limbs based on pattern recognition algorithms. *Neural Systems and Rehabilitation Engineering, IEEE Transactions on*, 22(4):756–764.

[Oskoei and Hu, 2007] Oskoei, M. A. and Hu, H. (2007). Myoelectric control systems - a survey. *Biomedical Signal Processing and Control*, 2(4):275–294.

[Parker et al., 2006] Parker, P., Englehart, K., and Hudgins, B. (2006). Myoelectric signal processing for control of powered limb prostheses. *Journal of Electromyography and Kinesiology*, 16(6):541–548.

[Parra et al., 2005] Parra, L. C., Spence, C. D., Gerson, A. D., and Sajda, P. (2005). Recipes for the linear analysis of EEG. *NeuroImage*, 28(2):326–341.

[Pasquina et al., 2015] Pasquina, P. F., Evangelista, M., Carvalho, A., Lockhart, J., Griffin, S., Nanos, G., McKay, P., Hansen, M., Ipsen, D., Vandersea, J., et al. (2015). First-in-man demonstration of a fully implanted myoelectric sensors system to control an advanced electromechanical prosthetic hand. *Journal of neuroscience methods*, 244:85–93.

[Peerdeman et al., 2011] Peerdeman, B., Boere, D., Witteveen, H., Huis in 'tVeld, R., Hermens, H., Stramigioli, S., Rietman, H., Veltink, P., and Misra, S. (2011). Myoelectric forearm prostheses: State of the art from a user-centered perspective. *The Journal of Rehabilitation Research and Development*, 48(6):719.

[Pilarski et al., 2011] Pilarski, P., Dawson, M., Degris, T., Fahimi, F., Carey, J., and Sutton, R. (2011). Online human training of a myoelectric prosthesis controller via actor-critic reinforcement learning. In *2011 IEEE International Conference on Rehabilitation Robotics (ICORR)*.

[Powell et al., 2014] Powell, M., Kaliki, R. R., Thakor, N. V., et al. (2014). User training for pattern recognition-based myoelectric prostheses: Improving phantom limb movement consistency and distinguishability. *Neural Systems and Rehabilitation Engineering, IEEE Transactions on*, 22(3):522–532.

[Prabhav et al., 2014] Prabhav, N. R., Devasahayam, S. R., and Babu, K. S. (2014). Implanted myoneural interface for artificial hand control. *International Journal of Biomedical Engineering and Technology*, 14(1):13–33.

[Putti, 2005] Putti, V. (2005). Historical prostheses. *Journal of Hand Surgery (British and European Volume)*, 30(3):310–325.

[Radmand et al., 2014] Radmand, A., Scheme, E., and Englehart, K. (2014). A characterization of the effect of limb position on EMG features to guide the development of effective prosthetic control schemes. In *Engineering in Medicine and Biology Society (EMBC), 2014 36th Annual International Conference of the IEEE*, pages 662–667.

[Rahimi and Recht, 2008] Rahimi, A. and Recht, B. (2008). Weighted Sums of Random Kitchen Sinks: Replacing minimization with randomization in learning. In *NIPS*, pages 1313–1320.

[Ramoser et al., 2000] Ramoser, H., Muller-Gerking, J., and Pfurtscheller, G. (2000). Optimal spatial filtering of single trial eeg during imagined hand movement. *Rehabilitation Engineering, IEEE Transactions on*, 8(4):441–446.

[Reiter, 1948] Reiter, R. (1948). Eine neue elektrokunsthand. *Grenzgebiete der Medizin*, 1(4):133–135.

[Roy et al., 2007] Roy, S., De Luca, G., Cheng, M., Johansson, A., Gilmore, L., and De Luca, C. (2007). Electro-mechanical stability of surface EMG sensors. *Medical and Biological Engineering and Computing*, 45(5):447–457.

[Samek et al., 2012] Samek, W., Vidaurre, C., Müller, K.-R., and Kawanabe, M. (2012). Stationary common spatial patterns for brain–computer interfacing. *Journal of neural engineering*, 9(2):026013.

[Scheme and Englehart, 2011] Scheme, E. and Englehart, K. (2011). Electromyogram pattern recognition for control of powered upper-limb prostheses: state of the art and challenges for clinical use. *Journal of Rehabilitation Research and Development*, 48(6):643–659.

[Scheme et al., 2011] Scheme, E., Englehart, K., and Hudgins, B. (2011). Selective classification for improved robustness of myoelectric control under Non-Ideal conditions. *Biomedical Engineering, IEEE Transactions on*, 58(6):1698–1705.

[Scheme et al., 2014] Scheme, E., Lock, B., Hargrove, L., Hill, W., Kuruganti, U., and Englehart, K. (2014). Motion normalized proportional control for improved pattern recognition-based myoelectric control. *Neural Systems and Rehabilitation Engineering, IEEE Transactions on*, 22(1):149–157.

[Schölkopf et al., 1998] Schölkopf, B., Smola, A., and Müller, K.-R. (1998). Nonlinear component analysis as a kernel eigenvalue problem. *Neural computation*, 10(5):1299–1319.

[Schölkopf and Smola, 2002] Schölkopf, B. and Smola, A. J. (2002). *Learning with Kernels: Support Vector Machines, Regularization, Optimization, and Beyond*. MIT Press.

[Seeger, 2008] Seeger, M. (2008). Cross-validation optimization for large scale structured classification kernel methods. *Journal of Machine Learning Research*, 9:1147–1178.

[Sensinger et al., 2009] Sensinger, J. W., Lock, B. A., and Kuiken, T. A. (2009). Adaptive pattern recognition of myoelectric signals: exploration of conceptual framework and practical algorithms. *Neural Systems and Rehabilitation Engineering, IEEE Transactions on*, 17(3):270–278.

[Shawe-Taylor and Cristianini, 2004] Shawe-Taylor, J. and Cristianini, N. (2004). *Kernel methods for pattern analysis*. Cambridge University Press.

[Sherman, 1964] Sherman, E. D. (1964). A russian bioelectric-controlled prosthesis. *Canadian Medical Association Journal*, 91(24):1268–1270.

[Simon et al., 2012] Simon, A. M., Lock, B. A., and Stubblefield, K. A. (2012). Patient training for functional use of pattern recognition-controlled prostheses. *Journal of prosthetics and orthotics*, 24(2):56–64.

[Smith et al., 2011] Smith, L. H., Hargrove, L. J., Lock, B. A., and Kuiken, T. A. (2011). Determining the optimal window length for pattern recognition-based myoelectric control. *Neural Systems and Rehabilitation Engineering, IEEE Transactions on*, 19(2):186–192.

[Smith et al., 2014] Smith, L. H., Kuiken, T. A., and Hargrove, L. J. (2014). Real-time simultaneous and proportional myoelectric control using intramuscular EMG. *Journal of Neural Engineering*, 11(6):066013.

[Vidal, 1973] Vidal, J.-J. (1973). Toward direct brain-computer communication. *Annual review of Biophysics and Bioengineering*, 2(1):157–180.

[Vidaurre et al., 2011a] Vidaurre, C., Kawanabe, M., von Bunau, P., Blankertz, B., and Müller, K.-R. (2011a). Toward unsupervised adaptation of lda for brain–computer interfaces. *Biomedical Engineering, IEEE Transactions on*, 58(3):587–597.

[Vidaurre et al., 2011b] Vidaurre, C., Sannelli, C., Müller, K.-R., and Blankertz, B. (2011b). Machine-learning based co-adaptive calibration. *Neural computation*, 23(3):791–816.

[Vidovic et al., 2015] Vidovic, M. M.-C., Hwang, H.-J., Amsüss, S., Hahne, J. M., Farina, D., and Müller, K.-R. (2015). Improving the robustness of myoelectric pattern recognition for upper limb prostheses by covariate shift adaptation. *Neural Systems and Rehabilitation Engineering, IEEE Transactions on, in Press.*

[von Bünau et al., 2009] von Bünau, P., Meinecke, F. C., Király, F. C., and Müller, K.-R. (2009). Finding stationary subspaces in multivariate time series. *Physical Review Letters*, 103(21):214101.

[Webster, 2007] Webster, J. G. (2007). *Medical Instrumentation Application and Design*. Wiley & Sons, 4th ed. edition.

[Weir et al., 2009] Weir, R., Troyk, P., DeMichele, G., Kerns, D., Schorsch, J., and Maas, H. (2009). Implantable myoelectric sensors (IMESs) for intramuscular electromyogram recording. *Biomedical Engineering, IEEE Transactions on*, 56(1):159–171.

[Wolpaw and Wolpaw, 2012] Wolpaw, J. and Wolpaw, E. W. (2012). *Brain-computer interfaces: principles and practice*. Oxford University Press.

[Wurth and Hargrove, 2014] Wurth, S. M. and Hargrove, L. J. (2014). A real-time comparison between direct control, sequential pattern recognition control and simultaneous pattern recognition control using a fitts law style assessment procedure. *Journal of neuroengineering and rehabilitation*, 11:91.

[Young et al., 2013] Young, A., Smith, L., Rouse, E., and Hargrove, L. (2013). Classification of simultaneous movements using surface EMG pattern recognition. *Biomedical Engineering, IEEE Transactions on*, 60(5):1250–1258.

[Young et al., 2011] Young, A. J., Hargrove, L. J., Kuiken, T., et al. (2011). The effects of electrode size and orientation on the sensitivity of myoelectric pattern recognition systems to electrode shift. *Biomedical Engineering, IEEE Transactions on*, 58(9):2537–2544.

[Zecca et al., 2002] Zecca, M., Micera, S., Carrozza, M. C., and Dario, P. (2002). Control of multifunctional prosthetic hands by processing the electromyographic signal. *Critical Reviews in Biomedical Engineering*, 30(4-6):459–485.

[Zhang et al., 2013] Zhang, H., Zhao, Y., Yao, F., Xu, L., Shang, P., and Li, G. (2013). An adaptation strategy of using LDA classifier for EMG pattern recognition. In *Engineering in Medicine and Biology Society (EMBC), 2013 35th Annual International Conference of the IEEE*, pages 4267–4270.

[Ziai and Menon, 2011] Ziai, A. and Menon, C. (2011). A linear regression model for estimation of isometric wrist joint torques with varying arm configurations using emg

signals. In *Robotics and Biomimetics (ROBIO), 2011 IEEE International Conference on*, pages 1230–1235. IEEE.

[Ziehe et al., 2004] Ziehe, A., Laskov, P., Nolte, G., and Müller, K.-R. (2004). A fast algorithm for joint diagonalization with non-orthogonal transformations and its application to blind source separation. *The Journal of Machine Learning Research*, 5(1):777–800.